AFWL-TR-79-48

AFWL-TR-
79-48

(2) LEVEL III

BOREHOLE SHEAR DEVICE FEASIBILITY AND PRELIMINARY STUDIES

Roger Sidey, et al.

Dames and Moore
Los Angeles, CA 90071

August 1980

Final Report

Approved for public release; distribution unlimited.

AIR FORCE WEAPONS LABORATORY
Air Force Systems Command
Kirtland Air Force Base, NM 87117

This final report was prepared by Dames and Moore, Los Angeles, California, under Contract F29601-78-C-0058, Job Order 88091314 with the Air Force Weapons Laboratory, Kirtland Air Force Base, New Mexico. Capt Michael A. Reed (NTESG) was the Laboratory Project Officer-in-Charge.

This report has been reviewed by the Public Affairs Office and is releasable to the National Technical Information Service (NTIS). At NTIS, it will be available to the general public, including foreign nations.

This technical report has been reviewed and is approved for publication.

Michael A Reed

MICHAEL A. REED
Captain, USAF
Project Officer

FOR THE DIRECTOR

Gary P. Ganong

GARY P. GANONG
Lt Colonel, USAF
Chief, Tech & Applications Branch

Stewart W. Johnson

STEWART W. JOHNSON
Lt Colonel, USAF
Chief, Civil Engr Research Div

DO NOT RETURN THIS COPY. RETAIN OR DESTROY.

UNCLASSIFIED

SECURITY CLASSIFICATION OF THIS PAGE (When Data Entered)

REPORT DOCUMENTATION PAGE	READ INSTRUCTIONS BEFORE COMPLETING FORM
1 REPORT NUMBER: AFWL-TR-79-48 / 2. GOVT ACCESSION NO.: AD-A090 697	3 RECIPIENT'S CATALOG NUMBER
4 TITLE (and Subtitle): BOREHOLE SHEAR DEVICE FEASIBILITY AND PRELIMINARY STUDIES	5 TYPE OF REPORT & PERIOD COVERED: Final Report
	6. PERFORMING ORG. REPORT NUMBER: 10926-001-86
7 AUTHOR(s): Roger Sidey, Luis Rodriguez, Joaquin Marti, Douglas White	8. CONTRACT OR GRANT NUMBER(s): F29601-78-C-0058
9 PERFORMING ORGANIZATION NAME AND ADDRESS: Dames and Moore, Los Angeles, CA 90071	10. PROGRAM ELEMENT, PROJECT, TASK AREA & WORK UNIT NUMBERS: 62601F/88091332
11 CONTROLLING OFFICE NAME AND ADDRESS: Air Force Weapons Laboratory (NTESG), Kirtland AFB, NM 87117	12. REPORT DATE: August 1980 13. NUMBER OF PAGES: 214
14 MONITORING AGENCY NAME & ADDRESS (if different from Controlling Office)	15 SECURITY CLASS. (of this report): UNCLASSIFIED 15a. DECLASSIFICATION DOWNGRADING SCHEDULE

16 DISTRIBUTION STATEMENT (of this Report)

Approved for public release; distribution unlimited.

17 DISTRIBUTION STATEMENT (of the abstract entered in Block 20, if different from Report)

18 SUPPLEMENTARY NOTES

19 KEY WORDS (Continue on reverse side if necessary and identify by block number)

Borehole Device
Shear Modulus
Shear Waves
Soil Testing

20 ABSTRACT (Continue on reverse side if necessary and identify by block number)

The present studies try to overcome the difficulties inherent to the determination of in-situ shear modulus of soils over the complete range of strains. A new apparatus is proposed: the BSD (Borehole Shear Device). It essentially consists of a self-boring cylinder which has the capabilities of expanding radially to recover the pre-existing horizontal stress levels in the soil and of rotating harmonically about its axis. This allows constructing the curve

(Continued)

DD FORM 1 JAN 73 1473

UNCLASSIFIED

SECURITY CLASSIFICATION OF THIS PAGE (When Data Entered)

Block 20 (Continued)

relating the secant modulus to the strain level, based on the field measurements of torque and rotation of the cylinder. The device is expected to work up to failure strains in non-gravelly soils down to depths on the order of 50 m.

PREFACE

The authors express their gratitude to Dr. Richard H. Bassett of King's College, London, who, as an external consultant to Dames and Moore, provided invaluable comments and discussions throughout this project, particularly in regard of the engineering design and geotechnical aspects of the work.

In respect of the relatively new technology of self boring which is discussed in this report, the authors are most grateful to PM Geotechnical Analysts Ltd., of Cambridge, U.K. for their invaluable suggestions and technical discussion.

Thanks are also extended to Mr. Denis Hitchings of Imperial College, London, also an external consultant to Dames and Moore, for his continuous help in modifying and successfully using his finite-element system FINEL.

Construction of the prototype was undertaken by Prototype Engineering Limited of Croydon, under the supervision of Mr. Brian Stevens.

CONTENTS

LIST OF TABLES

LIST OF FIGURES

1. INTRODUCTION

1.1 PREAMBLE

There are many natural and man-made events which subject soils to large dynamic forces and the survival of buildings in the vicinity is strongly dependent upon the manner in which these soils respond. To realistically assess vulnerability it is therefore essential to have a good quantitative knowledge of soil dynamic response. Of particular interest to the US Air Force is the response of soil to the loads associated with a nuclear explosion. An accurate knowledge of this response is required for the design and assessment of many military structures such as command centers, missile silos and other surface or under-ground facilities.

Modern numerical tools allow performing sophisticated dynamic analyses which model the interaction of soils and structures. Indeed, the US Air Force is presently conducting an effort to improve its numerical capabilities in regard of that specific problem, both in two and three space dimensions. In fact, the numerical problem can be considered almost solved. Most of the required capabilities already exist and the effort remaining is essentially that of blending them into a single computer program of the required generality.

Of greater concern is the difficult problem of obtaining an accurate constitutive description of the soil. To the writers' knowledge, there is not sufficient confidence in any of the existing soil constitutive

laws to allow making reliable predictions of the behaviour of soil when subjected to complex stress paths under dynamic conditions. Even at the fundamental level, it is not obvious whether concepts such as the traditional "effective stress" still apply under the high transient stresses generated by blast loading.

It is fair to state that in the last two decades numerical capabilities have improved at a much faster rate than soils testing. At present, most soils testing is conducted in the laboratory on relatively small soil samples. These samples suffer from the unknown effects of disturbance and stress relief which, due to the strong history dependence of soils, often introduce large uncertainties in the validity of the results obtained by those tests. A clear example of this is the large difference in shear modulus which is normally observed at identical strain levels between laboratory resonant column tests and in-situ seismic measurements.

There are many other uncertainties inherent in present day soils testing methods. Variables can only be measured at internal or external boundaries in the material, the influence of which is not always obvious. The effect of sample size and soil inhomogeneity is difficult to assess, and still more important, testing has normally only one or two (seldom three) degrees of freedom, whereas a true constitutive description requires at least six components of the stress and strain tensor. In the absence of better data one must make assumptions to generalize the results of tests such as triaxial and simple shear to the full three-dimensional situation.

The conclusion is that too much is often expected from the tests. It is equally clear that it is not a simple matter to overcome these problems. The work described in this report will hopefully constitute a step towards a better material description by providing a method which minimizes some of the problems of the present testing procedures for derivation of the dynamic shear modulus of soils.

1.2 PURPOSE OF THE WORK PERFORMED

Dynamic calculations in soil are very often based on generalisations or direct use of a one-dimensional constitutive law which, in shear is characterised by a secant shear modulus, expressed as:

$$\frac{\mu}{\mu_r} = \left(\frac{\sigma'}{\sigma'_{rf}}\right)^n \mu(\varepsilon) \qquad (1)$$

where μ is the secant shear modulus ($\mu = \tau/\varepsilon$, where τ is the shear stress)

σ' is the effective confining pressure

ε is the shear strain

n is a constant

the subscript r applies to values of the variables at the reference state (characterized by small strains and $\sigma' = \sigma'_{rf}$ is a reference effective confining pressure).

The objective of the apparatus described in the present report is to produce the function $\mu(\varepsilon)$ along the soil profile for the complete

range of strains of interest. The function $\mu(\varepsilon)$ is intended to be representative of the in-situ soil conditions; hence, an attempt has been made to minimize the soil disturbance during the test.

1.3 SCOPE OF WORK

In trying to provide a basis towards the operation of a device able to perform the aforementioned task, the scope of the present work can be summarized in the following items:

(a) A brief review of the state-of-the-art as regards the determination of the dynamic shear modulus of soils.

(b) A feasibility analysis of a borehole device for in-situ determination of the dynamic shear modulus.

(c) Design, construction and laboratory testing of the mechanism which couples the device to the borehole wall.

The feasibility analysis includes several different aspects:

(I) Conceptual design of the overall device and its operation.

(II) Analytical and numerical studies to determine the stress, strain and displacement fields at the strain levels of interest; also, studies to predict the normal operation of the device as well as the influence on its performance of

factors such as soil layering and soil disturbance around the borehole.

(III) The construction of a procedure to obtain the shear modulus - shear strain curve in-situ, based on the values of the variables during operation in the field.

It must be however remembered that the device proposed in this report is not intended to solve the problem of measuring the shear modulus of soil completely, but simply to alleviate some of the most serious inconsistencies of present practice.

2. STATE-OF-THE-ART

Dynamic analyses of soil response are frequently required for a variety of problems, including blasting, earthquakes, etc. Such analyses must always be based on the dynamic properties of the soil. The present chapter briefly reviews those properties and the current methods of obtaining them.

The information which is ideally required for performing a dynamic soil analysis consists of the full constitutive equations of the soil. This is too formidable a task to be attempted as yet. Idealised forms of the constitutive laws, which approach the soil behaviour over the range of conditions of interest, must therefore be assumed in order to decide which properties are to be determined.

By passing the completely linear approaches, which are not of great interest here, the first non linear approximations which would be applied with some generality were based on the assumption that a one-dimensional propagation of shear waves would be an adequate representation of soil dynamics problems (Schnabel et al, 1972)[1]. Under these circumstances, the soil is totally defined by the relation:

$$\mu(\varepsilon_e)\ \varepsilon + \eta(\varepsilon_e)\ \dot{\varepsilon} \qquad (1)$$

where τ is the shear stress (*)

ε is the shear strain, $\dot{\varepsilon}$ is the rate of increase of shear strain

μ is a strain-dependent secant shear modulus

η is a strain-dependent viscosity

ε_e is an equivalent strain

(*) All symbols are defined in their first appearance and in Appendix A.

Such an approach has constituted the basis of many lines of analysis, primarily due to the fact that it can be formulated in an "equivalent linear" manner by using for the values of the modulus and the vicosity those corresponding to a certain percentage of the maximum shear strain (equivalent strain) developed at each point in the soil profile. The approach has been generalized to more dimensions and other alternative procedures have been devised; but the determination of the function $\mu(\varepsilon)$ still remains a basic concern in practically any soil dynamics analysis.

The function $\mu(\varepsilon)$ is known to be more or less constant for strain levels smaller than 10^{-6} or even almost 10^{-5}. At this point, non-linearities appear and the shear modulus starts decreasing; clearly, it should tend to zero as the strain level increases indefinitely (see for example: Seed and Idriss, 1970)[2].

The standard procedure for determining $\mu(\varepsilon)$ at present is explained below. Geophysical techniques are used to measure the in-situ velocity of compressional and shear waves. Those two velocities can then be used together with the well known elastic relationships to derive the value of the dynamic Poisson's ratio and of the shear modulus for the lower range of strains.

$$\mu = \rho v_s^2 \tag{2}$$

$$\nu = \frac{(v_p/v_s)^2 - 2}{2\left[(v_p/v_s)^2 - 1\right]} \tag{3}$$

where ρ is the density

ν is the dynamic Poisson's ratio

v_p, v_s are the velocities of propagation of compressional and shear waves respectively.

In materials which are suitable for sampling, laboratory tests are then conducted in conditions which attempt to reproduce the in-situ configuration. Shear tests of the resonant column type are used for strain levels up to 10^{-4} or 10^{-3}. Those are complemented either with simple shear tests or with strain-controlled dynamic triaxial tests for the upper range of strains, including failure of the material if necessary. In case of using triaxial tests, the property obtained is the Young's modulus; assuming that the dynamic Poisson's ratio is constant and hence independent of the strain level, the value of the Poisson's ratio derived in the field is then used together with the Young's modulus, E, in order to derive the value of the shear modulus sought.

$$\mu(\varepsilon) = \frac{E(\varepsilon)}{2(1+\nu)} \qquad (4)$$

The above procedure presents a number of conceptual inconsistencies due to the three diverse experimental philosophies embodied; as it could be expected, such inconsistencies are clearly displayed by the results obtained. At the overlapping range of strains, field and laboratory techniques have been found to yield values of the shear modulus which differ by factors varying from 1.2 to 4.0 (Stokoe et al, 1978)[3]. Such differences are believed to be due to the disturbance which occurs during sampling and to the stress relief undergone by the sample when removed from its native environment; in general, they show the difficulty of simulating field conditions in a laboratory test (Stokoe and Richart, 1973)[4]. A number of procedures have been devised to correct the laboratory curve so that it passes through the field

value of the modulus : both parallel and proportional corrections have been advocated (Anderson et al, 1978)[5]. Theories have also been proposed which postulate that a thixotropic effect stiffens the soil with time until an energy balance within the soil is attained (Anderson et al, 1976)[6]. Such procedures and theories are valuable but, used in this context, they simply constitute attempts to patch up the weakness inherent in the experimental tricotomy which the method suffers.

Let us examine in more detail some of the procedures used for in-situ determination of the shear modulus of soils. The most common ones are based on seismic wave propagation phenomena. The instrumentation required for those tests is basically composed of a seismic wave source and one or more pick-up devices; nature and location of these components requires a careful understanding of wave generation and propagation phenomena. General theory of propagation of waves in elastic media can be found in Timoshenko and Goodier (1951)[7] and Ewing et al (1957)[8]. Since the material behaviour remains essentially elastic during most wave propagation tests, these general studies provide the necessary background.

Seismic tests in which source and detectors are located on the surface of the soil were developed first and have been discussed by Duke (1969)[9]. Methods based in reflection and refraction techniques were described by Richart et al (1970)[10]. In any case, the input source can be impulsive or vibratory. In case of impulse tests, the energy source is provided by detonation of explosives or by mechanical means. The arrival times of the direct and/or reflected and/or refracted body or surface waves are measured

in an array of transducers and used to determine average values of wave velocities along the different paths assumed. Refraction surveys give in addition the depths to the different refractors, which can be used to check the reliability of the results obtained.

The impulse source is chosen depending on the type of waves desired. Shear waves are the most suitable ones for determination of the shear modulus because their velocity is directly related to it. Also, at high degrees of saturation, the compressional wave is likely to represent more the velocity of propagation through the water and, therefore, produces little information on the behaviour of the soil skeleton.

A description of various suitable sources of shear-waves is given by Mooney (1974)[11]. Impulse methods often produce considerable amounts of P- waves and consequently S-wave arrivals are difficult to identify; this problem can be somewhat overcome by using a seismic source which allows reversal of the energy input. Schwarz et al (1974)[12] used this technique to determine the shear wave velocity in marine foundations. The procedure consists on subtracting seismic records produced with opposite energy inputs; the reason is that, under those conditions, P-wave components should be equal while S-wave components should be exactly opposite. Lande (1974)[13] describes a technique in which the reaction force on a horizontal plate produced by a water cannon is used as a source of horizontally polarized waves. Different orientations of the water cannon allow production of P- and/or S-waves as well as application of the phase reversal method.

Surface tests with sustained seismic sources have been performed using constant or systematically varying sinusoidal inputs. The source is normally a mechanical or electro-mechanical vibrator and the signals are recorded at various points at or below the surface of the soil. A procedure has been described by Kurzeme (1971)[14] in which horizontally polarized shear waves are produced by means of a torsional vibrator. The method which has been primarily used in pavement investigation, consists in analysing the measured velocity dispersion with frequency using an idealised material and structural model. Shear wave velocity and thickness of the various layers can be determined; the quality of the results depends on how closely the model simulates the real soil conditions.

All of the aforementioned tests utilise body wave velocities to determine the shear modulus of soils. A method using Rayleigh waves was described by Jones (1960,[15] 1962)[16]. This technique, which was initiated in Germany during the thirties, consists in measuring the wave length and phase velocity of the vibrations propagated along the surface of the soil. Shear wave velocity can then be calculated assuming a ratio of v_R to v_s resulting from elastic theory (Richart et al 1970)[10]. For the range of Poisson's ratios commonly found in soil materials, errors due to the above assumption are less than 10%. Due to the fact that the shear modulus of soil is not constant with depth, the phase wave velocity - depends on the frequency of vibration. Fowler (1972)[17] has found empirically that the velocity determined from propagation of a surface wave is applicable to a depth of equal to half of the wave length.

A method using this technique is described by Ballard et al, (1975)[18] in which an impulsive source is used to generate Rayleigh waves. Instrumentation and field procedures are similar to those used in the refraction method; phase velocity can be determined by numbering the peaks and troughs of the oscillations and following them through adjacent traces. This method is limited in application by the inability to exercise selective control over the generated frequencies and, hence to the depths associated with those frequency values.

Various methods have been developed to measure the direct shear wave velocity between surface and subsurface points. They normally utilize a single borehole; the seismic source is located on the surface of the soil (downhole) or in the borehole (uphole). In the first case, transducers are placed in the borehole; in the second, they are at the surface and/or in the borehole. Several types of seismic sources have been used and references are given by Stokoe et al, (1972)[19].

The crosshole seismic technique is a method which has received a great deal of attention in the last few years. It basically consists in measuring the time that body waves take to travel along a horizontal path between two points in the soil mass. The source and one or more transducers are located in separate boreholes. Swain (1962)[20] and Stokoe et al, (1972)[19] used the technique with impulsive motions generated by impact. Tanimoto et al, (1973)[21] discussed the problems of using only two boreholes; those arise due to the differences between the characteristics of the motions of the transducer in the operating source and those of the transducer in the receiving

hole as well as from large differences in the strain level along the wave path. A low energy impulse source has been developed by Auld (1977)[22]; it is composed of a stationary part and a hammer, the stationary par consists of a hydraulic cylinder block with eight horizontal pistons, four pistons for expansion to grip the borehole walls and the others for contraction. The hammer can strike either downwards or upwards thus allowing application of the phase reversal technique.

The use of vibratory sources of shear waves in crosshole configurations has been tried by Ballard et al (1969)[23] and it has been successfully developed by Ballard (1975)[18]. It consists of a vibratory source in conjunction with a spring wedged device in contact with the borehole wall. Vertically polarized shear waves are propogated and the results obtained are processed for determining the shear wave velocity.

All methods mentioned so far are used for determining the in-situ shear modulus for small strains (up to 10^{-6}). Some of them only generate small strains; in cases where large strains are generated, the configuration of the test is chosen so that the large strains do not influence the measurements. The measurement of the shear modulus in-situ for large strains has proved to be a difficult task indeed. Large strain amplitudes can be obtained using explosives as seismic sources. The main problems associated with explosives is that they generate large amounts of P-waves and that the results produced are difficult to analyze and non-repeatable.

Some investigators have tried to produce large strains by means of vibratory sources. Miller et al, (1972)[24] utilized a vibratory high-energy

driving source; velocity transducers were located in two adjacent holes. Shear waves originated from the sinusoidal input, are propagated to the monitoring boreholes. Although the source was initially designed to produce large strains, it has been used only for small strains due to difficulties of interpretation of the signals related to interference with background noise.

An attempt to measure the shear modulus as a function of strain level using an in-situ technique has been presented by Miller et al, (1975)[25] and Troncoso (1975)[26]. The method essentially consists in a crosshole impulse test; the generating source is composed of an anchor firmly coupled to the surrounding soil and a striking hammer which impacts the top of the anchor. Coupling of the anchor to the soil is accomplished by means of an radial stress. The recording stations consist in velocity transducers firmly coupled to the soil by means of high pressure rubber balloons. The shear wave velocity between two stations is calculated from arrival times of wave peaks. The strain level developed at each station is calculated using the elastic relationship which equals it to the ratio of the measured particle velocity divided by the shear wave velocity. The procedure is designed to work up to strain levels of about 10^{-3} although it does not appear to have been used in natural soils beyond 10^{-4}.

Several important problems are associated with the method as reported. The large strains occur close to the source. At this point, particle velocity is equated to source velocity; this often leads to errors due to slip which is difficult to avoid and has greater tendency to appear as the strain and

hence the input energy increase. Furthermore, the device generates P-waves which, close to the source, have not yet separated from the S-waves, thus introducing uncertainties in interpretation. The formula for calculating local strain values also starts introducing errors as the material behaves more non-linearly, which is the behavior of greater interest. Finally, it must be noted that wave forms are preserved only in linear materials; non-linear behavior distorts the wave forms. Hence, wave parameters calculated from arrival times of wave peaks are likely to introduce errors increasing with the strain level.

Independently of the type of borehole test for high strains, it can easily be seen that, even under linear propagation, strains will decrease as Bessel functions; as a consequence of the cylindrical symmetry this decay will be progressively faster as greater non-linearities (or greater strains) are induced in the soil. If it is also realised that the soil has only a limited shear strength around the borehole which can be activated to propagate the input to the progressively larger regions of surrounding soil, it is quite clear that, in most realistic situations, the zone of large strains is going to be confined to the immediate vicinity of the source. This is confirmed by the analyses presented in this report. Any type of crosshole methods, even with very short distances between the source and transducers (which creates many other experimental problems) are likely to have difficulties arising from vast non-uniformities in wave propagation arising from the widely varying strain levels. Also, any method relying on arrival times of any kind, is likely to introduce errors associated with the different velocities of propagation of different strain levels. Because of the above

reasons, it seems to the authors that a single-point measurement technique, independently of the details of the test proposed, may be a better option than up-, down- or cross-hole alternatives for in-situ measurement of the shear modulus of soil at large strain levels.

3. ANALYTICAL SOLUTIONS

It seems quite clear that the full problem of a finite cylinder rotating in an inhomogeneous and non-linear domain cannot be solved by present analytical procedures. However, since close-form solutions are very useful for studying the influence of the different parameters, it has been considered appropriate to introduce certain simplifications to the problem in order to allow the derivation of a number of analytical solutions.

The first simplification included is that the length to diameter ratio of the shoe (rotating cylinder) is large. This assumption effectively decreases the order of the problem from two spatial dimensions to one; the time dimension is independent of that simplification.

Second, as the maximum frequencies foreseen for the device are on the range of 10 to 20 Hz and typical shear wave velocities will span from one to a few hundred metres per second, it appears that associated wave lengths will be substantially larger than the domain under investigation. In that situation, the static strain distribution cannot be expected to differ greatly from the real part of the dynamic one.

Finally, the soil will be considered as a homogeneous half-space; although linearity and full isotropy are not required at this stage, axisymmetric property distributions are assumed throughout this report. Not all of the above assumptions are needed for allowing derivation of close-form solutions, as will be seen later. However, those

obtained will be presented here following an approximate order of increasing complexity or, equivalently, of decreasing number of assumptions.

3.1 LONG CYLINDER - STATIC

Let us consider an infinitely long cylinder of radius r_o embedded in a homogeneous continuum. Let τ_o be the static shear stress transmitted at the interface between the cylinder and the continuum. The equilibrium of any annulus boundred by r_o and an arbitrary radius r requires (Figure 1):

$$\tau(r) = \frac{\tau_o r_o^2}{r^2} \qquad (1)$$

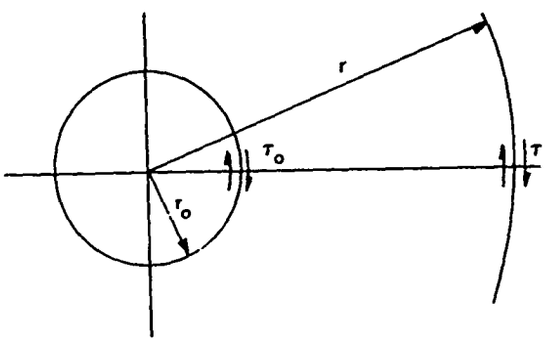

Figure 1. Shear stress distribution

It is then clear that the only non-vanishing strain $\varepsilon_{r\theta}$ (called ε for simplicity) fulfills, independently of the constitutive relation:

$$\frac{\tau_o r_o^2}{r^2} = \tau(\varepsilon) \qquad (2)$$

where $\tau = \tau(\varepsilon)$ is the constitutive relation of the material in simple-shear.

Equation (2) allows the derivation of the strain distribution under fairly general constitutive laws. Five such laws have been used as examples. The laws are summarized in Table 1, together with their formulation and main characteristics:

Table 1. Constitutive laws used in the derivation of strain fields

NAME	FORMULATION	INITIAL MODULUS	LIMITING STRESS
ELASTICITY	$\tau = \mu_o \varepsilon$	μ_o	∞
HYPERBOLIC LAW	$\tau = \dfrac{\mu_o \varepsilon}{1 + \mu_o \varepsilon / \tau_m}$	μ_o	τ_m
POWER LAW	$\tau = A\varepsilon^n \quad (o<n<1)$	∞	∞
HYPERBOLIC TANGENT	$\tau = \tau_m \tanh \dfrac{\mu_o \varepsilon}{\tau_m}$	μ_o	τ_m
RAMBERG-OSGOOD	$\varepsilon = A\tau^n + \tau/\mu_o \quad (n>1)$	μ_o	∞

For each one of the above laws, the corresponding strain distributions are presented below:

a) Elasticity

The constitutive law is:

$$\tau = \mu_o \varepsilon$$

The strain distribution becomes:

$$\varepsilon = \frac{\tau_o r_o^2}{\mu_o r^2} \tag{3}$$

b) Hyperbolic Law

Substituting the constitutive law into equation (2):

$$\tau \frac{r_o^2}{r^2} = \frac{\mu_o \varepsilon}{1 + \dfrac{\mu_o}{\tau_m} \varepsilon}$$

Hence, the strain distribution is:

$$\varepsilon = \frac{\tau_o}{\mu_o \left[\frac{r^2}{r_o^2} - \frac{\tau_o}{\tau_m} \right]} \qquad (4)$$

or, for easier comparison with equation (3):

$$\varepsilon = \frac{\tau_o r_o^2}{\mu_o} \; \frac{1}{r^2 - \frac{\tau_o r_o^2}{\tau_m}}$$

which reverts to the elastic distribution for large τ_m or at large distances for the cylinder.

c) Power Law

Operating as above:

$$\frac{\tau_o r_o^2}{r^2} = A\varepsilon^n \quad (n<1)$$

$$\varepsilon = \left[\frac{\tau_o r_o^2}{A r^2} \right]^{1/n} \qquad (5)$$

which approaches the elastic distribution as n approaches unity.

d) Hyperbolic Tangent

$$\frac{\tau_o r_o^2}{r^2} = \tau_m \tanh \frac{\mu_o \varepsilon}{\tau_m}$$

$$\varepsilon = \frac{\tau_m}{\mu_o} \operatorname{atanh} \left[\frac{\tau_o r_o^2}{\tau_m r^2} \right] \qquad (6)$$

Again the elastic distribution is recovered at large distances or, in any case, for large τ_m.

e) Ramberg-Osgood Type

The equation proposed is a typical skeleton curve used in studies of cyclic behaviour.

$$\varepsilon = A\tau^n + \frac{\tau}{\mu_o}$$

The strain distribution becomes:

$$\varepsilon = A\left[\frac{\tau_o r_o^2}{r^2}\right]^n + \frac{\tau_o r_o^2}{\mu_o r^2} \qquad (7)$$

Elastic behavior is obtained as n approaches 1 or A approaches zero or the distance becomes large.

In order to study the effect of the material description in the strain distribution, a typical stress-strain curve was fitted by the proposed models (Figure 2). The resulting strain distributions are plotted together in Figure 3. As can be seen, elastic strains decrease with the inverse of the square of the distance from the axis of the borehole; the effect of the non-linearity of the stress-strain law is essentially felt as a faster than elastic rate of decrease of the shear strain. When the initial modulus coincides, all stress-strain laws predict identical strains at large distances.

Once the strain distribution is known, the torque required and the corresponding displacement field can be easily obtained.

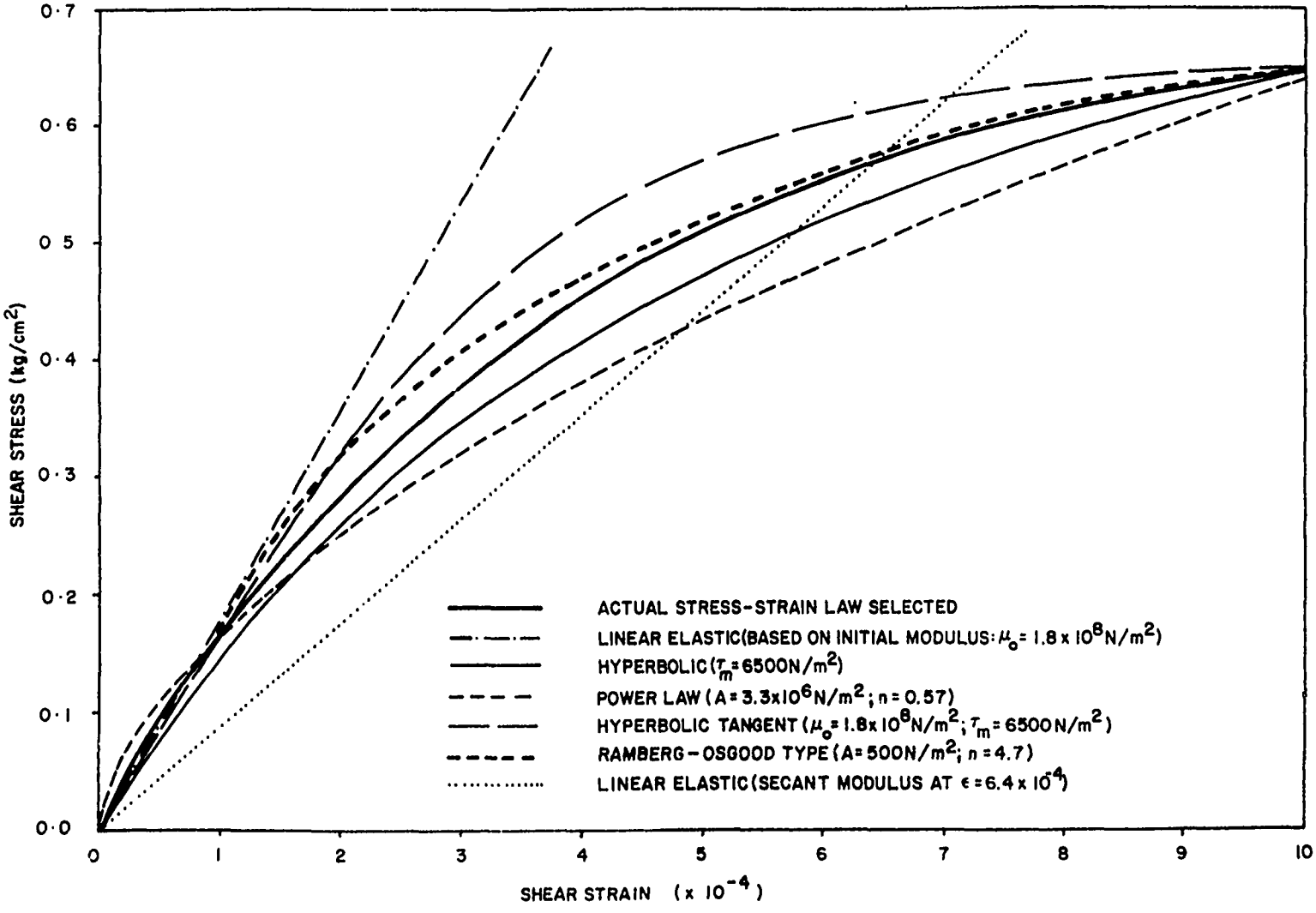

Figure 2. Comparison of some different stress-strain laws

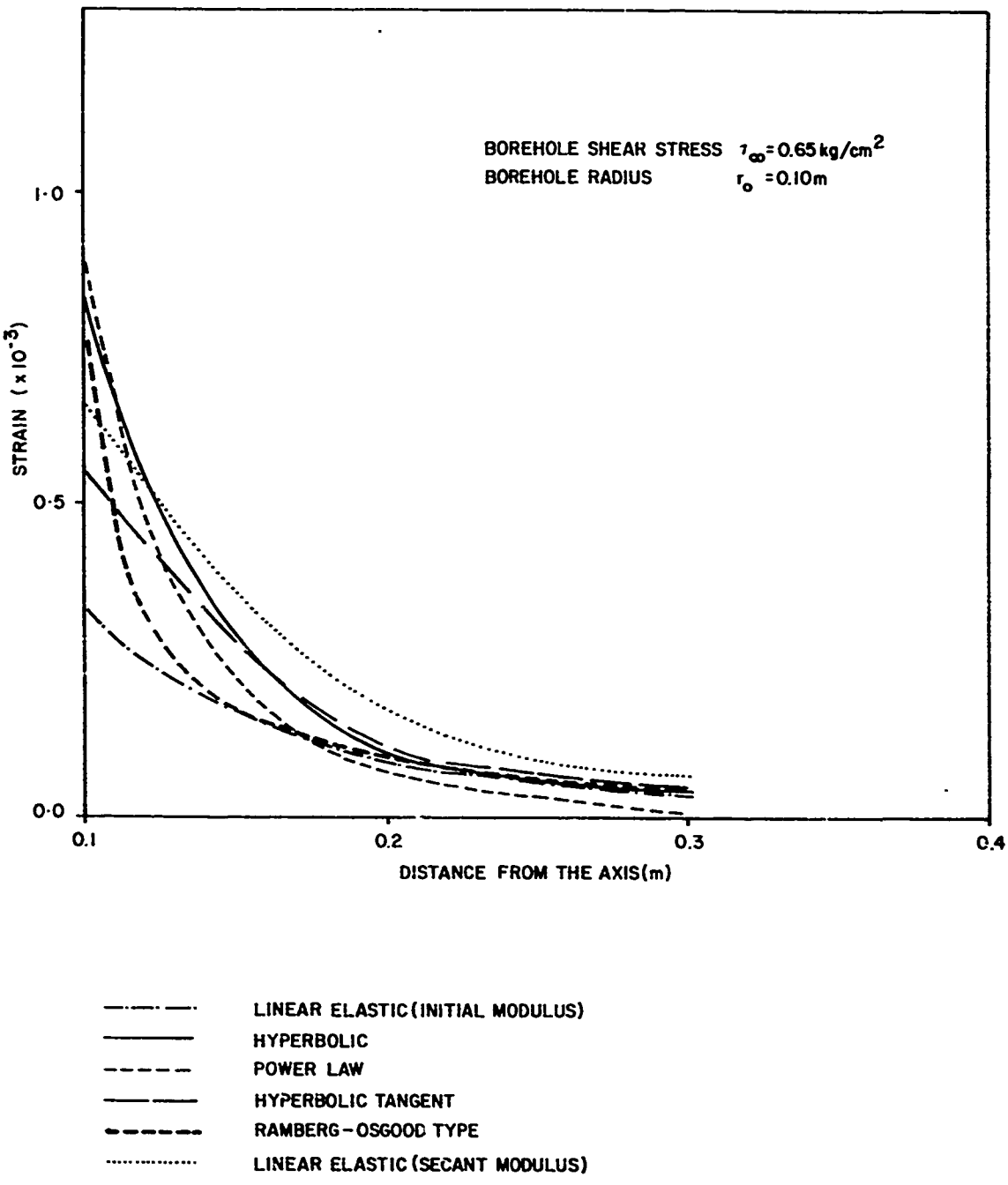

Figure 3. Comparison of the corresponding strain distributions

The torque per unit length is:

$$T_\ell = 2\pi r_o^2 \tau_o \tag{8}$$

The displacement field is derived from the relation:

$$\cdot = \frac{\partial u}{\partial r} - \frac{u}{r} \tag{9}$$

where u is the θ - component of the displacement (all other components vanish).

For example, for the elastic case:

$$\frac{\partial u}{\partial r} - \frac{u}{r} = \frac{\tau_o r_o^2}{\mu_o r^2} \tag{10}$$

This equation can be readily integrated. The partial derivative becomes an ordinary one, as u only depends on r. Assuming that the displacement vanishes at infinity, the solution is (see Appendix IV for the derivations):

$$u = -\frac{\tau_o r_o^2}{2\mu_o r} \tag{11}$$

The above result can also be expressed as a function of the displacement at the interface of u_c or the angle rotated θ_o. Table 2 provides those forms of the solution.

Table 2. Summary of elastic results

VARIABLE / AS A FUNCTION OF	τ_o	u_o	θ_o
τ	$\frac{\tau_o r_o^2}{r^2}$	$-\frac{2\mu_o u_o r_o}{r^2}$	$-\frac{2\mu_o \theta_o r_o^2}{r^2}$
ε	$\frac{\tau_o r_o^2}{\mu_o r^2}$	$-\frac{2u_o r_o}{r^2}$	$-\frac{2\theta_o r_o^2}{r^2}$
u	$-\frac{\tau_o r_o^2}{2\mu_o r}$	$\frac{u_o r_o}{r}$	$\frac{\theta_o r_o^2}{r}$
T_ℓ	$2\pi r_o^2 \tau_o$	$-4\pi\mu_o u_o r_o$	$-4\pi\mu\theta_o r_o^2$

The above formulae, in spite of their simplicity and the number of assumptions involved, are of notable use in later considerations.

Derivations similar to the elastic ones can be carried out for other constitutive relations. The hyperbolic model will be studied here because of its later utilization for interpretation of field data. The displacement distributions fulfills now the equation:

$$\frac{du}{dr} - \frac{u}{r} = \frac{\tau_o r_o^2}{\mu_o} \frac{1}{r^2 - \frac{\tau_o r_o^2}{\tau_m}}$$

again subject to the boundary condition:

$$\lim_{r \to \infty} u = o$$

The intergration of this linear equation is carried out in Appendix C and yields the solution:

$$u = -\frac{\tau_m r}{2\mu_o} \ln\left(1 - \frac{\tau_o r_o^2}{\tau_m r^2}\right) \tag{12}$$

Other related formulae can be obtained from equation (12) as it was done for the elastic case. In particular, by taking $r=r_o$ and $\theta_o = u_o/r_o$, the following result is immediately obtained:

$$\tau_o = \tau_m \left[1 - e^{-\frac{2\mu_o \theta_o}{\tau_m}}\right] \tag{13}$$

relating the stress at the boundary to the rotation. The torque per unit length is then:

$$T_\ell = 2\pi r_o^2 \tau_m \left[1 - e^{-\frac{2\mu_o \theta_o}{\tau_m}}\right] \tag{14}$$

3.2 LONG CYLINDER - DYNAMIC

The present section is only concerned with soils which can be represented by a homogeneous axisymetric continuum, constituted by a linear viscoelastic solid of constant complex moduli. Under those conditions, the combined viscoelastic equations in terms of displacements can be readily derived from:

$$\rho \frac{\partial^2 u_r}{\partial t^2} = (\lambda+2\mu) \frac{\partial \Delta}{\partial r} - \frac{2\mu}{r} \frac{\partial w_z}{\partial \theta}$$

$$\rho \frac{\partial^2 u_\theta}{\partial t^2} = \frac{\lambda+2\mu}{r} \frac{\partial \Delta}{\partial \theta} + 2\mu \frac{\partial w_z}{\partial r} \qquad (15)$$

where:

$$\Delta = \frac{\partial u_r}{\partial r} + \frac{u_r}{r} + \frac{1}{r} \frac{\partial u_\theta}{\partial \theta}$$

$$w_z = \frac{1}{2r} \left(r \frac{\partial u_\theta}{\partial r} + u_\theta - \frac{\partial u_r}{\partial \theta} \right)$$

and λ, μ are complex Lame constants

In the present case $u_r = 0$ and $\frac{\partial}{\partial \theta} = 0$; then, the first of equations (15) becomes an identity while the second one takes the form:

$$\frac{\partial^2 u_\theta}{\partial t^2} = v_s^2 \left[\frac{\partial^2 u_\theta}{\partial r^2} + \frac{1}{r} \frac{\partial u_\theta}{\partial r} - \frac{u_\theta}{r^2} \right] \qquad (16)$$

where $v_s^2 = \frac{\mu}{\rho}$ is the square of the complex velocity of shear-wave propagation.

The boundary conditions for equation (16) are vanishing displacements at infinity and harmonic input at the cylinder-soil interface, whether in the form of controlled displacements or controlled stresses. Again representing by u the only non-vanishing component of the displacement, those boundary conditions can be expressed mathematically as:

$$\lim_{r \to \infty} u = 0$$

and $u = u_o e^{i\omega t}$ for $r = r_o$ (controlled displacements)

or $\tau = \tau_o e^{i\omega t}$ for $r = r_o$ (controlled stress)

Since only the steady-state solutions are sought, initial conditions are not required.

Equation (16) can be integrated by the standard method of separation of variables, that is, finding the solutions of the form:

$$u(r,t) = \bar{R}(r)\ \bar{T}(t)$$

where R depends only on r and $\bar{T}$ only on t (the bar is used simply to differentiate the symbol from that used for torque)

Substituting into equation (16):

$$\frac{\bar{T}''}{\bar{T}} = v_s^2 \left[\frac{\bar{R}''}{\bar{R}} + \frac{1}{r} \frac{\bar{R}'}{\bar{R}} - \frac{1}{r^2} \right] \qquad (17)$$

Since the left hand side of equation (17) is only a function of time and the right hand side depends only on the distance, both sides are equal to a constant, henceforth named $-\omega^2$. Equation (17) then generates:

$$\frac{\bar{T}''}{\bar{T}} = -\omega^2 \tag{18}$$

$$v_s^2\left[\frac{\bar{R}''}{\bar{R}} + \frac{1}{r}\frac{\bar{R}'}{\bar{R}} - \frac{1}{r^2}\right] = -\omega^2 \tag{19}$$

All solutions of equation (18) are of the form:

$$\bar{T} = \bar{T}_o e^{i\omega t}$$

where $\bar{T}_o$ is a constant.

Equation (19) can be regrouped; by changing variables to the dimensionless distance $\frac{\omega r}{v_s}$ the equation takes the form of a Bessel differential equation:

$$\left(\frac{\omega r}{v_s}\right)^2 \frac{d^2\bar{R}}{d\left(\frac{\omega r}{v_s}\right)^2} + \left(\frac{\omega r}{v_s}\right) \frac{d\bar{R}}{d\left(\frac{\omega r}{v_s}\right)} + \bar{R}\left[\left(\frac{\omega r}{v_s}\right)^2 - 1\right] = 0 \tag{20}$$

the general solution of which is:

$$\bar{R}\left(\frac{\omega r}{v_s}\right) = A'J_1\left(\frac{\omega r}{v_s}\right) + B'Y_1\left(\frac{\omega r}{v_s}\right) \tag{21}$$

where J_1 is a Bessel function of the first kind

Y_1 is a Bessel function of the second kind

A' and B' are arbitrary complex constants

Equation (21) can be expressed in terms of Hankel functions in a more convenient way:

$$\bar{R}\left(\frac{\omega r}{v_s}\right) = A\, H_1^{(1)}\left(\frac{\omega r}{v_s}\right) + B\, H_1^{(2)}\left(\frac{\omega r}{v_s}\right) \tag{22}$$

where $H_1^{(1)}(\cdot) = J_1(\cdot) + i\, Y_1(\cdot)$

$H_1^{(2)}(\cdot) = J_1(\cdot) - i\, Y_1(\cdot)$

A and B are again arbitrary complex constants.

The general solution to equation (16) can now be seen to be:

$$u(r,t) = \sum_n \left\{ \left[A_n H_1^{(1)}\left(\frac{\omega_n r}{v_s}\right) + B_n H_1^{(2)}\left(\frac{\omega_n r}{v_s}\right) \right] e^{i\omega_n t} \right\} \tag{23}$$

By observing the assymptotic behaviour of the Hankel functions:

$$H_1^{(1)}\left(\frac{\omega_n r}{v_s}\right) e^{i\omega_n t} \sim \sqrt{\frac{2v_s}{\pi\omega_n r}}\, e^{i\left(\frac{\omega_n r}{v_s} + \omega_n t - \frac{3\pi}{4}\right)}$$

$$= \sqrt{\frac{2v_s}{\pi\omega_n r}}\, e^{-i\frac{3\pi}{4}}\, e^{i\frac{\omega_n}{v_s}(r + v_s t)}$$

$$H_1^{(2)}\left(\frac{\omega_n r}{v_s}\right) e^{i\omega_n t} \sim \sqrt{\frac{2v_s}{\pi\omega_n r}}\, e^{i\left(-\frac{\omega_n r}{v_s} + \omega_n t + \frac{3\pi}{4}\right)}$$

$$= \sqrt{\frac{2v_s}{\pi\omega_n r}}\, e^{i\frac{3\pi}{4}}\, e^{i\frac{\omega_n}{v_s}(-r + v_s t)}$$

It is then readily apparent that $H_1^{(1)}$ corresponds to waves converging towards the axis r=o while $H_1^{(2)}$ represents waves diverging from the axis. It can further be noticed that real wave numbers correspond to travelling waves while imaginary wave numbers represent standing waves. In this situation, for displacement controlled boundary conditions, the general solution for the displacement becomes:

$$u = r_o\theta_o \frac{H_1^{(2)}\left(\frac{\omega r}{v_s}\right)}{H_1^{(2)}\left(\frac{\omega r_o}{v_s}\right)} e^{i\omega t} \tag{24}$$

where ω is the input frequency.

Simple differentiation of equation (24) provides the strain field:

$$\varepsilon = \frac{\omega r_o \theta_o}{v_s} \frac{H_2^{(2)}\left(\frac{\omega r}{v_s}\right)}{H_1^{(2)}\left(\frac{\omega r_o}{v_s}\right)} e^{i\omega t} \tag{25}$$

and similarly:

$$\tau = \frac{\omega r_o \theta_o \mu}{v_s} \frac{H_2^{(2)}\left(\frac{\omega r}{v_s}\right)}{H_1^{(2)}\left(\frac{\omega r_o}{v_s}\right)} e^{i\omega t} \tag{26}$$

$$T_\ell = \frac{2\pi r_o^3 \omega\theta_o \mu}{v_s} \frac{H_2^{(2)}\left(\frac{\omega r}{v_s}\right)}{H_1^{(2)}\left(\frac{\omega r_o}{v_s}\right)} e^{i\omega t} \tag{27}$$

Although it is not shown here, it is immediate to notice that the static solutions are easily recovered from the above formulae by taking limits when $r_o \to \infty$ (substitute the Bessel functions by their assymptotic approximations).

Since the material is linear, the above equations (24) and (27) can be used to obtain the results for the stress controlled boundary. For $r = r_o$, equation (22) becomes:

$$\tau_o = \frac{\omega r_o \theta_o \mu}{v_s} \frac{H_2^{(2)}\left(\frac{\omega r_o}{v_s}\right)}{H_1^{(2)}\left(\frac{\omega r_o}{v_s}\right)} e^{i\omega t} \tag{28}$$

which substituted into equations (24) to (27) yields:

$$u = \frac{\tau_o v_s}{\mu\omega} \frac{H_1^{(2)}\left(\frac{\omega r}{v_s}\right)}{H_2^{(2)}\left(\frac{\omega r_o}{v_s}\right)} e^{i\omega t} \tag{29}$$

$$\varepsilon = \frac{\tau_o}{\mu} \frac{H_2^{(2)}\left(\frac{\omega r}{v_s}\right)}{H_2^{(2)}\left(\frac{\omega r_o}{v_s}\right)} e^{i\omega t} \tag{30}$$

$$\tau = \tau_o \frac{H_2^{(2)}\left(\frac{\omega r}{v_s}\right)}{H_2^{(2)}\left(\frac{\omega r_o}{v_s}\right)} e^{i\omega t} \tag{31}$$

$$T_\ell = 2\pi r_o^2 \tau_o e^{i\omega t} \tag{32}$$

3.3 FINITE CYLINDER - STATIC AND DYNAMIC

For an elastic half-space bounded by a free or fixed surface, the problem of a finite cylinder rotating in a borehole normal to the surface has been partially solved by Boyer and Oien (1972)[27]. The full fields of each variable were not derived but torque-angle ratios were provided as a function of the parameters of interest. The problem will be presented here following the reference mentioned. The approach used there is somewhat similar to that used in the previous section, but the mathematical treatment becomes rather involved and the reader is referred to the original paper for more specific details.

The equation to be solved is:

$$\frac{1}{r}\frac{\partial}{\partial r}\left(r\frac{\partial u}{\partial r}\right) - \frac{u}{r^2} + \frac{\partial^2 u}{\partial z^2} + \Omega^2 u = 0 \qquad (33)$$

where $\Omega = \frac{\omega h}{2v_s}$, ω being the input frequency, h the height of the cylinder

v_s the shear wave velocity.

u is the θ component of the displacement

r, θ, z are the cylindrical coordinates and all distances are scaled by division by h/2.

The boundary conditions, placing the origin of coordinates at the center of gravity of the cylinder, take the form:

$u = R\theta$ at $r = R$ $|z| < \frac{1}{2}$

$\tau_{r\theta} = 0$ at $r = R$ $|z| > \frac{1}{2}$

$u = 0$ at $r \to \infty$

$$\tau_{z\theta} = 0 \qquad \text{at } r > R \quad z = D \quad \text{(if free surface)}$$

$$u = 0 \qquad \text{at } r > R \quad z = D \quad \text{(if fixed surface)}$$

where R and D are the dimensionless radius of the borehole and height to the surface, respectively, and $\theta = \theta_0 e^{i\omega t}$. Figure 4 illustrates the meaning of the variables:

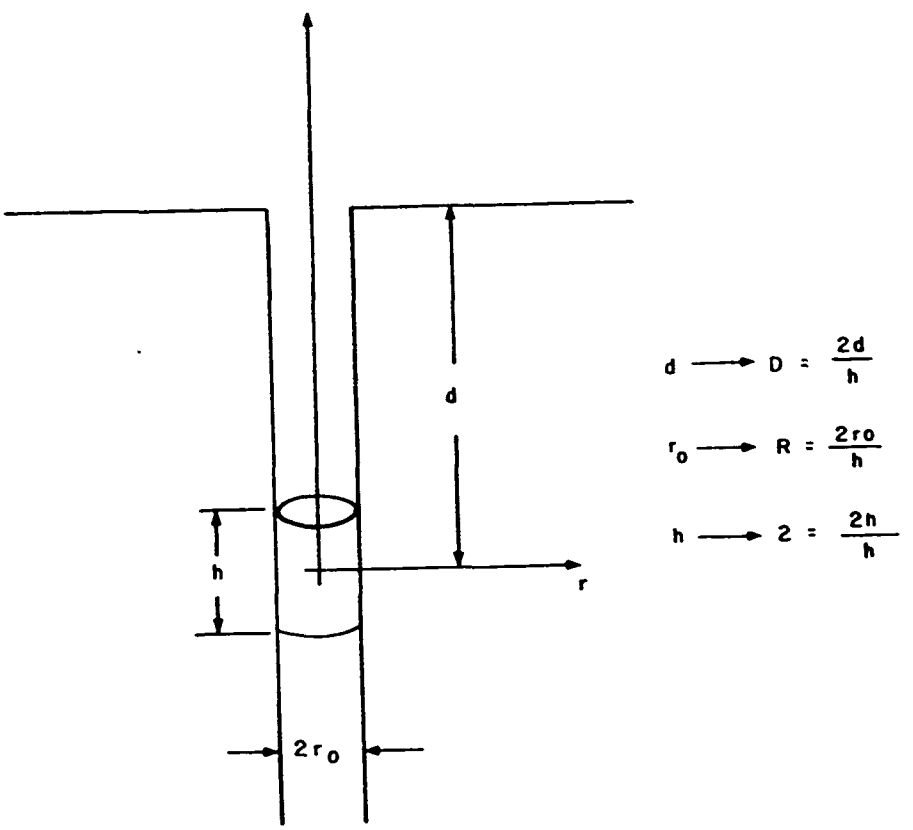

Figure 4. Geometric variables and their corresponding dimensionless values

Under the circumstances described, the torque can be expressed as:

$$T = 2\pi r_o^2 n v_c F \tag{34}$$

where F can be thought of as a complex influence function of the form:

$$F = f_R - i \frac{\omega r_o}{v_s} f_I \tag{35}$$

The values of f_R and f_I are presented in Figures 5 to 8 for several depths and geometries of the cylinder.

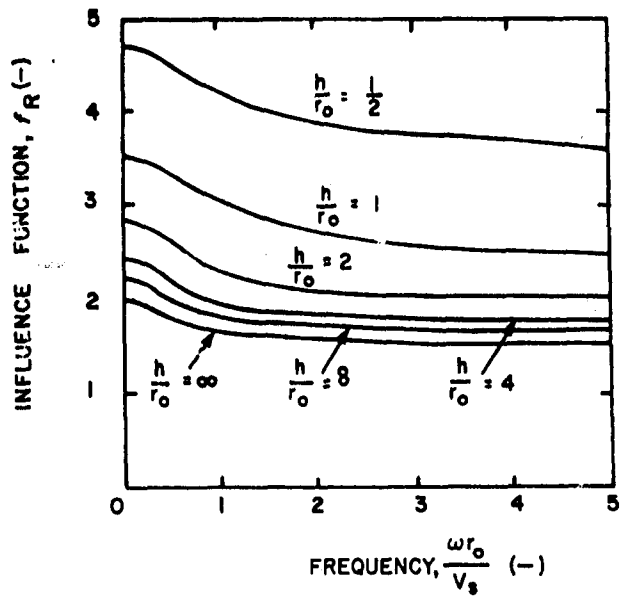

Figure 5. Real part of the influence function vs. frequency for several cylinder geometries in an unbounded medium. (After Boyer and Oien, 1972)

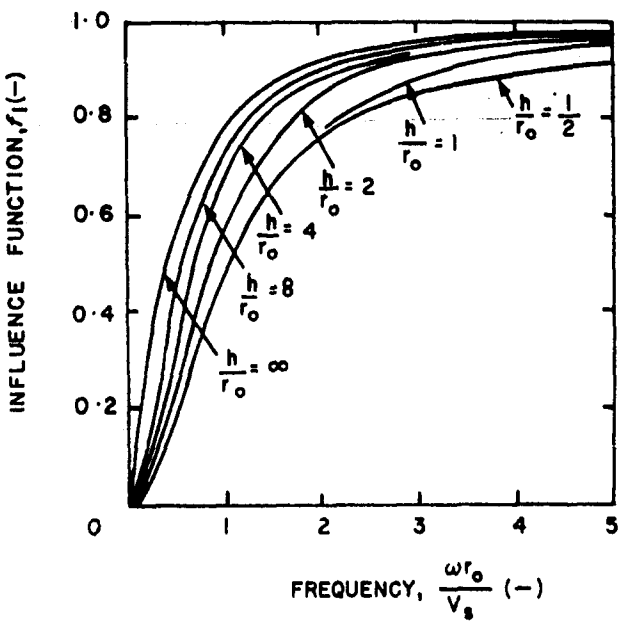

Figure 6. Normalised imaginary part of the influence function vs. frequency for several cylinder geometries in an unbounded medium. (After Boyer and Oien, 1972)

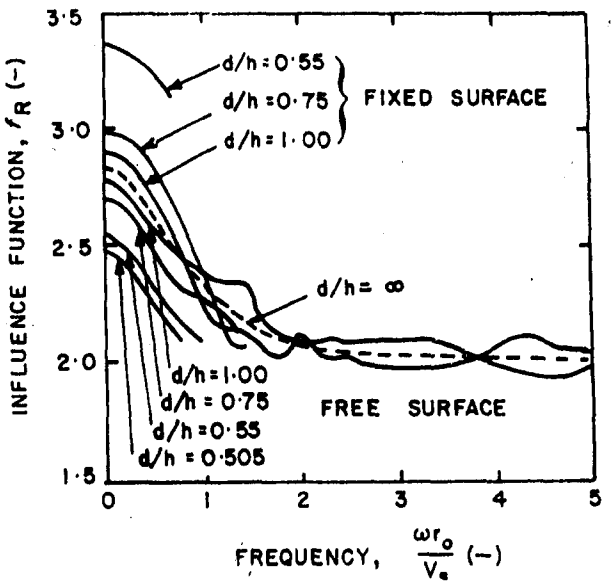

Figure 7. Real part of the influence function vs. frequency for a cylinder with geometry $h/r_o = 2.0$ at various distances from either a free or fixed surface. (After Boyer and Olen, 1972)

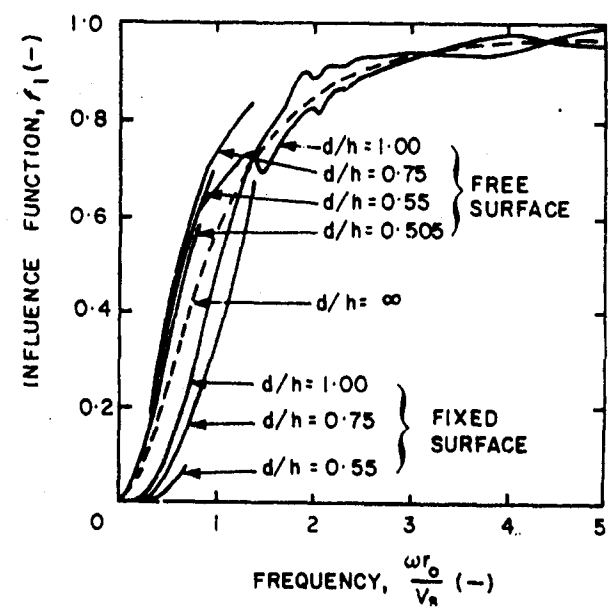

Figure 8. Normalised imaginery part of the influence function vs. frequency for a cylinder with geometry $h/r_o = 2.0$ at various distances from either a free or fixed surface. (After Boyer and Olen, 1972)

4. NUMERICAL ANALYSIS

It was pointed out at the onset of Chapter 3 that close-form solutions, in spite of their usefulness, required for their derivation the incorporation of a number of assumptions. Numerical analysis has the disadvantage of providing answers only at discrete points of the space of input parameters; however, it allows solving the problem without unnecessary assumptions for each specific set of input data.

The purpose of the numerical analysis reported in the present chapter is to assess the magnitude of the errors introduced in the analytical treatment and to correct them when deemed necessary. Those activities are orientated towards the final goal of providing a realistic method of obtaining the value of the secant shear modulus of the soil as a function of strain level, based on field measurements of torque and rotation during the operation of the BSD.

4.1 METHODOLOGY

The field operation of the BSD has two characteristics which are of decisive importance in the selection of the numerical approach: those are the facts that the actuator is cycled at a single frequency and under steady-state conditions. In those circumstances, a finite element analysis working in the frequency domain shows its best advantages. Non-linearities can then be handled via an equivalent-linear method, where the solution procedure is iterated until the deformation levels achieved are consistent with the values of the modulus used.

Based on the above considerations, the program FINEL, developed by Mr. D. Hitchings at Imperial College, London, was selected for carrying out the computations. General information on FINEL, including its methodology and capabilities, can be found in Appendix D.

The version of FINEL used in the present project assumes axial symmetry of geometry and input conditions. In order to adapt it best to the particular configuration of the problem under consideration, several modifications were introduced in the computer program:

- The equivalent-linear procedure was implemented. As mentioned, this allows the use of a shear modulus "consistent" with the strain level produced at each point. This consistency will be discussed in further sections.

- Special non-reflecting boundaries were introduced to allow the use of a small finite-element mesh while appropriately modelling the radiation of energy out of the finite-element region. The cylindrical surface of the region was provided with a boundary similar to that proposed by Lysmer and Waas (1972)[28] but modified for axisymmetric as opposed to plane-strain conditions; such boundary is theoretically perfect as long as the soil outside the boundary behaves linearly and is horizontally layered. The top boundary was equipped with an optional non-reflecting boundary of the type described by Lysmer and Kuhlemeyer (1969)[29]; energy is absorbed at the boundary by means of suitably selected viscous dashpots.

Figure 9 shows the numerical idealisation of the test used in the analysis. As it was mentioned before, the only requirement for adequate performance of the cylindrical boundary is that all non-linearities take place inside the modelled domain. This condition applies particularly to the constitutive non-linearities associated with the high strain levels. The plane boundary is not theoretically "perfect", in the sense that its efficiency depends on the angle of incidence of the incoming waves. However, since the difficulties arise only for small angles of incidence, the geometry of the problem guarantees the adequacy of such boundary. Further, even if any energy from the BSD were to reflect at the upper boundary, it would be absorbed at the cylindrical one rather than be reflected towards the BSD region. The theory supporting each of the two boundaries is given in Appendix B.

As for the lower boundary of the domain, the plannar symmetry condition makes it a free boundary. Such symmetry is broken at very shallow depths. However, as can be seen from Chapter 3 (Fig. 7 and 8) the symmetry condition is established for all pratical purposes as soon as the depth of the centre of the BSD exceeds its height, which occurs in all practical cases. The reason for this fact is that below such depth and at the low frequencies of interest, the presence of the free surface does not significantly alter the torque-angle relationship. An exception to that symmetry occurs in the case of layering intersecting the domain of investigation; however, for the case of properties varying uniformly with depth, the dimensions of the domain are sufficiently small to make such variation unimportant.

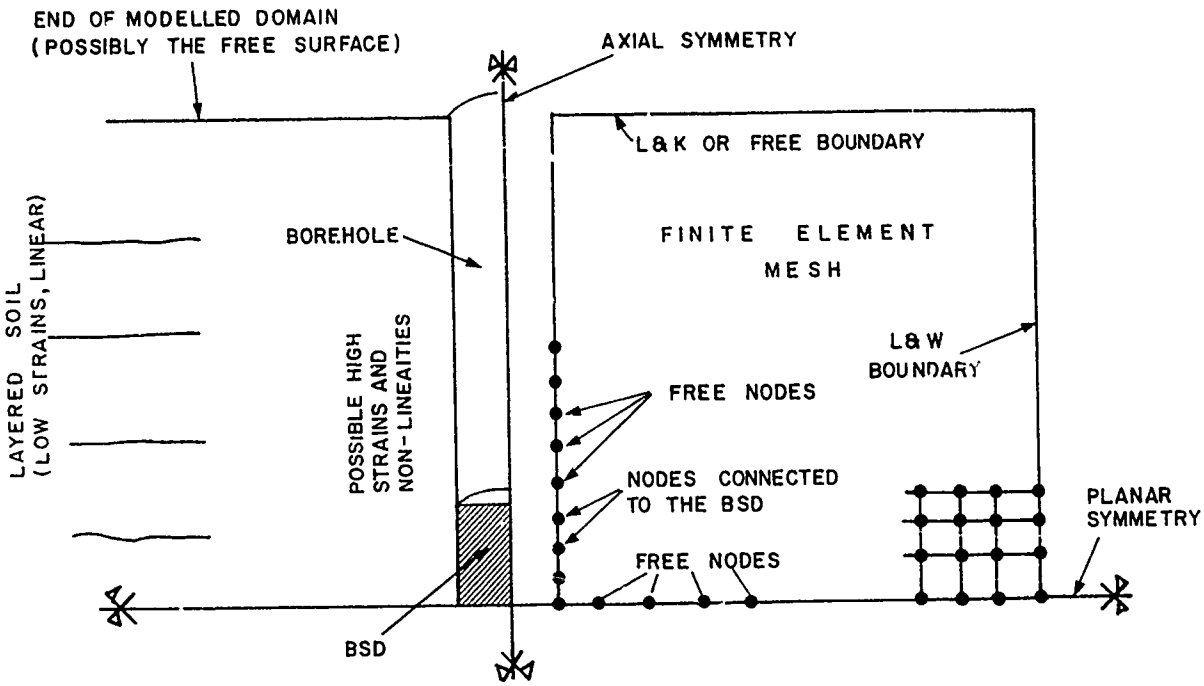

Figure 9. Characteristics of the physical situation being modelled (left) and the corresponding numerical idealisation (right)

Finally, the nodes at the borehole wall in contact with the BSD are subjected to the boundary condition:

$$u = u_o e^{i\omega t}$$

while all other nodes in the borehole walls are considered free to move.

It is interesting to note here that, although the strains considered are large enough to introduce constitutive non-linearities, geometrical non-linearities are not taken into account in the analysis due to the relatively small rotations involved. Consequently, the only non-vanishing displacement is u_θ and the only non-zero strains are $\varepsilon_{r\theta}$ and $\varepsilon_{z\theta}$; these strains are related to the displacement field by the small displacement formulation.

Finally, because of the small size of the domain investigated in comparison with the wave lengths induced (small dimensionless input frequency), the effect of material damping becomes negligible with respect to that of radiation damping. It has therefore been neglected in the numerical calculations.

4.2 DUPLICATION OF ELASTIC RESULTS

The purpose of duplicating e results already known from close-form solutions is essentially that of verifying the adequacy of the methodology selected for the numerical analysis. Of particular interest in this respect is the validation of the non-reflecting boundaries which were added to FINEL

for the present study. Apart from routine checks of little interest here, two basic tests will be included in the present section because of the insight that they provide into the general treatment of the problem and because they can be used as proof of the validity of the answers generated by the computer program.

The two basic tests mentioned are described in detail in the next subsections. They include:

a) Infinitely long cylinder rotating harmonically in an elastic medium. All variables are known from analytical solutions. This test is designed for general verification of the computer program and, in particular, of the axisymmetric non-reflecting boundary. Although the modelling is two-dimensional, the problem is only one-dimensional.

b) Finite cylinder rotating harmonically in an elastic medium. The torque-angle relationships are known from analytical solutions. This test is designed for validation of the program under a truly two-dimensional situation and, in particular, for verification of the plane non-reflecting boundary. It will be seen later that, based on this example, upper bounds can be found to the effects of layering in distorting the field measurements.

4.2.1 Infinitely Long Cylinder

The following input parameters were used for the case of an infinitely long cylinder rotating harmonically in an elastic medium:

Soil density	ρ	= 2000 Kg/m^3
Shear modulus	μ	= 1.8×10^8 N/m^2
Borehole radius	r_o	= 0.1 m
Input frequency	ω	= 100 rad/sec
Angular displacement	u_o	= 10^{-4} m (half-amplitude)

The above conditions are representative of a typical field situation, assuming that the soil behaves elastically. Shear-wave propagation velocity is 300 m/sec, based on the values of μ and ρ selected.

Analytical solutions were provided for those conditions in Chapter 3. Figures 10 and 11 present the comparison of analytical and numerical solutions for the real and imaginary parts of the displacement field, respectively. Figures 12 and 13 depict similar results for the strain field. Note that, under the conditions examined, the imaginary part of the response is very small while the real part is practically equal to the static solution; this is true for both displacements and strain fields.

As can be seen in the referenced figures, the agreement of the finite-element calculations and the close-form solutions is extremely good. In order to give an idea of the importance of the cylindrical non-reflecting boundary, it should be mentioned here that errors in excess of 100% were not uncommon in the neighborhood of the boundary, when fixed or free conditions were used. A notable improvement over free of fixed boundary conditions could be obtained by using the

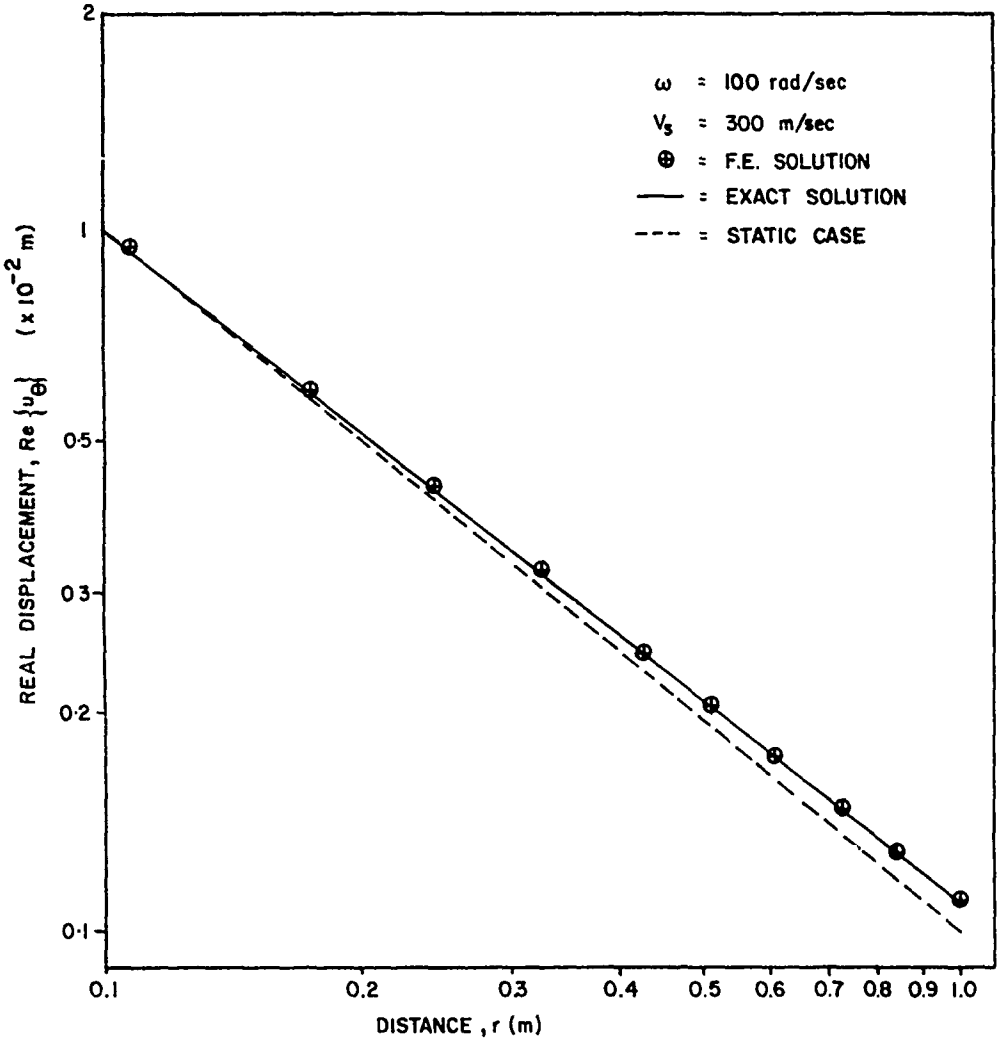

Figure 10. Comparison of analytical and numerical solutions - real part of the displacement

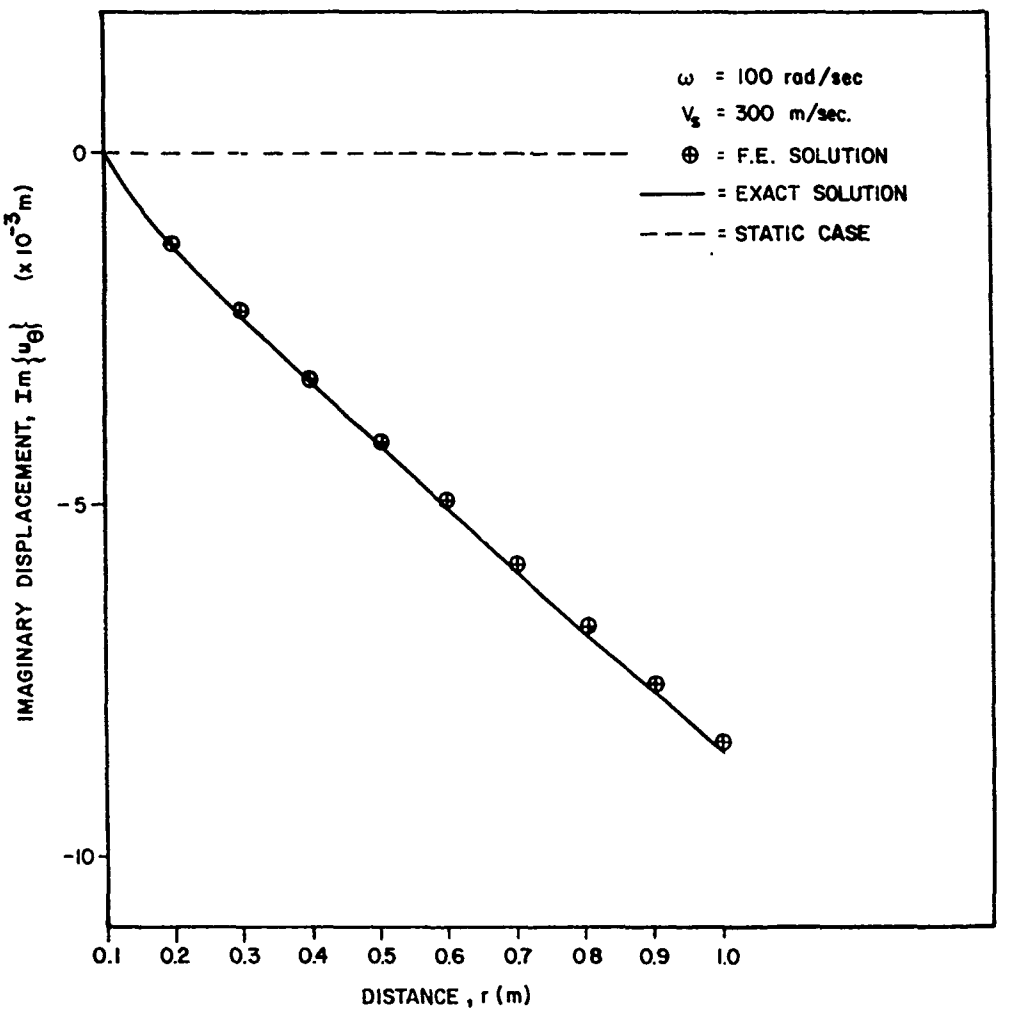

Figure 11. Comparison of analytical and numerical solutions - imaginary part of the displacement

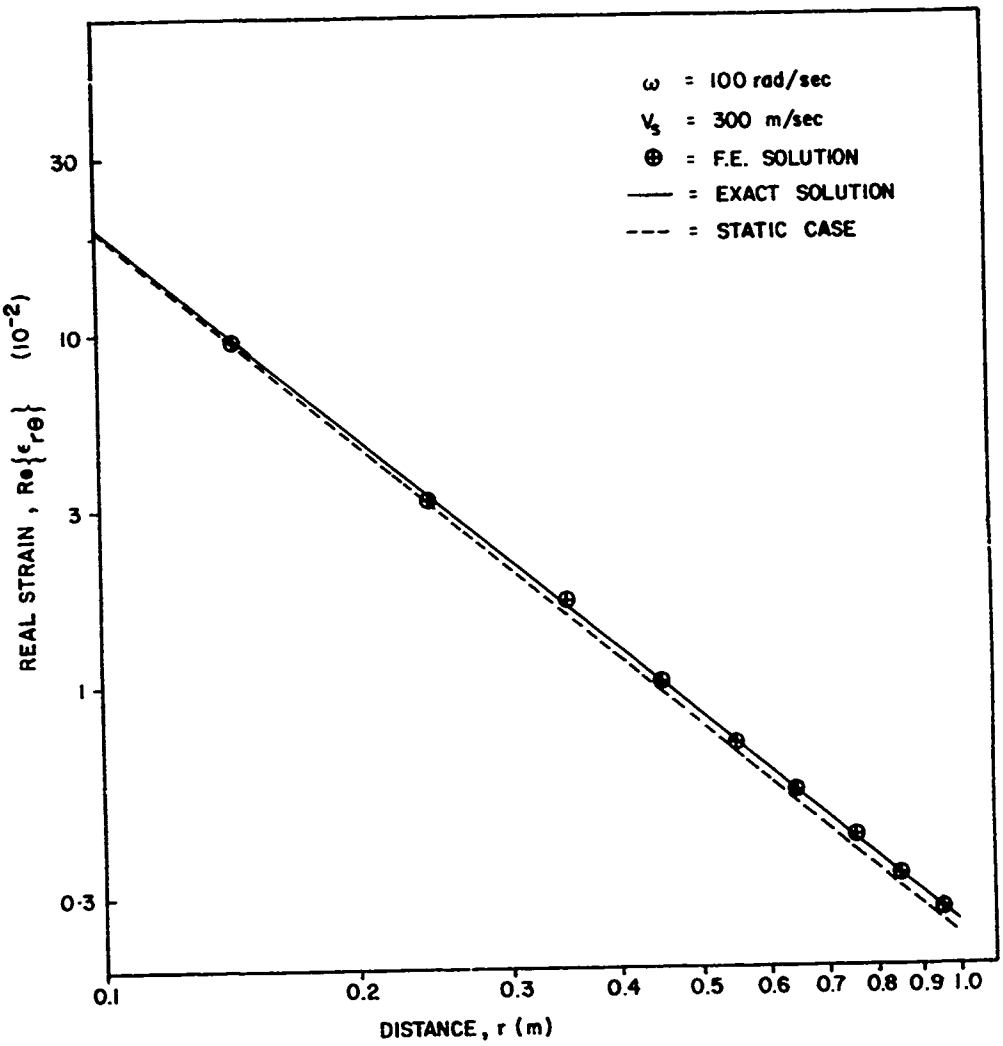

Figure 12. Comparison of analytical and numerical solutions - real part of the strain

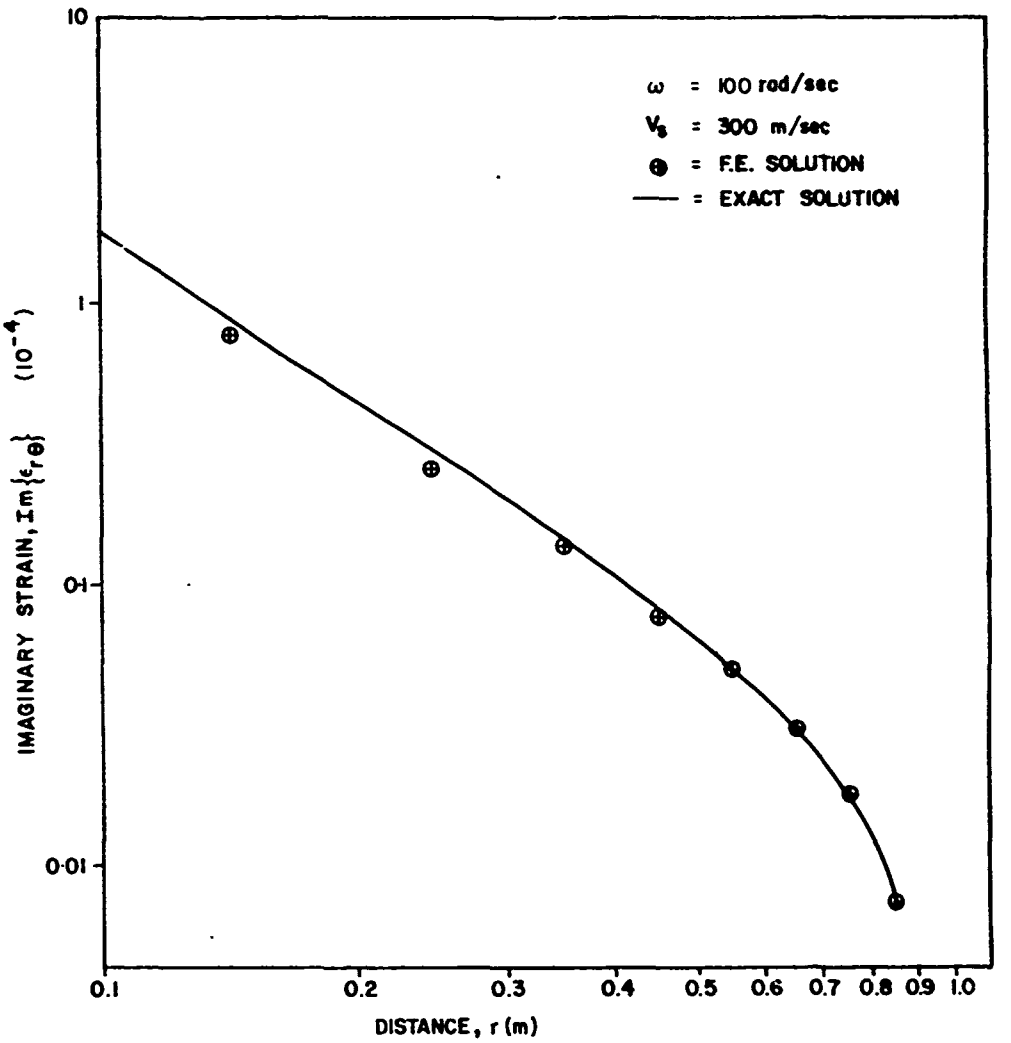

Figure 13 Comparison of analytical and numerical solutions - imaginary part of the strain

plane-strain Lysmer - Waas boundary; this condition is perfect as the radius grows to infinity but still generates substantial errors at the relatively small radii of the geometries of interest. It is due to those circumstances that a decision was made to develop and implement the axisymmetric boundary.

4.2.2 Finite Cylinder

The case of a harmonically rotating cylinder of finite length was studied under the same conditions and parameters used in the analysis of the infinite cylinder. A number of tests were carried out in order to ascertain the validity of the results of the program and the adequacy of the plane non-reflecting boundary; this was done by comparison with the close form solutions obtained in the previous chapter.

Of special interest here is a series of tests performed on the mesh shown in Figure 14 . The cylinder is 0.5 m long and the distance from its centre to the top boundary is again 0.5 m. Three alternative conditions were used at the top boundary: free, simulating the free surface; fixed, modelling an infinitely rigid layer and non-reflecting, to represent infinite embedment. Table 3 presents the comparison of the torque - rotation ratios obtained by the program and from the close-form solutions. Values of the influence function F defined in Figure 5 are used for this comparison.

Table 3 Comparison of the real part of the influence function F for d/h = 1

	F.E. SOLUTION	ANALYTICAL SOLUTION (after Boyer & Oien, 1972)	
	$\frac{h}{r_o} = 5$	$\frac{h}{r_o} = 5$	$\frac{h}{r_o} = 2$
FIXED SURFACE	2.35	-	2.90±0.05
FREE SURFACE	2.31	-	2.78±0.05
INFINITE EMBEDMENT	2.32	2.36±0.05	2.85±0.05

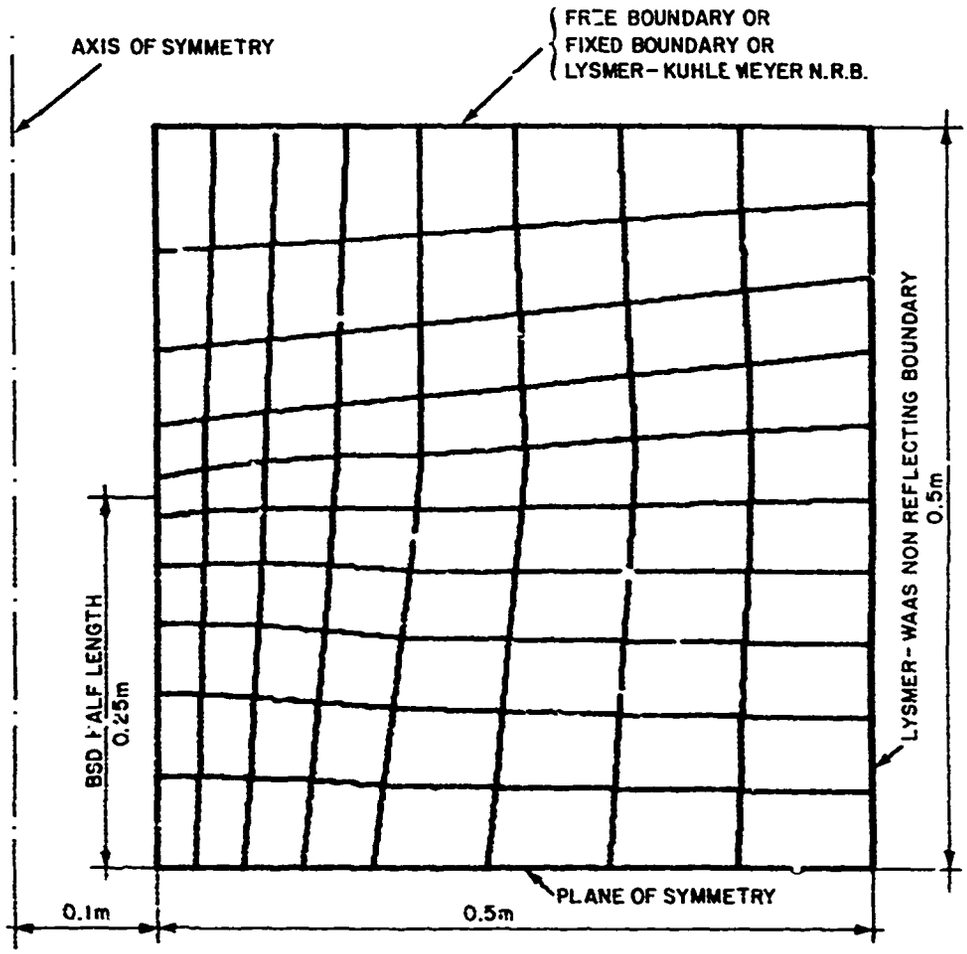

Figure 14. Finite-element grid used for evaluation of boundary effects.

Notice that the analytical solution for fixed and free boundaries cannot be expected to coincide with the numerical results since both correspond to different cylinder geometries; besides, the numerical results include two rather than one fixed or free planes due to the symmetry conditions imposed (unlike the analytical values). The results in the third column correspond to the geometry which is closest to the present BSD design within the set of analytical results available. The tolerances shown in the analytical values represent the possible errors in reading from the figures of Boyer and Oien (1972)[27].

The strain fields developed in the above cases are shown in Figures 15 to 20. It can be noticed that the higher strains are barely affected by the presence of a fixed or free boundary located half a cylinder length away from the end of the cylinder. This conclusion can also be drawn from the torque-rotation ratios. As expected, the results for infinite embedment lie in between the cases of fixed and free boundary conditions on the top plane. It can therefore be stated that although the plane non-reflecting boundary is working adequately, the importance of its implementation on a satisfactory modelling of this problem is considerably less than in the case of the cylindrical boundary.

One more point worth noticing is that $\varepsilon_{\theta z}$ becomes infinity at the extreme of the cylinder. However, for the geometries of interest, its contribution to the required torque is small. Its importance would increase as the cylinder becomes very short compared to its diameter.

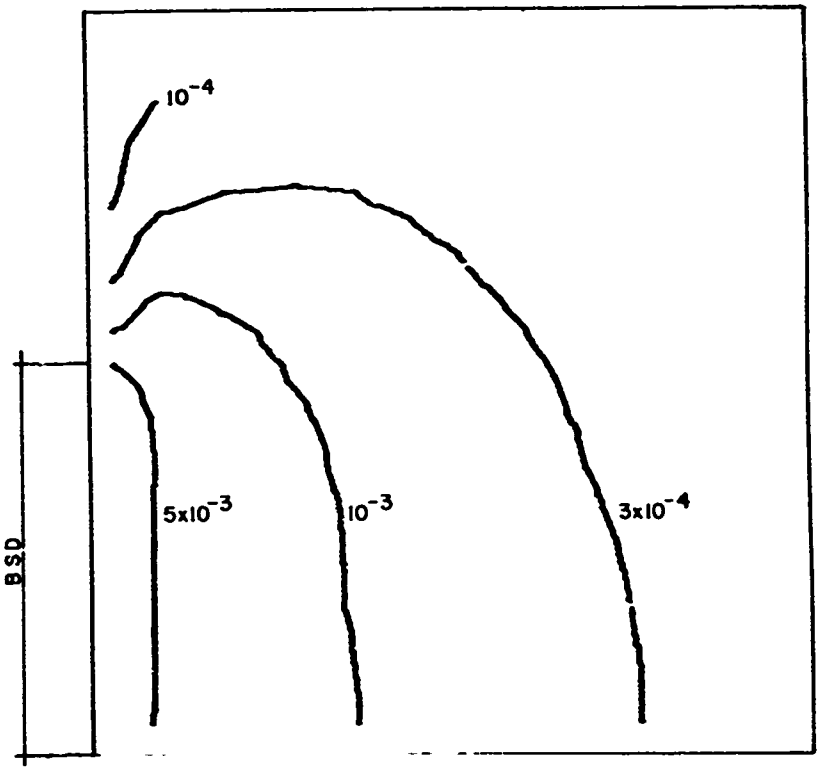

Figure 15. $\epsilon_{r\theta}$ strain distribution
top surface free

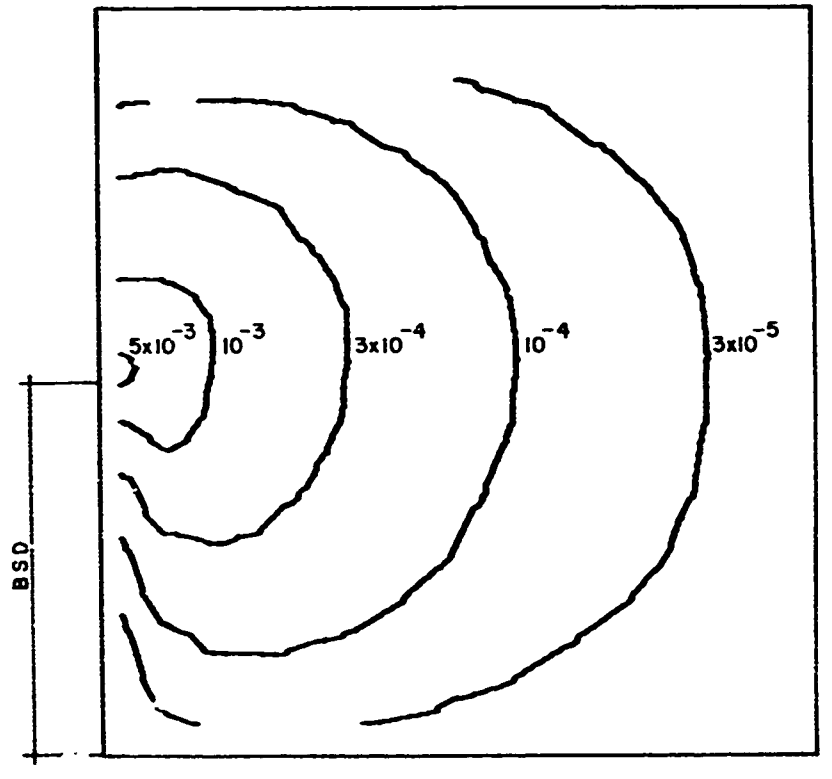

Figure 16. $\epsilon_{\theta z}$ strain distribution
top surface free

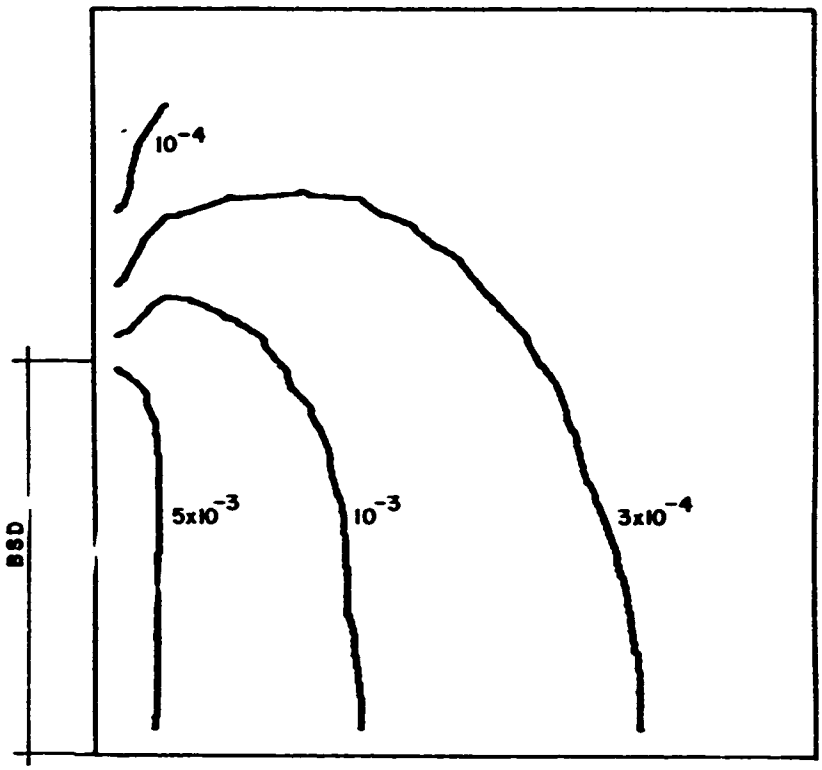

Figure 17. ε_{re} strain distribution
top surface non-reflecting

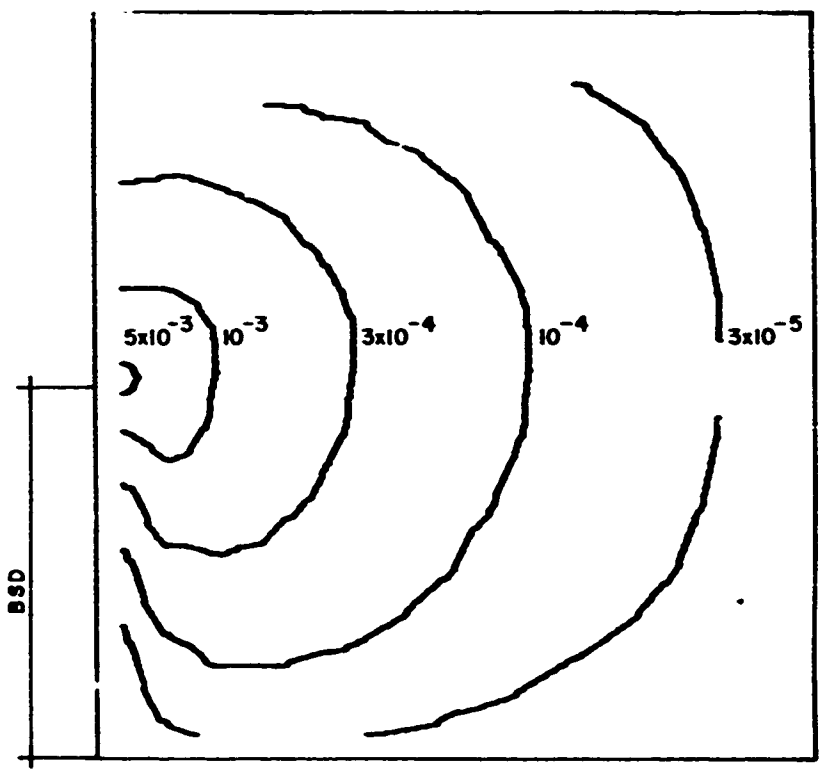

Figure 18. ε_{ez} strain distribution
top surface non-reflecting

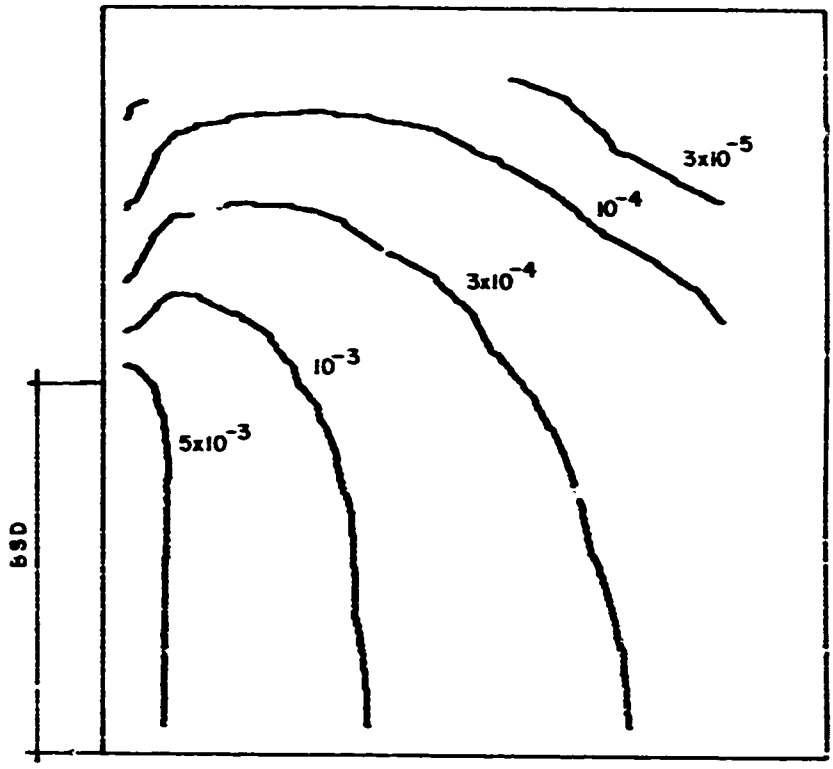

Figure 19. ε_{re} strain distribution
top surface fixed

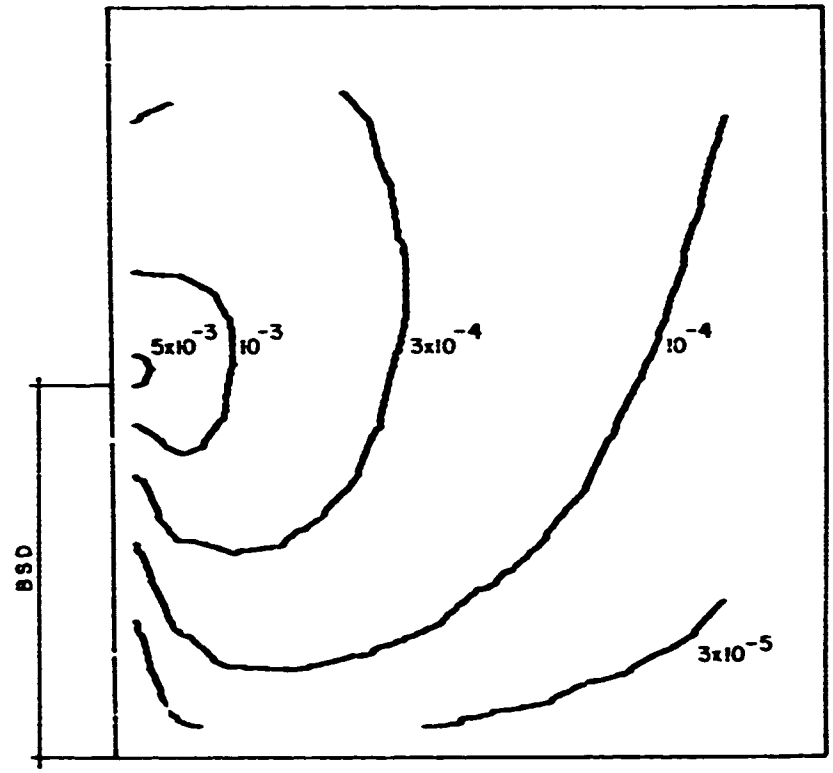

Figure 20. ε_{ez} strain distribution
top surface fixed

4.3 NON-LINEAR ANALYSIS

The tests reported under the present section are orientated to two purposes:

- To verfiy the implementation of the "equivalent-linear" method and its ability to represent the constitutive non-linearities of the problem.
- To study the influence of the non-linearity of the problem on the ratio of torques required in the cases of infinite and finite cylinder.

The object of the two goals mentioned, particularly the second one, will become more clear in Chapter 6. There, a procedure will be proposed to construct an arbitrary μ-ε (shear modulus - strain level) curve for the soil, based on the T-θ (torque - rotation) measurements obtained in the field. The present section is, in a way, the justification of the assumptions embodied in that procedure.

Two points must, however, be made here concerning the "equivalent linear" method. The first one is that the method originates from a one-dimensional philosophy and its generalization to two dimensions is by no means unique. The modulus for each shear strain may be related to the corresponding strain, to a specific one of the two strains, to the modulus of both or to any other shear strain measure. Each hypothesis has advantages and disadvantages but the present state of the art in dynamic soil modelling does not provide a definite argument in favour of any of them. Under these conditions, and given the fact that $\varepsilon_{r\theta}$ is larger than $\varepsilon_{\theta z}$ almost everywhere

and the most important one to reproduce correctly, we have made the somewhat arbitrary decision of assuming that, at each point within the soil and each moment in time, there is a single value of the secant modulus relating shear strains and the corresponding shear stresses, furthermore, the deterioration of such modulus is totally controlled by $\varepsilon_{r\theta}$ alone.

The second point is that the "equivalent linear" procedure was developed and has been primarily applied in the field of earthquake engineering; there, the dynamic and inertial aspects of true wave propagation prevail over the static or quasi-static distributions of stress which are only controlled through stiffness characteristics. Furthermore, the behavior of the soil consists mainly of transient responses to trains of irregular cycles. As a consequence, in earthquake engineering, the "consistency" of the strain level and the secant modulus is customarily satisfied by taking for the latter the modulus corresponding to 65% (approximately) of the maximum strain developed at each point of the soil. The above conditions do not apply exactly to the problem being examined here. Hence, some research was done in optimizing the strain level at which the secant modulus is taken as "consistent". It is clear that, under static conditions, 100% of the strain would be the optimum value. The conclusions of our investigation were that, although convergence was somewhat hindered, values close to 100% of the strain provided the best answers. As a consequence, a value of 100% was used in all the runs, including those in the present section.

One more aspect should be mentioned before going into the tests. Since a certain constitutive law has to be assumed in order to be able to obtain some quantitative results, a hyperbolic stress-strain law has been

postulated on the soil for the purpose of the numerical tests included under the present section. It is reasonable to assume that the verifications performed for a hyperbolic law would in fact hold if other non-linear stress-strain laws had been used. Although, strictly speaking, since no single law is universally applicable, one would need to repeat the process with all other possible laws, this is not actually required since the final recommended procedure is based on the hyperbolic law. However, it is important to stress that, in spite of the fact that the procedure will be based on the hyperbolic law, it will not be assumed that the soil behaves according to such law; rather, as will be seen in Chapter 6, the constitutive law will be reproduced by a series of hyperbolic approximations.

4.3.1 Infinitely Long Cylinder

The primary purpose of these tests is to check the "equivalent-linear" procedure. We have neither been able to locate nor deemed sensible to try and produce any non-linear close-form solutions for the present boundary value problem under general dynamic conditions. However, in view of the fact that, at the range of frequencies of interest, the static solution closely approximates the real part of the dynamic solution, comparisons have been established between analytical solutions of the former and the finite-element predictions of the latter.

In the next two tests, the soil constitutive law is hence hyperbolic and can be described by means of the μ-ε curve shown in Figure 21 . The input parameters common to both tests are:

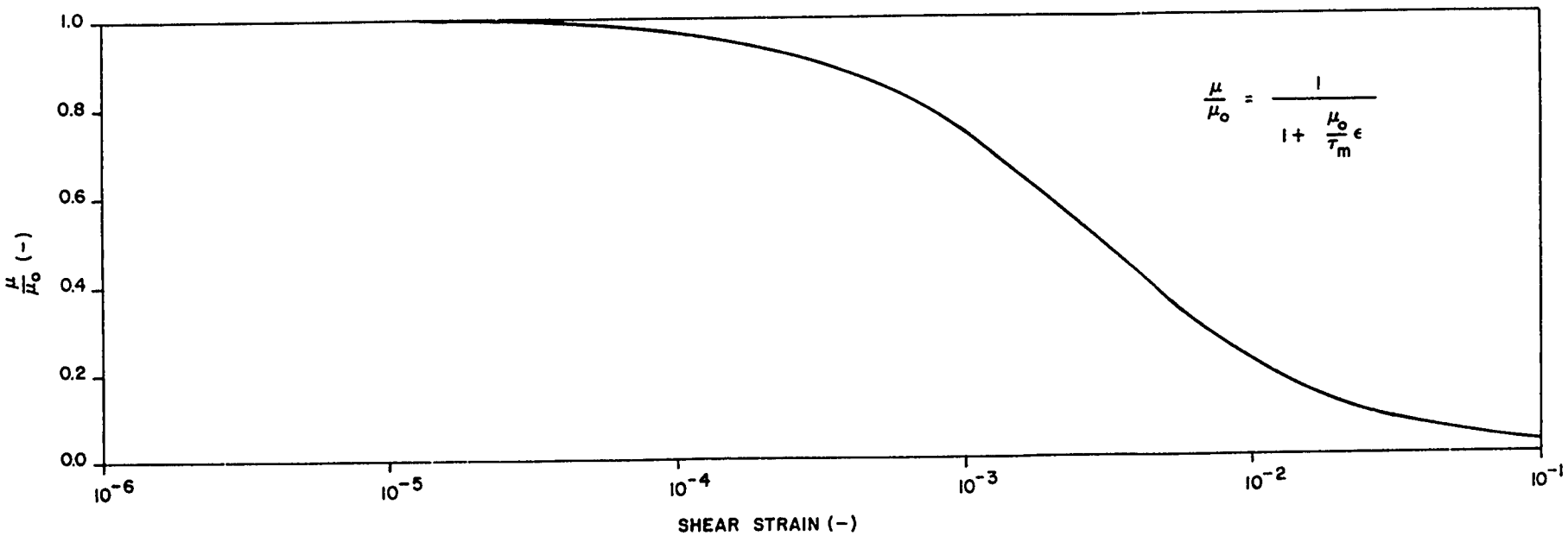

Figure 21. Secant modulus vs. strain curve used in the non-linear hyperbolic calculations $\mu_o = 1.8 \times 10^8 N/m^2$; $\tau_m = 5 \times 10^5 N/m^2$

Soil density	ρ	$= 2 \times 10^3$ Kg/m^3
Initial shear modulus	μ_o	$= 1.8 \times 10^8$ N/m^2
Limiting shear strength	τ_m	$= 5 \times 10^5$ N/m^2
Borehole radius	r_o	$= 0.1$ m

Two different angular displacements were given at the borehole wall: in the first case, $u_o = 10^{-4}$ m and in the second, $u_o = 3.5 \times 10^{-4}$ m. Two different input frequencies were also used: ω = 10 rad/s and ω = 100 rad/s The comparisons between the analytical static solution and the real part of the dynamic numerical solution are presented for strains (Figure 22 and 23) and displacements (Figure 24 and 25). The required torques are shown in Table 4.

Table 4. Comparison of torques in hyperbolic soil

INPUT ANGULAR DISPLACEMENT, u_o (m)	REQUIRED TORQUE, T(Nm/m)		
	CLOSE-FORM STATIC	F.E. REAL PART OF DYNAMIC	
		ω=10rad/s	ω=100rad/s
1.0×10^{-4}	1.61×10^4	1.64×10^4	1.64×10^4
3.5×10^{-4}	2.89×10^4	3.15×10^4	3.15×10^4

4.3.2 Finite Cylinder

The above tests were repeated under identical conditions with a cylinder of finite length (0.5 m) located at large depth in a borehole. The finite-element mesh used in the calculations is shown in Figure 26. Again,

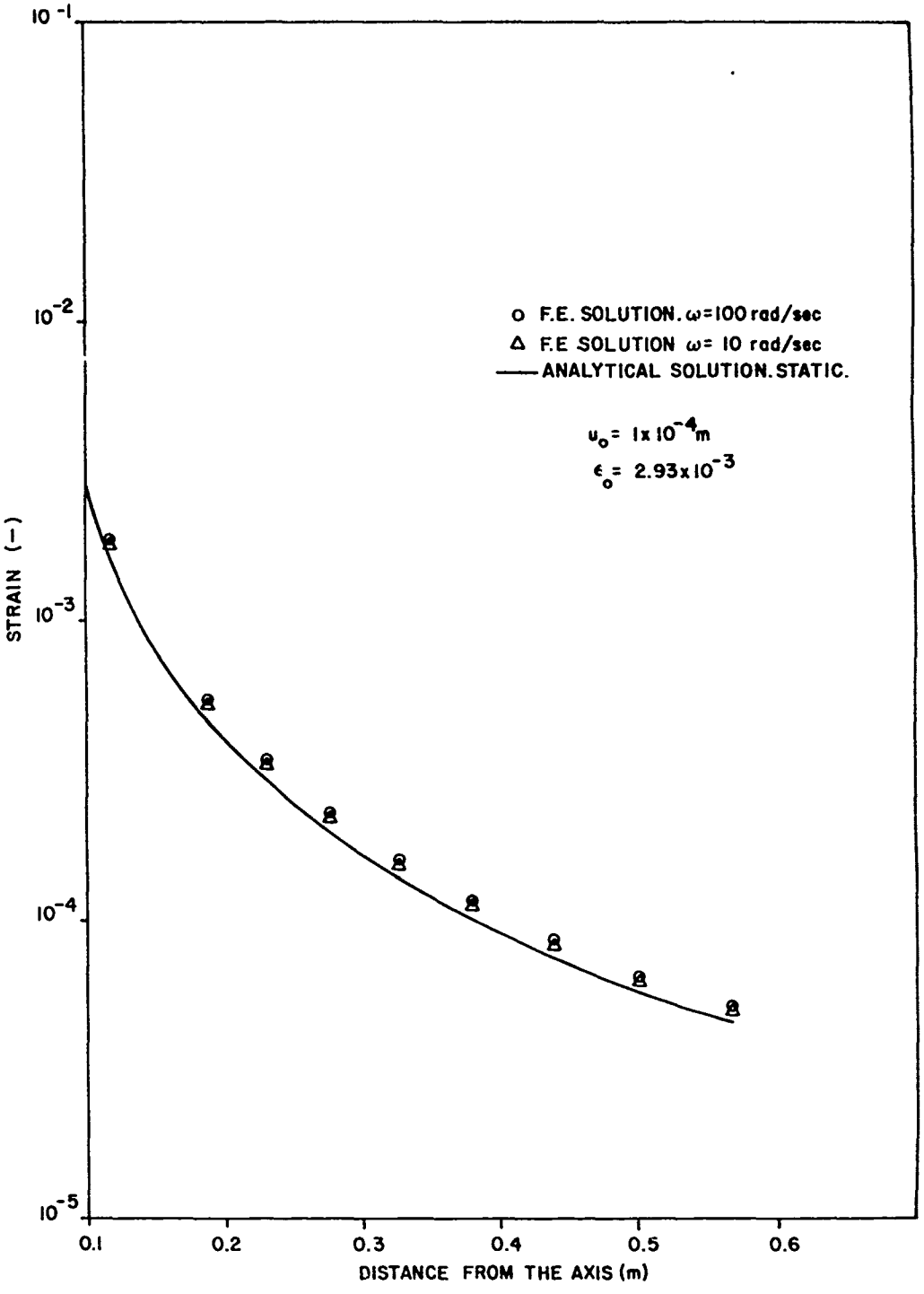

Figure 22. Comparison between analytical and numerical strain values

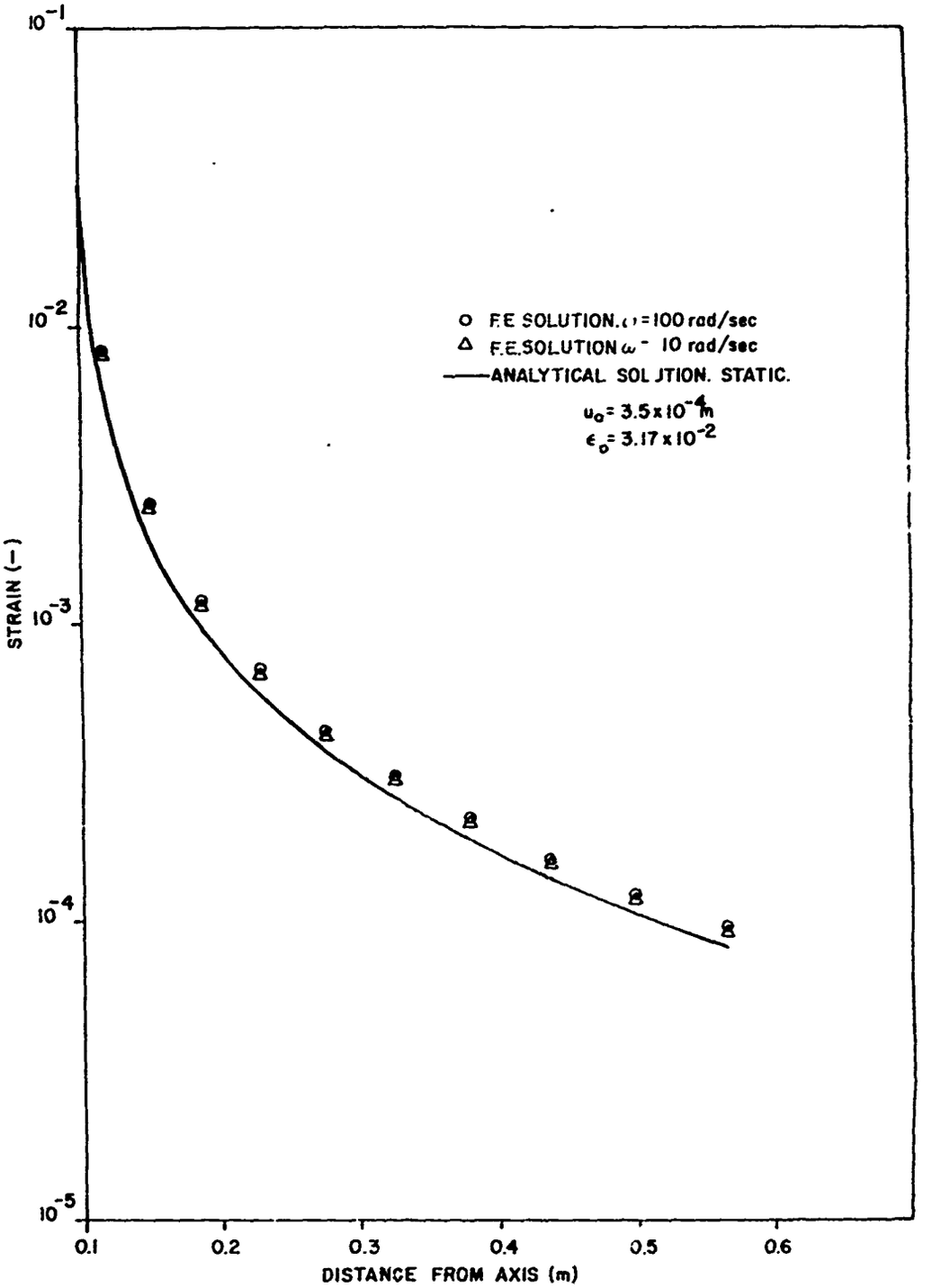

Figure 23. Comparison between analytical and numerical strain values

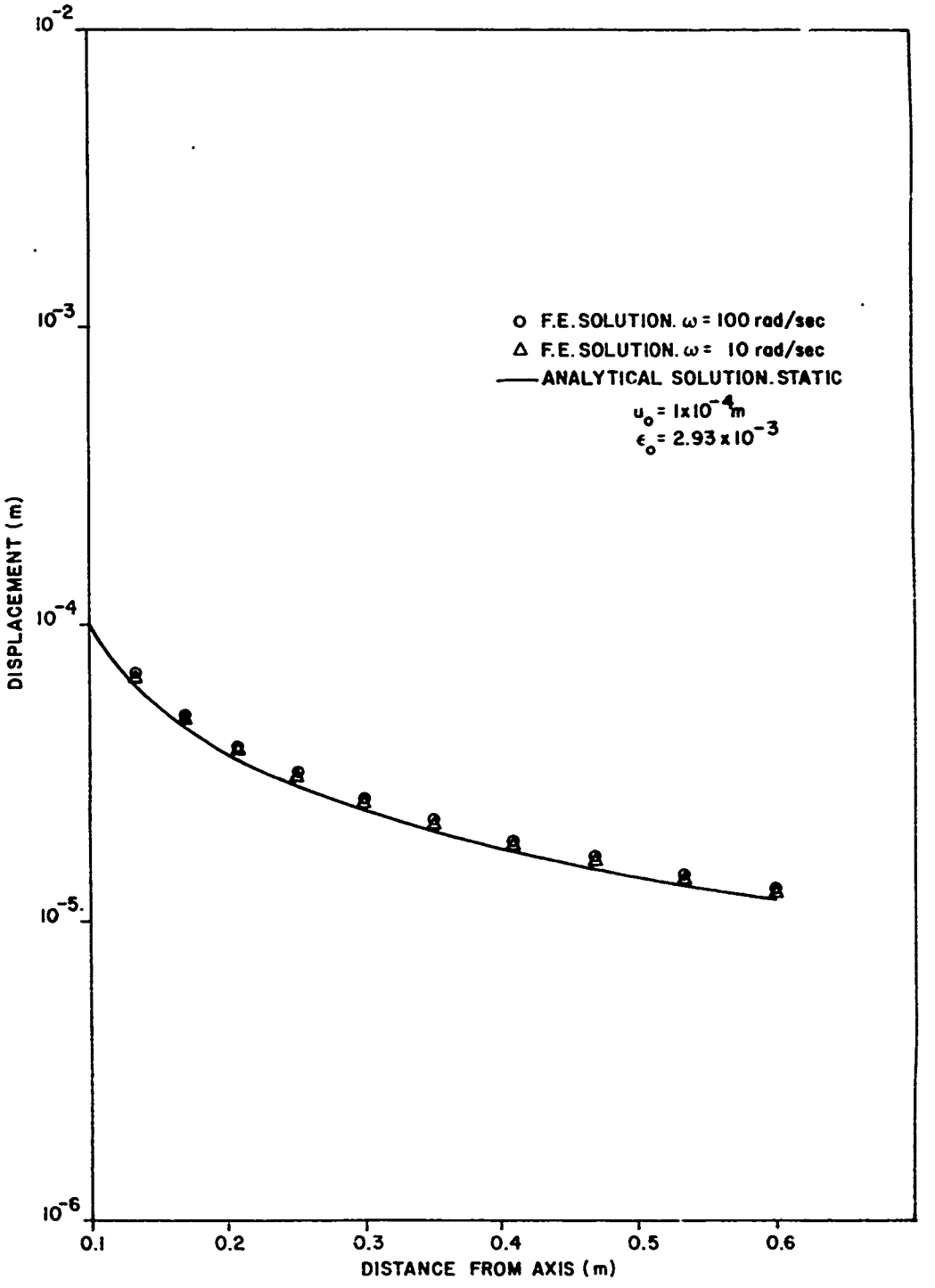

Figure 24. Comparison between analytical and numerical displacement values

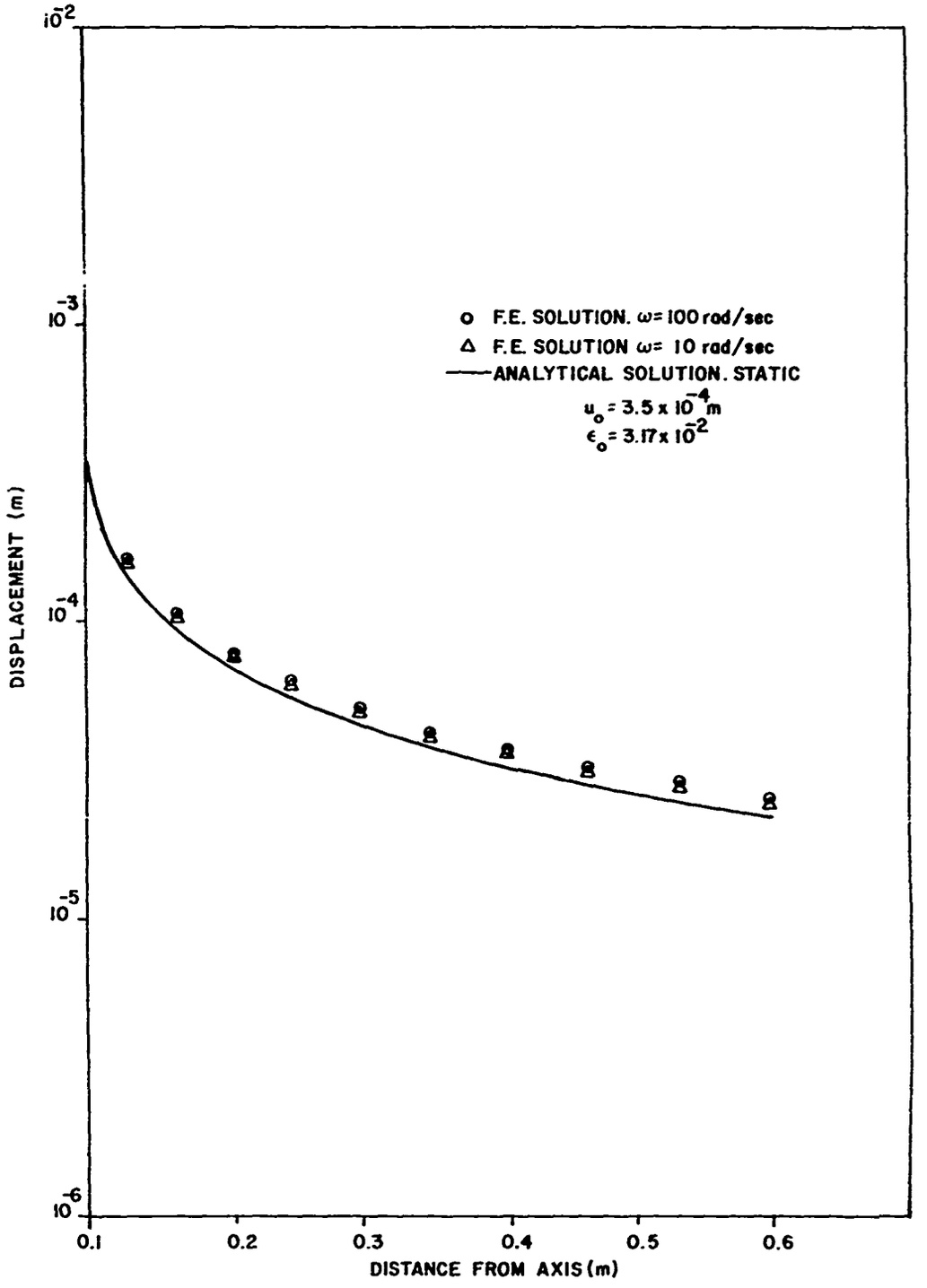

Figure 25. Comparison between analytical and numerical displacement values

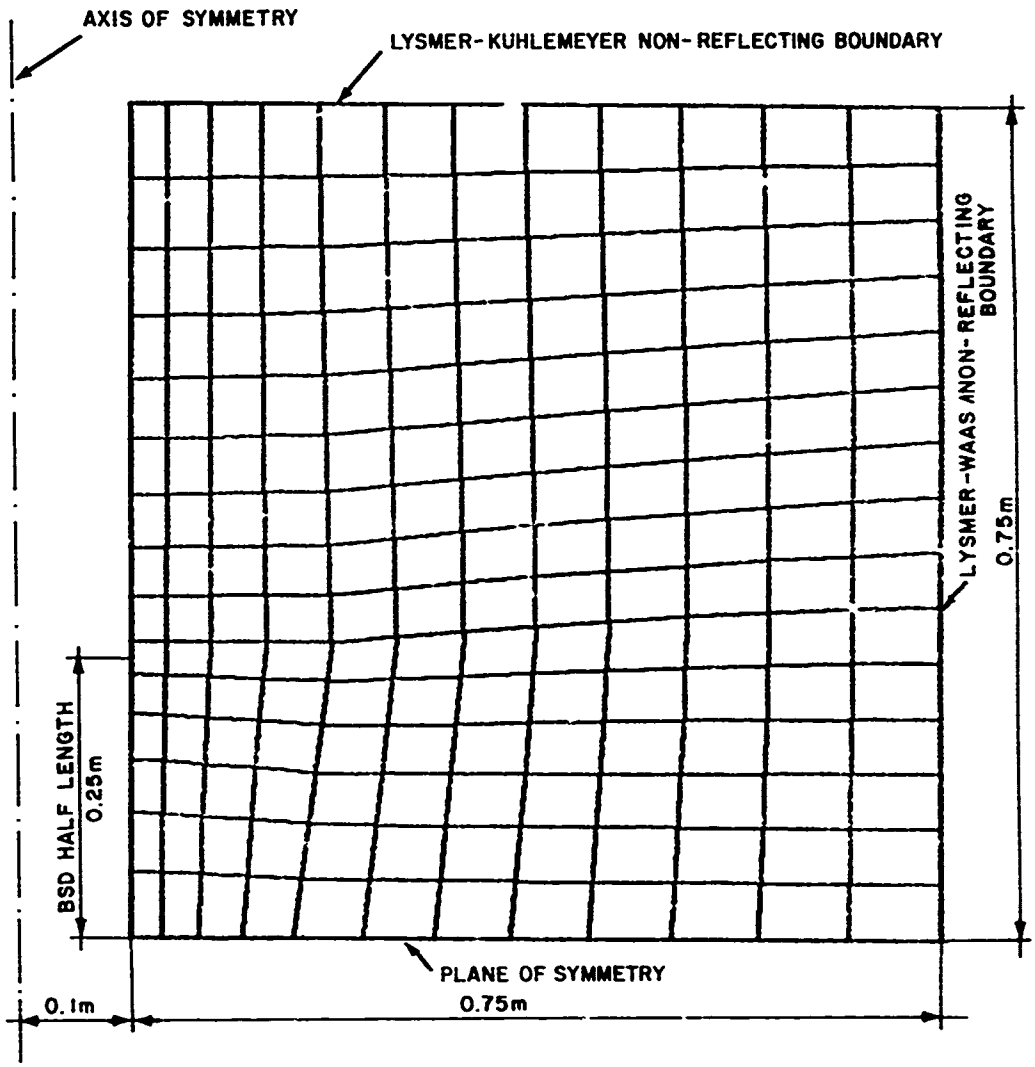

Figure 26. Finite element mesh used for calculations with cylinders of finite length

the real component of both strain distributions ($\varepsilon_{r\theta}$ and $\varepsilon_{\theta z}$) has been plotted by the computer (Figures 27 and 30). As it was mentioned earlier in this report, it can be easily observed that the greater the non-linearity of the part of the stress-strain law involved, the faster the decay of the strains with distance from the cylinder.

The values of torque required to induce the imposed boundary displacements cannot be verified against analytical solutions and are given in Table 5.

Table 5. Torque values for finite cylinder in hyperbolic soil

INPUT ANGULAR DISPLACEMENT, u_o (m)	TORQUE REQUIRED TO PRODUCE IT, T (N m)
1.0×10^{-4}	9.20×10^{3}
3.5×10^{-4}	1.79×10^{4}

Quite naturally, the torque required divided by the displacement produced decreases as the soil becomes more non-linear due to the degradation of the secant stiffness.

4.3.3 Torque Ratios

It was mentioned at the onset of Section 4.3 that one of the purposes of the non-linear analysis was to determine the influence of the non-linearity on the ratio of torques for the case of long and short cylinders. This point constitutes the object of the present section.

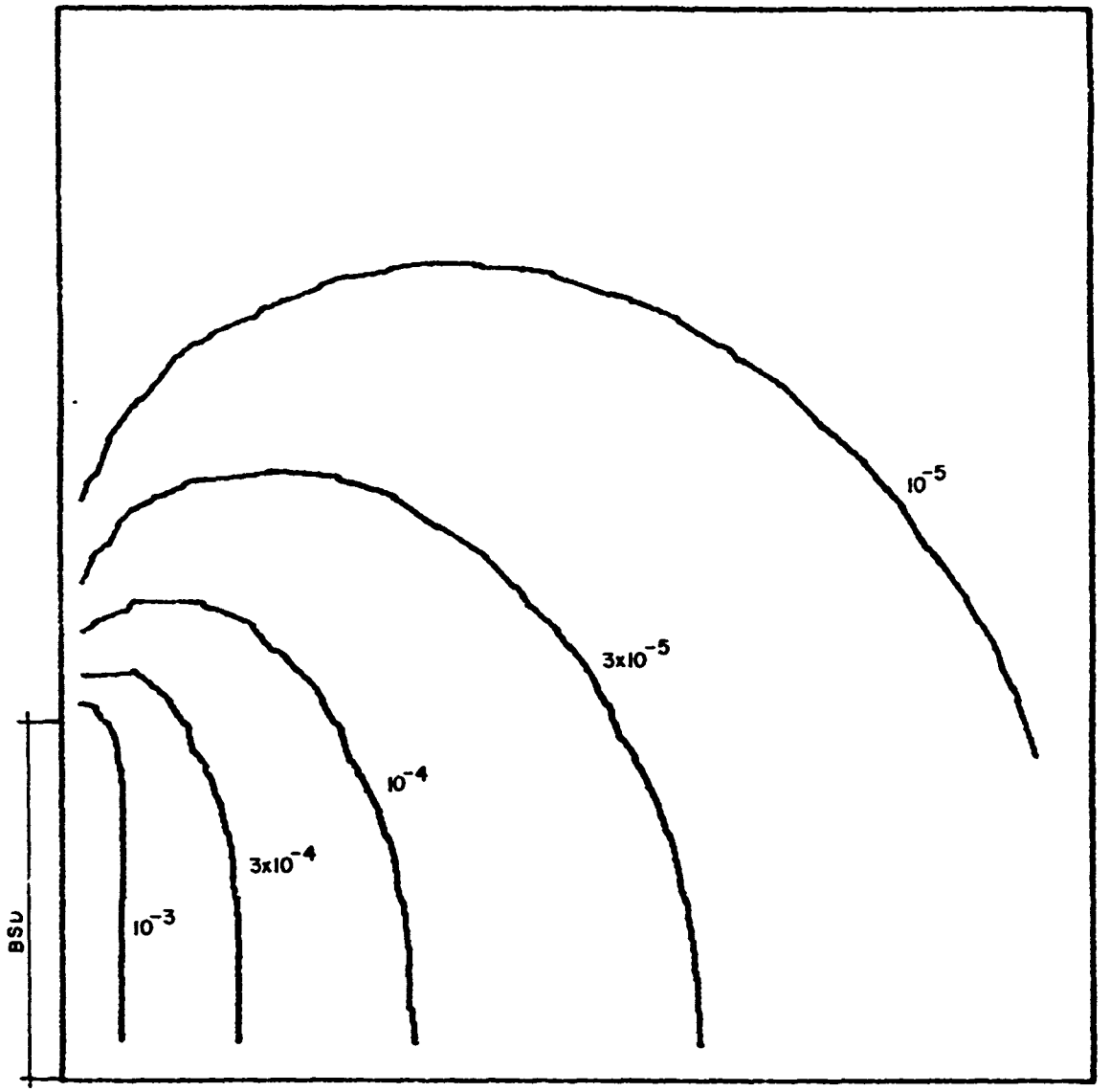

Figure 27. $\varepsilon_{r\theta}$ strain distribution for a non linear constitutive law ($U_o = 1x10^{-4}m$)

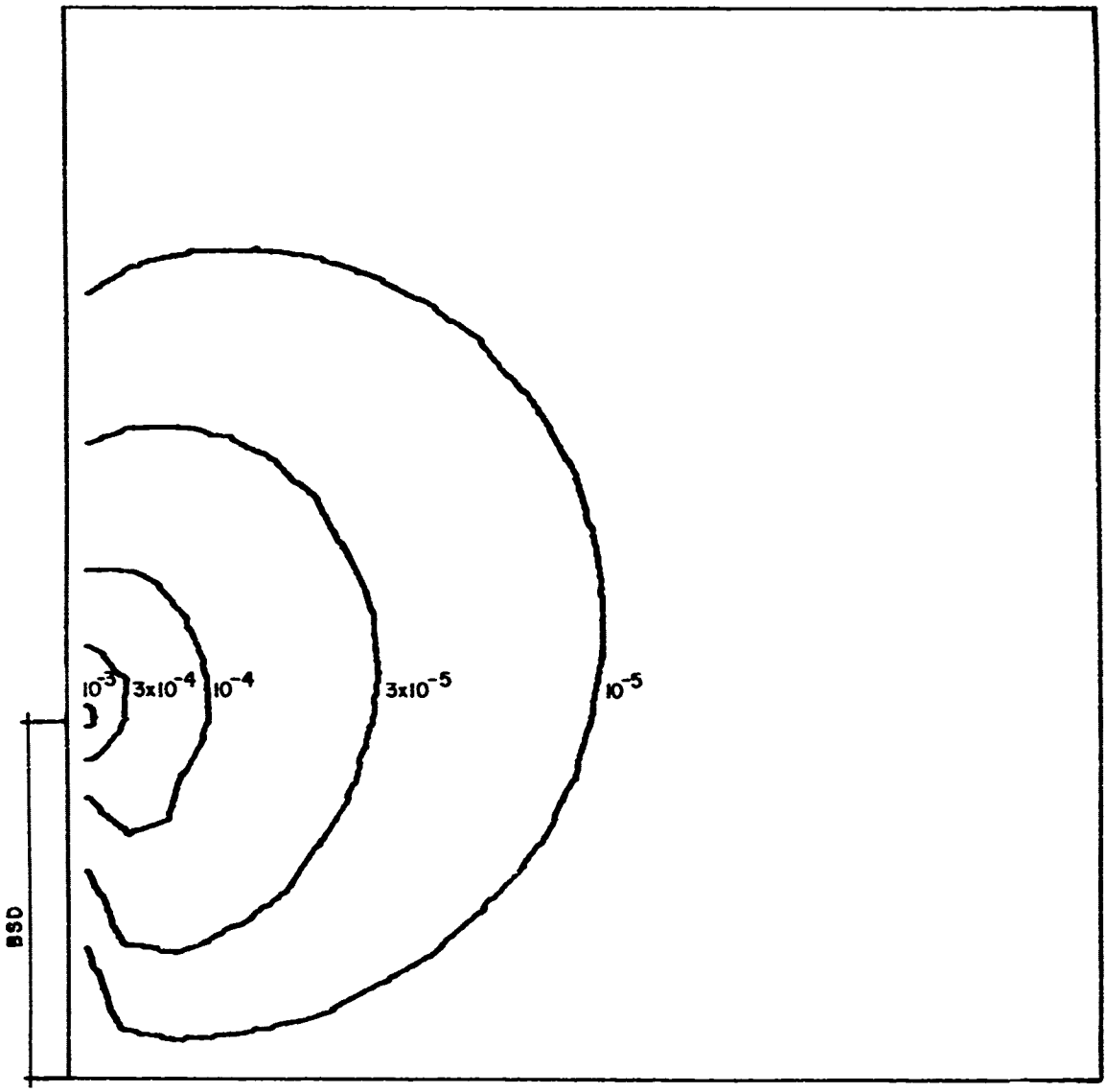

Figure 28. $\varepsilon_{\theta z}$ strain distribution for a non linear constitutive law ($U_o=1x10^{-4}$ m)

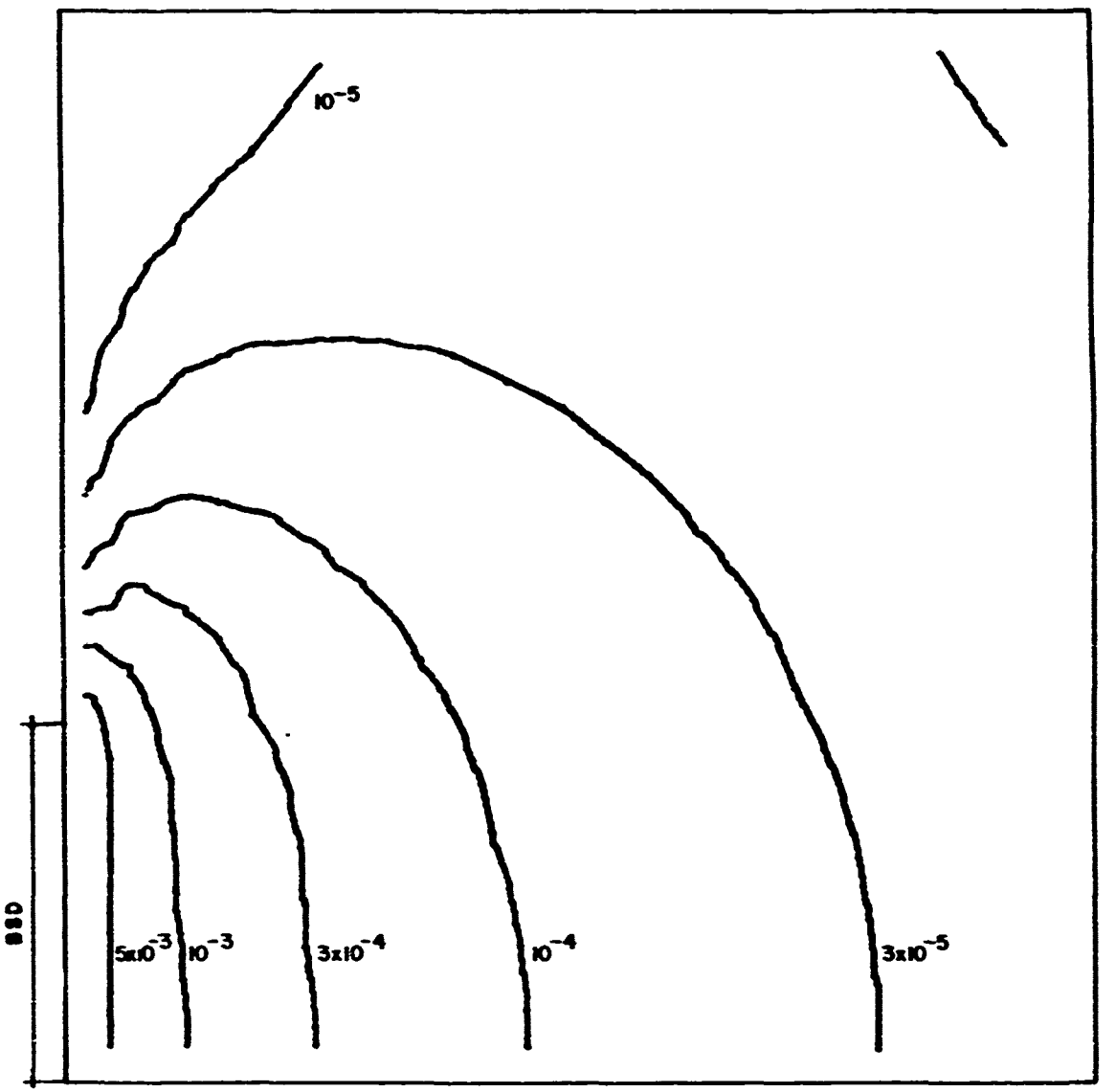

Figure 29. ε_{rr} strain distribution for a non linear constitutive law ($U_o = 3.5x10^{-4}$ m)

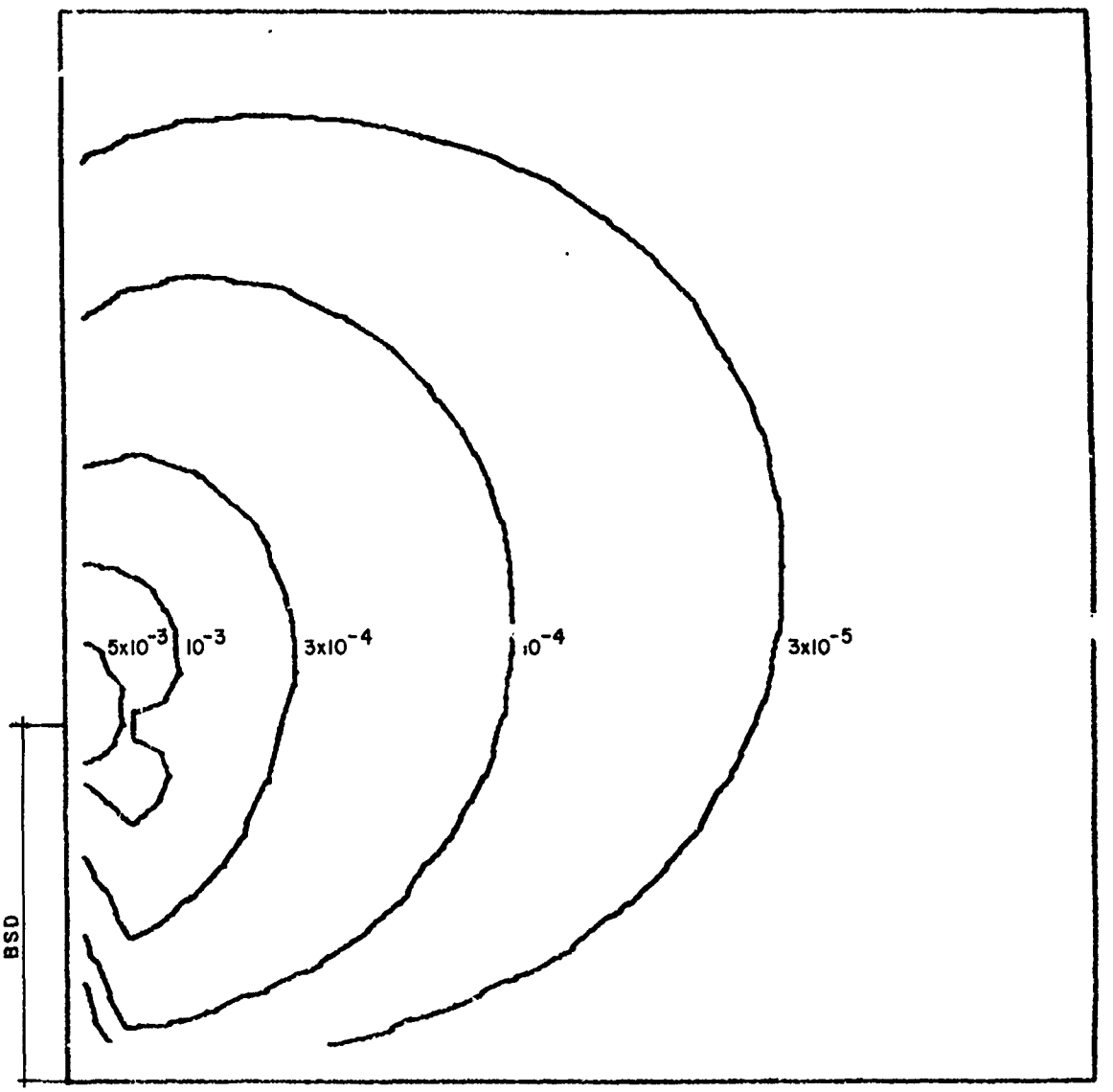

Figure 30. ϵ_{ez} strain distribution for a non linear constitutive law (U_o=3.5x10^{-4}m)

The torque T_F required to produce a steady-state rotation θ on a finite cylinder of length h can be expressed in terms of the torque T_L required to induce the same effect in an infinitely long cylinder. We will concentrate on the real part of the torque since it was already shown that the imaginary part is very small. The expression will be of the type:

$$T_F = T_L F \tag{1}$$

From dimensional analysis, in the elastic case F_E (the subscript E stands for elastic is only a function of:

$$F_E = F_E\left(\frac{h}{r_o}, \frac{d}{h}, \frac{\omega r_o}{v_s}\right) \tag{2}$$

A quick look to Figures 5 to 8 shows that the influence of $\frac{d}{h}$ can be neglected when $\frac{d}{h} > 1$; since this is always true, F can always be taken as its value when $\frac{d}{h} \to \infty$. Similarly, due to the facts that a) Figures 5 and 7 start the curves horizontally and b) $\frac{\omega r_o}{v_s}$ is very small, $\frac{\omega r_o}{v_s}$ can be considered zero for the purpose of determing F. Hence:

$$F_E = F_E\left(\frac{h}{r_o}\right) \tag{3}$$

where $\frac{h}{r_o} = 5$ in the present design of the BSD.

In the case of non-linear soil, the small influence of frequency was already seen in Section 4.3.1. As for the influence of $\frac{d}{h}$, it is clear that, although it cannot be directly quantified, it must be even smaller than in the elastic case due to the fact that the strains decrease faster

with distance from the cylinder. One more parameter has to be considered in the case of hyperbolic soil; several equivalent ones could be used, for example, ε_o (the value of the maximum $\varepsilon_{r\theta}$ strain developed). Then, in the case of hyperbolic soil:

$$F_H = F_H\left(\frac{h}{r_o}, \varepsilon_o\right) \tag{4}$$

The value of $\frac{h}{r_o}$ is still 5. The value of ε_o increases with the rotation level; clearly,

$$F_H = F_E \text{ when } \varepsilon_o << 1 \tag{5}$$

since the soil behaves elastically for sufficiently small strains (Section 3.1b). The question is how does F_H vary with ε_o as the latter increases. The results obtained in the tests are shown in Table 6.

Table 6. F_H factor for hyperbolic soil

MAXIMUM $\varepsilon_{r\theta}$ STRAIN DEVELOPED, ε_o (-)	F_H FACTOR (-)
SMALL	2.31
2.93×10^{-3}	2.25
3.17×10^{-2}	2.27

As can be seen in the above Table, the factor F_H remains essentially constant over the range of strain levels of interest; the differences are so small that they are almost on the order of the accuracy of the results presented.

4.4 INFLUENCE OF LAYERING

To this point, all the analysis has been made on the assumption that the soil is a homogenous medium. In all probability, layers will exist in the real soil profiles where the BSD is to be used. The present section aims to define the influence of layering on the torque and rotation measurements on which the soil modulus calculations will be based.

It has been shown that the influence of a fixed or free boundary on the torque required to produce a certain rotation of the cylinder is greater in the linear than in the non-linear case. In fact, it is easy to see that, as the strains increase, $\tau_{r\theta}$ around the cylinder approaches the limiting strength of the material, irrespective of any free or fixed surfaces, no matter how close to the cylinder. Therefore, the elastic case, and hence the small strain operations, are the most sensitive to the proximity of very hard or very soft layers above or below the BSD.

Fortunately, even in the elastic case, there does not seem to be reason for concern. The worst condition will arise if an infinitely rigid or infinitely soft layer are at a short distance from the BSD. But even for this worst condition of the worst case, Table 3 clearly shows that, as long as the extreme of the BSD is more than 25cm away from the infinitely rigid or soft layer, the influence in the torque is less than 1% (half of what is shown in Table 3 which includes two symmetric fixed or free surfaces rather than one). Even when the distance is on the order of 10cm, the torque can only be seen to vary on the order of 10% in the far more disadvantageous configuration of Figure 7 ($h/r_o = 2$, rather than 5).

The above fact is a direct consequence of the fast decay in the vertical direction of the $\epsilon_{\theta z}$ strains, which are responsible for transmitting the BSD project to levels higher or lower than the location of the BSD.

In summary, since a) the geotechnical profile will be known, b) the operation will concentrate on relatively large strains and c) there are no infinitely rigid or soft layers in nature, it is not likely that errors as high as 2% will be introduced in the measurements as a consequence of soil layering.

4.5 EFFECT OF DISTURBANCE

It is well known that any method of creating an opening in the ground, no matter how careful, will inevitably produce a zone of disturbance around the opening. Such an effect has been considered at all stages of the BSD project, although not always with identical priority. At the early stages of the project, when the device was expected to propagate waves from the BSD to a pick-up, the importance of a narrow zone of disturbance was very limited. However, as preliminary analyses showed the impossibility of that operation and the conceptual design shifted to a single-point measurement configuration, the minimization of borehole disturbance became paramount. It was at that time that a decision was made to incorporate a self-boring tool at the front of the BSD.

Figure 31 presents two ideal curves as typically originated by a standard pressuremeter and a self-boring pressuremeter. Standard pressuremeters completely relieve the horizontal stress; the initial modulus obtained is low compared to the undisturbed one, due to both the stress relief and the disturbance caused. It is usually considered that the undisturbed situation has been reached where the $\sigma_r - u_r$ curve becomes a straight line as predicted by elastic considerations.

A self-boring pressuremeter however does not produce a total relief of the horizontal normal stress and causes much less disturbance (Hughes et al, 1977)[30]; also, the deterioration as a fixed rather than a radially smaller. If the BSD had been designed as a fixed rather than a radially expanding surface, it would have been appropriate to perform an

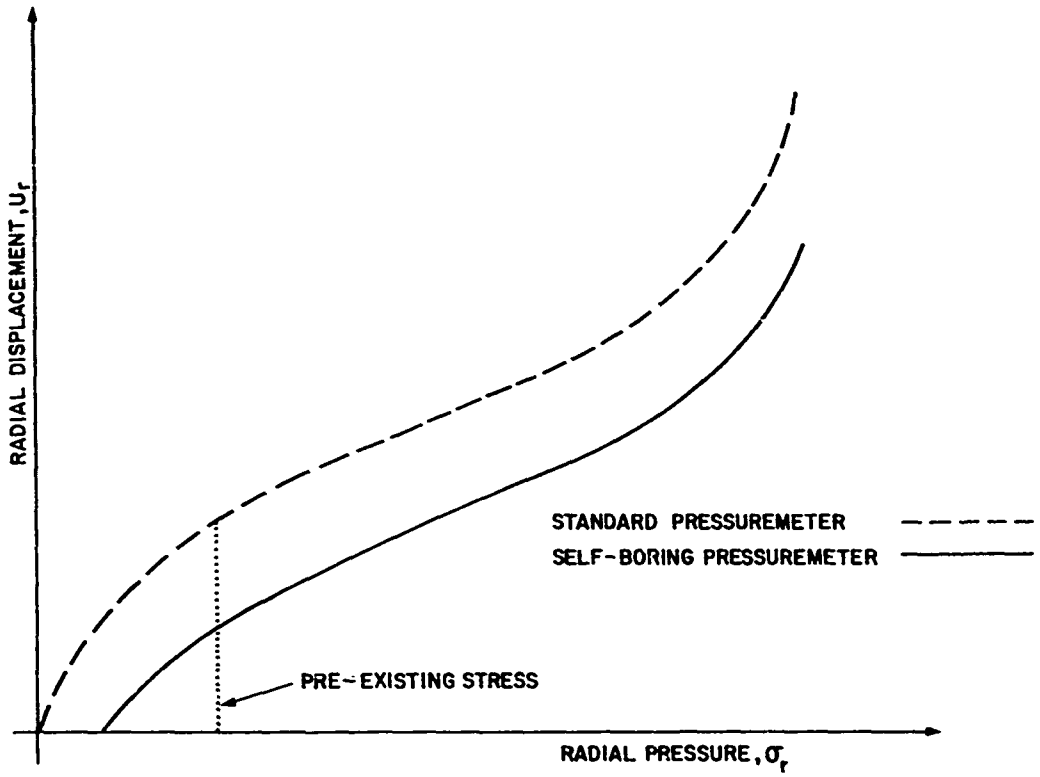

Figure 31. Pressure displacement curves from pressuremeters

analysis of the behavior of the device with the disturbed zone acting with a degraded value of the modulus. The width of the disturbed zone has been investigated by researchers at Cambridge by X-ray photography and seems to be on the order of 4 to 10 grain diameters or a maximum of 5mm (Windle et al, 1977)[31]. As to the degradation of the modulus, it could have been estimated from the initial slope of actual pressuremeter curves.

However, since the BSD is provided with a radially expanding shoe, the latter can be expanded until the pre-existing stress level is recovered; this point is located by analysis of the curvature changes of the curve shown in Figure 31. At that point, the large strain modulus is known to be approximately equal to its undisturbed value; indeed, such is the way in which the pre-existing stress is found in all radially expanding pressuremeters. Under those conditions, it is no longer necessary to conduct any numerical tests on the effect of the boring disturbance since, as far as the experimental data can tell, the radial expansion has been carried out exactly to the point in which the original value of the modulus has been recovered.

Although the above conclusion is theoretically reassuring, its verification by field testing with the actual prototype is strongly advised.

5.0 SYSTEMS DESIGN STUDY

5.1 INTRODUCTION

The purpose of this part of the project was to examine the practical aspects of the complete field measurement system. The scope of the study ranged from problems such as cost and complexity in manufacturing processes, to those related to handling and operation of the equipment in the field. Clearly, for such a broad scope, the aim was not to consider each aspect in detail but rather to endeavor to concentrate on fundamental problems affecting the feasibility of the proposed test; also, to identify areas where further work either experimental, analytical or in systems design was necessary or would contribute to the further development of the project.

The BSD is a new type of in-situ testing apparatus. Little was known about the detailed behaviour of the device until the analytical aspects of the work had been under way for some time. Consequently there have been some fundamental discoveries that have influenced significantly both the configuration of the originally proposed apparatus and the testing procedures.

A brief history of the developments leading to the current concept of the test is given in the next section. The following sections discuss various aspects of these developments in detail. Also discussed are the problems involved in incorporating these developments into the design of a practical field measurement system.

5.2 EVOLUTION OF THE BSD TEST

The principal factors affecting the configuration of the testing apparatus and the fundamental nature of the test itself have emerged largely from the analytical aspects of the work. They can be summarized as follows:

(a) It was found that, for most realistic geometries of the originally proposed apparatus, the dominant strain induced in the surrounding soil by the coupling cylinders is the $\varepsilon_{r\theta}$ component and not, as at first proposed, the $\varepsilon_{\theta z}$ component.

(b) Radiated power occurs only at relatively high frequencies. For a significant portion of the power applied to the coupling cylinder to be converted to radiated power (i.e. to generate shear waves), a relatively high frequency of excitation is required. At the torsional stiffnesses calculated for the in-situ coupling cylinder, an extremely high mechanical power would be required by the system. Much of this power would be effectively reactive, that is, exchanged within the system and not contributing to generating seismic waves.

Regarding the strain distribution, it was found that, for the original configuration of the apparatus where two coupling cylinders were driven by a downhole motor, the distance between the cylinders would have to be of the order of half the radius of the borehole for the $\varepsilon_{\theta z}$ strains to be comparable with the $\varepsilon_{r\theta}$ component. For such a geometry, a number of fundamental problems arise. Firstly the measurement region is small and concentrated in the disturbed region; also, the strain field becomes very complex and the edge effects introduced by local yielding of the soil at the ends of the cylinders influence the measurements very strongly. Furthermore,

there is the practical problem of generating and coupling the drive torque required in such a confined space.

Hence the $\varepsilon_{\theta z}$ strain concept was abandoned and the analytical and design efforts were concentrated around a device which was to be optimized for inducing the $\varepsilon_{r\theta}$ component of strain. The following were the major repercussions on the systems design work of this change in the orientation of the project:

(a) A two cylinder configuration was no longer essential. For the $\varepsilon_{r\theta}$ strains, the zone of high strain surrounds the coupling cylinder and extends radially outward. Hence a single coupling cylinder driven either inertially or from a remote reaction system would induce the required strain equally well. As a consequence of this, the systems design study was expanded to include the practical considerations involved in developing a single coupling cylinder borehole shear device.

(b) Control over the $\varepsilon_{r\theta}$ strain distribution is not achieved by varying the geometry of the in-situ apparatus, at least not to the extent of the original $\varepsilon_{\theta z}$ component. The region of high strain intimately surrounds the coupling cylinder and thus the characteristics of the coupling and the disturbance induced by placement are potentially limiting factors to the integrity of the test.

(c) At the commencement of the project, the choice between up/down hole, crosshole and point measurement or any combination therefore was a deliberately open issue. Following the change to the $\varepsilon_{r\theta}$ strains, however, the up-

hole technique was immediately eliminated and within a short period of time, the crosshole method was also ruled out. Obviously an uphole detector would have to rely on the unwanted $\varepsilon_{\theta z}$ component and for the crosshole method, the analytical solutions showed that for the detector to be measuring in the zone of high strain, it would have to be impractically close to the coupling cylinder.

The effect of power limitations on the frequency of operation of the test meant that it was not possible to modify the strain distribution by operating at high levels of radiated power. Here again a blow was dealt to the option of the crosshole method. Had it been possible to operate at frequencies where the crosshole distance was less than a wave-length, the method would have been worth pursuing.

Thus the BSD test evolved into a semi-static point measurement. Material properties are derived from the torque and angular displacement functions measured directly at the coupling cylinder. A sinusoidal, or more correctly, a periodic excitation is applied to the coupling cylinder/s in the form of a feedback controlled torque. The input to the system is monotonically increased to progressively load the soil throughout the strain range of interest. Both torque and the resultant angular displacement functions are recorded throughout the loading history and used subsequently to derive the μ-γ relationship for the soil under test. The original concept of two coupling cylinders driven by a downhole actuator is still discussed in this report, but it is dealt with as a technique which produces two simultaneous point measurements.

5.3 MODE OF OPERATION

Application of dynamic torsional drive to the coupling mechanism in the BSD can be achieved using either torque or displacement control; that is, using either the torque or angular displacement signals as feedback variables in the control system (see Fig. 32). The dynamics of the control system will be influenced by the control mode, but essentially, both modes of control are equally feasible.

The choice between control modes appears largely to be determined by soil mechanics considerations. Ideally, the apparatus would operate in strain control since the object of the test is to determine material properties over a prescribed range of shear strain. Using this mode of control, the apparatus could efficiently distribute the dynamic loading history around the prescribed region of operation, and there would be little risk of overloading the surrounding soil due to conditions of low strength. The BSD apparatus, however, does not afford a means for direct measurement of shear strain in the surrounding soil. The closest related variable that can be directly instrumented is simply the rotation of the coupling cylinder, and the relation between rotation and strain depends on the constitutive relation that the test is trying to obtain.

At high strains, the soil modulus will soften and strain gradients will increase in the area close to the coupling mechanism (see Fig 21, 22 and 23.) The BSD only provides a signal proportional to rotation and thus, using this signal as the feedback control variable, strains can only be controlled

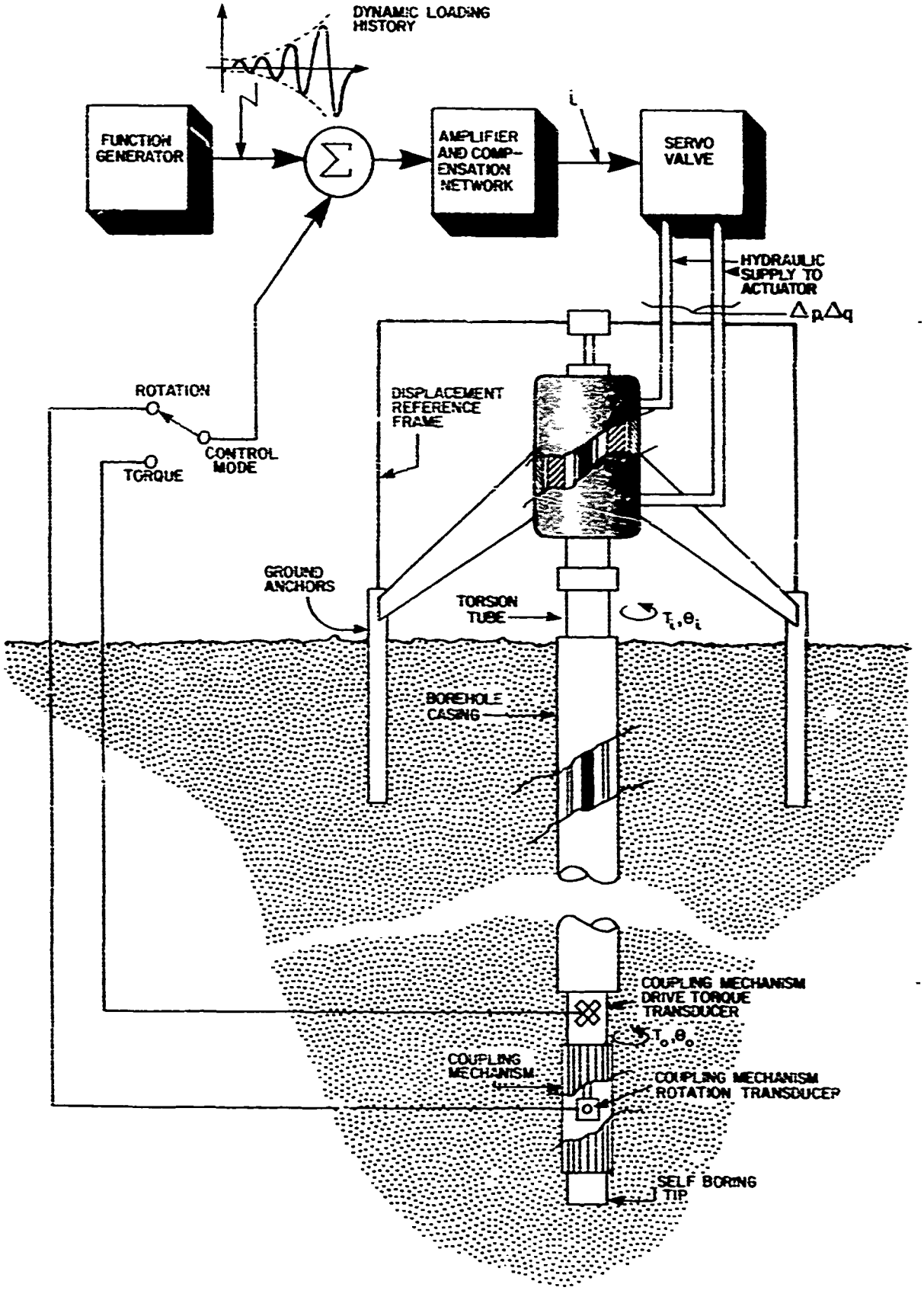
DYNAMIC LOADING HISTORY
FUNCTION GENERATOR
Σ
AMPLIFIER AND COMP-ENSATION NETWORK
i
SERVO VALVE
HYDRAULIC SUPPLY TO ACTUATOR
$\Delta p, \Delta q$
ROTATION
CONTROL MODE
TORQUE
DISPLACEMENT REFERENCE FRAME
GROUND ANCHORS
TORSION TUBE
T_i, θ_i
BOREHOLE CASING
COUPLING MECHANISM DRIVE TORQUE TRANSDUCER
T_o, θ_o
COUPLING MECHANISM
COUPLING MECHANISM ROTATION TRANSDUCER
SELF BORING TIP

in the low level, near-elastic range. In the high range, the strains indicated by the rotation signal using an elastic relation would always be smaller than the highest strain in the surrounding soil. Hence the danger would exist that the apparatus could advance the soil too rapidly through the loading history. Under these conditions, the rate of increase of strain per cycle of load could be large enough to limit seriously the amount of useful data obtainable from the measurement.

If, on the other hand, torque is used as the control variable, it appears more likely that the appropriate level of loading can be estimated better and that it can be more closely controlled throughout the loading history. This is felt to be so because there will always be a direct relation between the mean shear stress at the coupling mechanism/soil interface and the applied torque. The relation of this shear stress to shear strain will depend heavily on the soil properties, but a reasonable upper bound can be easily estimated based on competent geotechnical data for the site. This upper bound is determined from the shear strength of the soil, since the apparatus cannot couple torques, with their corresponding shear stresses, which exceed the shear strength of the soil. Thus, in order to ensure loading of the soil at high strains, it is reasonable to assume that the loadings should extend to yield of soil. As mentioned previously, estimation of this bound is relatively easy given good site data; not only is the procedure routine, but much practical experience coupled with field test results is available to assist in the calculation.

Given an upper bound or maximum value for the applied torque, the operation procedure would be to start the loading history at zero and, under controlled torque, increase the load at an appropriate rate to the calculated

yield value. The zero starting value would of course in practice correspond to the resolution of the system. This may be determined by backlash, striction or hysteresis in mechanical components; or, in a higher performance system, by random noise introduced by one or more of the system components.

It may be appropriate to modify the feedback signal in the control loop according to the rate of increase of strain but, fundamentally, the system would be described as a single-input, single-output torque control system.

5.4 RECOVERY OF SOIL PROPERTIES FROM FIELD DATA

The basic purpose of the development and operation of the BSD is the generation of a curve relating the secant shear modulus to the strain level. The present section is hence of the outmost importance since it is the one which provides the link between the in-situ operation and measurements, and the construction of the curve sought.

It has already been shown that, at the design frequencies of the apparatus, the associated wave lengths are long and the real part of the dynamic strain distribution approaches the static one. These facts permit proposing a relatively simple method of deriving the μ-ε curve.

5.4.1 Proposed Procedure

From Table 4 the torque required to induce a rotation θ on a long cylinder in elastic soil is:

$$T_{EL} = 4\pi r_o^2 \mu_o h\theta \qquad (1)$$

It was also shown (Section 3.3) that, if the cylinder can no longer be considered long, such torque becomes:

$$T_{EF} = 2\pi r_o^2 \mu_o h\theta F_E \qquad (2)$$

where F_E is an influence function given in Figures 5 to 8.

This means that, in elastic soil, the solution for a finite cylinder can be obtained from that for an infintely long cylinder as:

$$T_{EF} = T_{EL} \; F_E \tag{3}$$

For the cases of interest, it was justified in Section 4.3.3 the fact that F_E can be considered to depend on $\frac{h}{r_o}$ alone. For the present design, $\frac{h}{r_o} = 5$, for which value $F_E = 2.31$. In the case of a long cylinder in soil with a hyperbolic stress-strain law, the torque at small dimensionless frequencies (Section 3.1 and 4.3.1) can be expressed as:

$$T_{HL} = 2\pi r_o^2 h \tau_m \left(1 - e^{-\frac{2\mu_o \theta}{\tau_m}} \right) \tag{4}$$

It was also shown in Section 4.3.3 that the equivalent of eq. (4) for a short cylinder can be written:

$$T_{HF} = \pi r_o^2 h \tau_m \left(1 - e^{-\frac{2\mu_o \theta}{\tau_m}} \right) F_H \tag{5}$$

that is:

$$T_{HF} = T_{HL} . F_H \tag{6}$$

where F_H has been deduced numerically (Table 6) and appears to remain practically constanty over the range of strains of interest.

Since F appears to be approximately the same for elastic and hyperbolic soil models, even at high strains, let us assume for the moment that it will also be the same for other non-linear soil models. This assumption will be verified in the next subsection.

As mentioned in the previous section, the field procedure recommended consists of cycling the torque at gradually increasing levels starting from the lowest values allowed by the limit of resolution of the apparatus.

When the maximum strains are small, the initial modulus μ is easily determined from eq. 5:

$$T_{HF} = \pi r_o^2 h \tau_m \left[1 - \left(1 - \frac{2\mu_o \theta_o}{\tau_m} + \ldots\ldots \right) \right] F_E$$
$$= 2\pi r_o^2 h \mu_o F_E$$

as could be expected from eq. (1). Hence:

$$\mu_o = \frac{T_{HF}}{2\pi r_o^2 h F_E \theta} \tag{7}$$

For larger strains, it must be noticed that, in order to obtain the relationship between T and μ at a given strain level, the form of the constitutive law must be known. The problem is hence implicit. The following procedure is proposed.

Suppose the stress-strain law is truly hyperbolic. Then, once μ_o is known, a second test at higher θ is sufficient to determine τ_m from eq. (5) and hence to provide μ vs ε at all values of ε. Indeed:

$$\mu = \frac{\tau}{\varepsilon} = \frac{\mu_o}{1 + \frac{\mu_o}{\tau_m} \varepsilon} \tag{8}$$

where μ_o is already known, as for τ_m it can be found solving by iteration the implicit equation (5), which can be written in the form:

$$\tau_m = \frac{T}{\pi r_o^2 h\, F_H \left[1 - e^{-\frac{2\mu_o \theta}{\tau_m}}\right]} \tag{9}$$

A first approximation for τ_m is easily obtained by adding one term to the series expansion previously used:

$$T_{HF} = \pi r_o^2 h\, \tau_m \left\{ 1 - \left[1 - \frac{2\mu_o \theta}{\tau_m} + \frac{1}{2} \left(\frac{2\mu_o \theta}{\tau_m} \right)^2 + \ldots \right] \right\} F_H$$

which yields:

$$\tau_m = \frac{2\mu_o \theta}{1 + \frac{T_{HF}}{2\pi r_o^2 h \mu_o F_H \theta}} \tag{10}$$

Such an approximation is always sufficient for the first iteration due to the good convergence characteristics of eq. (9).

Even if the stress-strain law were not truly hyperbolic, the procedure for obtaining the μ-ε curve, as described above, would probably sufficient, particularly for the lower strains (probably up to about 10^{-3}). What such procedure would obtain is essentially a best fit of the real stress-strain law by means of a hyperbola. In order to avoid imposing a

hyperbolic stress-strain law onto the soil, the following improvement to the procedure described is proposed.

Suppose a test at low strains has already been conducted and μ_o is known. The next test is carried out at slightly higher strains and allows the computation of a τ_m value by means of eq. (9) and using eq. (10) as a first approximation. The rotation is again increased; the former value of τ_m is now used as a first approximation to solve eq. (9). This is continued until the soil fails.

Clearly, at each rotation level, the stress-strain law of the soil has been fitted with a hyperbolic law over the range of strains associated with the rotation imposed. Such hyperbolic law allows the derivation of the μ-ε relationship for all values of ε smaller than the maximum strain imposed. It is clear that when very high strains are involved, the approximation will be less satisfactory than when all strains are low; this is so because in the former case a larger portion of the stress-strain law is fitted with the hyperbola. This means that the value of μ corresponding to a strain ε will be optimum if derived from the value of τ_m obtained during the test in which ε was the maximum strain. Obviously, if the material is hyperbolic, all the τ_m values will be identical.

In summary the secant shear modulus μ at each strain level ε, based on the torque T required to induce a rotation θ, is taken as:

$$\mu\left(\varepsilon(\theta)\right) = \frac{\mu_o}{1 + \frac{\mu_o \varepsilon(\theta)}{\tau_m(\theta)}} \qquad (11)$$

where ε and τ_m are obtained from θ via the hyperbolic relationships.

5.4.2 Verification of the Proposed Procedure

In order to verify the adequacy of the procedure described, some "numerical field tests" have been performed. The purpose of these tests is to reproduce numerically the field operation. The soil is assumed to have a certain stress-strain law; in the soil, the BSD is operated numerically, thus producing torque and rotation values. The procedure described in the latter section is then used to generate a μ-ε curve which is compared to the original one in order to assess the errors made in the process. Tests with hyperbolic and non-hyperbolic soils have been performed and are described in this section. It should be reminded however that the examples included in the section provide an upper bound rather than a precise estimate of the errors involved. This is so because the soil in the field will respond exactly according to its true constitutive law, while the numerical soil includes errors in the response generated by the finite-element procedure itself. In a way, the present validation compounds the errors of the finite-element method with those of the procedure for generation of the μ-ε curve from T-θ data.

The first series of "numerical" field tests were run with a hyperbolic soil. Input data were as follows:

r_o = 0.1 m

h = 0.5 m

μ_o = 1.8×10^9 N/m^2

τ_m = 5×10^5 N/m^2

ω = 100 rad/sec

From the elastic run at strains smaller than 10^{-6}, μ_o was exactly recovered, as could be expected from the results shown in Section 4.2. Then a second test was run with identical input data except that the displacement at the BSD-soil interface was now:

$$u_o = 10^{-4} \text{ m}$$

corresponding to a rotation:

$$\theta = 10^{-3} \text{ rad}$$

The torque "measured" by the computer program was:

$$T = 9.2 \times 10^{3} \text{ Nm}$$

Solving then eq. (9) by iteration:

$$\tau_m = 4.83 \times 10^{5} \text{ N/m}^2$$

In Figure 33 the input curve is shown together with the one derived from the test. As could be expected, the agreement is very good for a hyperbolic stress-strain law since the approximation is also hyperbolic.

The true test of the procedure is to verify that it recovers a μ-ε curve even if the latter does not correspond to a hyperbolic stress-strain law. The same configuration of the above example was used again; in this test however, the stress-strain law was now defined by the thick line in Figure 34. It can be noticed that such curve intersects the hyperbolic ones and includes a horizontal segment at the end. Besides the elastic run, tests were performed at the following displacements and rotations:

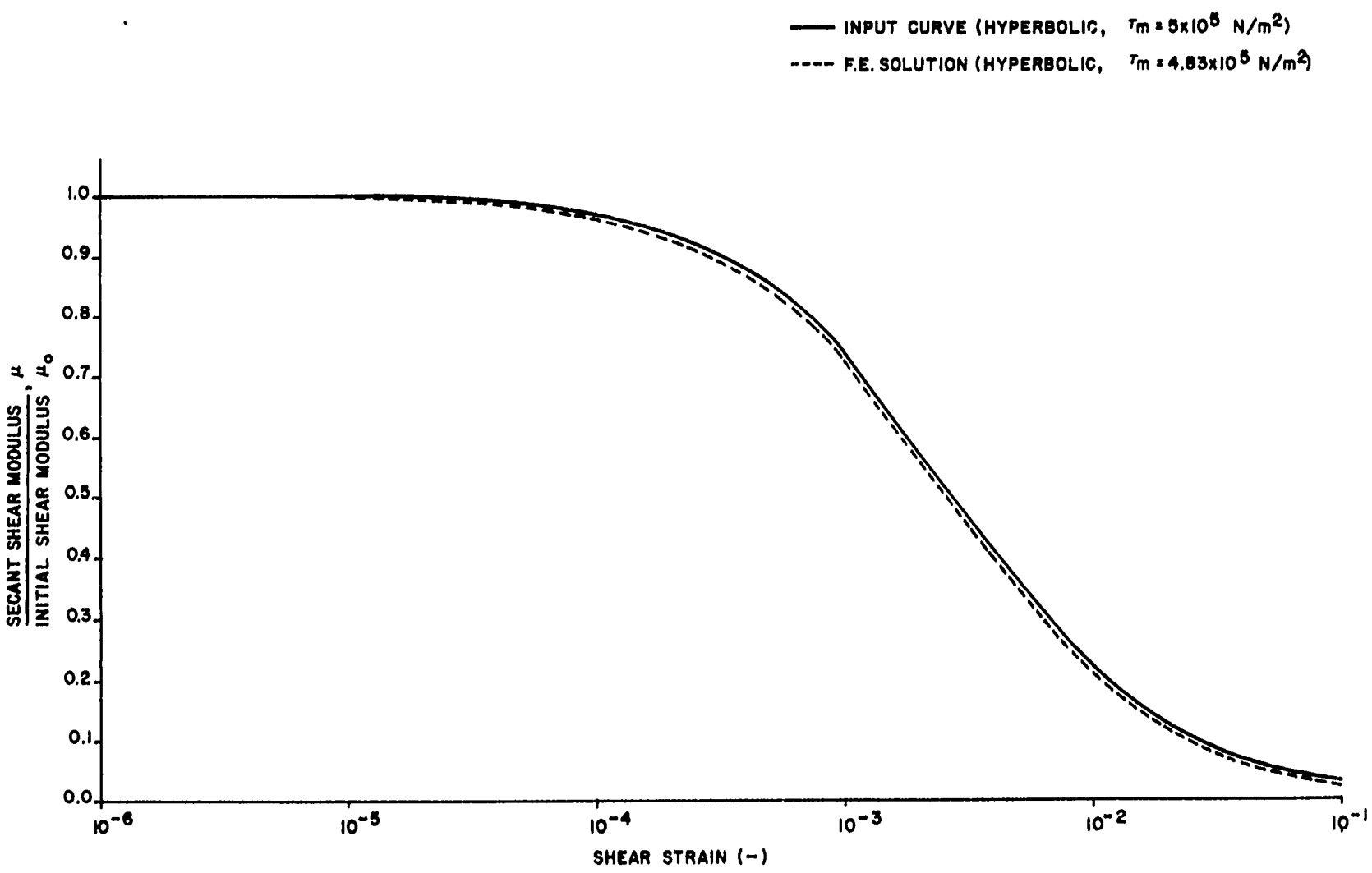

Figure 33. Numerical reproduction of a hyperbolic constitutive law

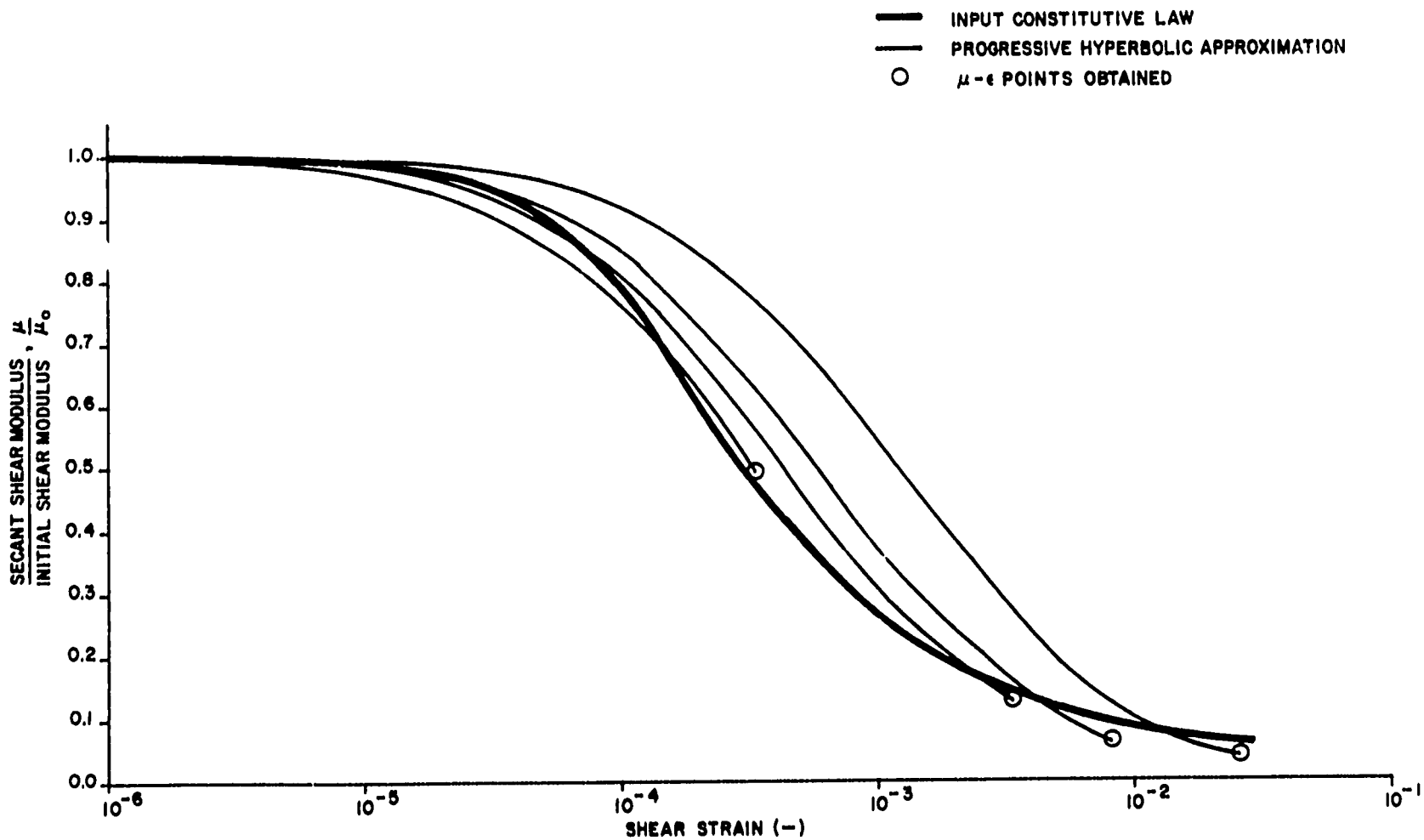

Figure 41. Reproduction of the input constitutive law by hyperbolic approximations

$u_o = 1x10^{-5}$ m

$u_o = 5x10^{-5}$ m

$u_o = 1x10^{-4}$ m

$u_o = 3.5x10^{-4}$ m

It is not difficult to reproduce the modulus values at strain levels at which the initial value has not deteriorated excessively. The most severe tests are the cases shown here where the secant modulus is 50% or less of the initial value. Table 7 presents a summary of the results obtained by the program and the values calculated by the procedure explained in Section 5.3.1.

Table 7. Results of the non-hyperbolic tests

u_o (m)	e (-)	T (Nm)	τ_{max} (N/m^2)	ε_{max} (-)
$1x10^{-5}$	$1x10^{-4}$	$9.71x10^{2}$	$5.75x10^{4}$	$3.28x10^{-4}$
$5x10^{-5}$	$5x10^{-4}$	$2.52x10^{3}$	$7.67x10^{4}$	$3.38x10^{-3}$
$1x10^{-4}$	$1x10^{-3}$	$3.61x10^{3}$	$1.02x10^{5}$	$8.32x10^{-3}$
$3.5x10^{-4}$	$3.5x10^{-3}$	$7.63x10^{3}$	$2.12x10^{5}$	$2.6\ x10^{-2}$

The μ-ε curve given as input, the four hyperbolic laws used in the successive approximations and the four points in which the hyperbolic laws are used to obtain a μ-ε point are all plotted together in Figure 34.

As can be seen, the agreement is better than could be expected from an approximate method, particularly since the errors compound those in the F.E. secant linerarisation with those in the derivation of μ-ε values via a hyperbolic approximation. As limitation, it should be pointed out that it is probably dangerous to use this scheme when the values of the secant modulus are below 10% of its initial value.

5.5 BSD TESTING HARDWARE

5.5.1 General

Figure 35 is a schematic diagram comparing the in-situ hardware for the two-cylinder and single cylinder BSD's. Both devices employ exactly similar coupling cylinders since, from the design or systems specifications point of view, it is immaterial whether they are driven from the surface or from a downhole actuator. For all realistic geometries of the apparatus, the torque-displacement relations derived from each coupling cylinder can be considered to be independent measurements. There are no special considerations such as modified stress distributions or design torques that influence the design of the coupling cylinder for either the single-/ or two-cylinder measurement systems.

5.5.2 The Self Boring Attachment

The self boring attachment is shown fitted to both systems. The purpose of this equipment is to remove and convey through the apparatus sufficient material to enable it to enter the virgin soil below the borehole casing with an absolute minimum of disturbance. The helical auger which is used to transport the soil cuttings through the apparatus is concentrically located, passing through the coupling mechanism and, in the case of the two-cylinder arrangement, passing also through the actuator. Provision of this free and uninterrupted central bore through the apparatus has been a major design constraint, particularly for the two-cylinder arrangement. The access bore for the auger must be of sufficient diameter to allow a reasonable size of auger and yet not to limit too severely the radial space available for the torque motor. The less radial

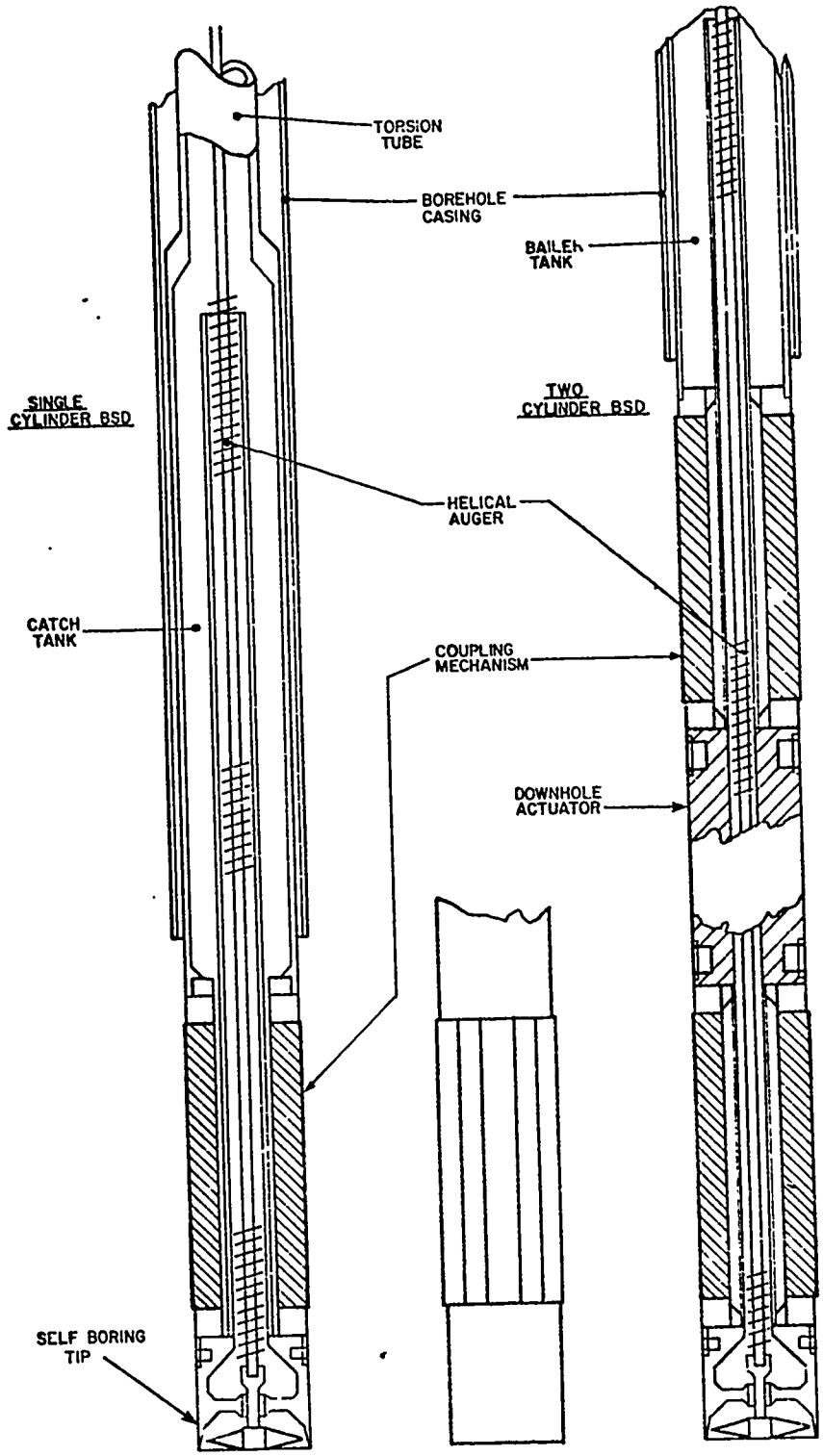

Figure 35. Comparison between in-situ hardware for the two-cylinder and single cylinder BSD's

space available for the actuator, the longer it becomes in order to develop a given torque. The auger, on the other hand, must transport a volume of soil cuttings of the order of that of the in-situ system. For the downhole acutator system, the problem is accentuated since the apparatus is considerably greater in volume than the single-cylinder system, with correspondingly greater distances over which the auger must convey the soil cuttings. Clearly, in the design of a two-cylinder BSD, a careful trade-off between the conflicting requirements of the components of these two system would be required. Both systems are shown equipped with a catch tank to store the soil cuttings. In the case of the two-cylinder system, it may be more convenient to use a bailer tank system where the tank is periodically raised up the hole in order to dispose of the cuttings.

5.5.3 Routing of Power, Instrumentation and Other Services

A major consideration in the design of the field equipment will be the routing of the various cables and hydraulic hoses which convey services to the downhole components. A convenient means of routing the instrumentation cables and a limited amount of hydraulic power is afforded in the coupling mechanism by the space at the bottom of the grooves in which the shear coupling keys fit. These services are conveyed by means of minature cables and small bore hydraulic tubes which easily fit into the clearance space at the bottom of the grooves (see Fig 36). In the case of the two cylinder mechanism, the actuator power hoses will require considerably more space. The only solution so far envisaged here is that they encroach on the central space provided for the helical auger. Tables 8, 9 and 10 are lists of the services coupled between the uphole and downhole systems. The list is divided between the two alternative systems, i.e.: the double and single

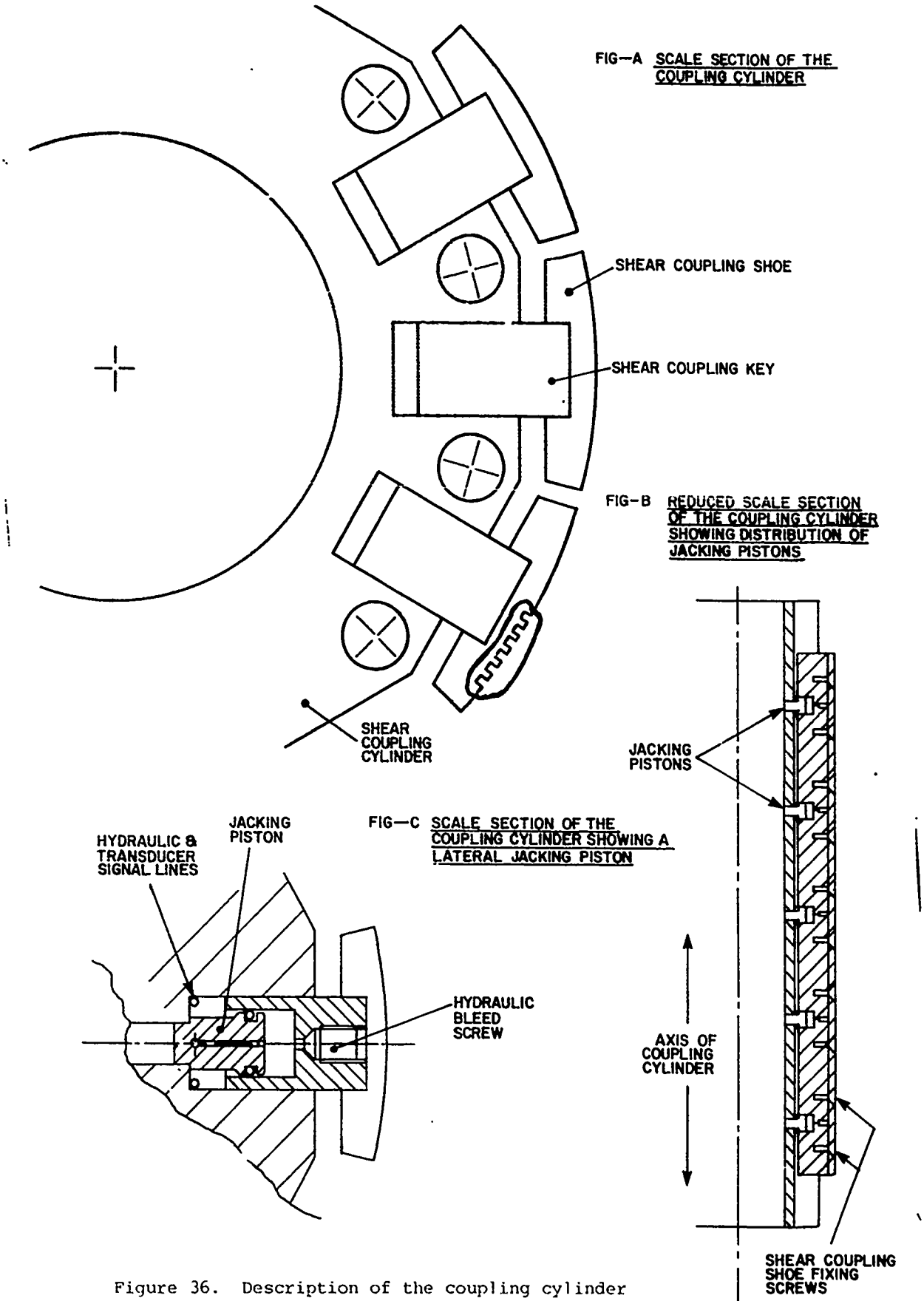

Figure 36. Description of the coupling cylinder mechanism

cylinder BSDs and then subdivided into individual system components. Certain features such as the instrumentation for the self-boring equipment may not ultimately be deemed necessary; they are however, included in this list for completeness.

Table 8. Power requirements of the BSD apparatus

	Single Cylinder BSD	Two Cylinder BSD
Torsional Drive Power	Rigid torsion tube sectioned into 2 metre lengths. The tube is thick or thin-walled depending upon whether oscillatory or direct coupling is employed. Outside diameter of tubing: 100 to 150 mm, max torque transmitted: 10^4 Nm.	High pressure hydraulic supply coupled via two 30 mm nominal diameter hoses. Typical supply rating: 2.5×10^7 Pa, (250 bars) at 0.5 litres/second.
Lateral Jacking and and Retracking Power	Two micro-bore (3 diameter maximum) high pressure hydraulic lines carrying bi-directional flow. Maximum jacking pressure: 150 bars, maximum compressible displaced volume of fluid: 0.035 litres	
	Hydraulic fluid conveyed by tubing attached to the wall of the torsion tube. Quick release, self sealing couplings installed at torsion tube joints.	Hydraulic fluid conveyed by flexible high pressure hose fused at intervals along main umbilical line.
Auger Drive Power	Sectioned torsion rod fitted with flush screw joints. Web-type centering brushes are fitted at torsion tube joints to maintain concentricity with torsion tube.	Sectioned torsion rod running in bushed radial-web type centering fixtures to maintain concentricity with borehole casing.
Cutting Tip Thrust	Applied from surface, coupled directly through torsion tube.	Applied either by temporarily installed jacking unit acting against borehole casing or coupled from surface via auger drive rod.

Table 9 Instrumentation of the BSD apparatus

	Single Cylinder BSD	Two cylinder BSD
Coupling Cylinder Drive	Multi-element strain-gauge torque transducer configured on torsion tube close to coupling auger.	Multi-element strain-gauge torque transducer configured on the actuator shaft.
Coupling Cylinder Rotation	Multi-element strain gauge flexural web arrangement coupled via rigid rod to surface reference frame. Web is coupled to inside bore of coupling cylinders by means of radially expending grips.	

Coupling Cylinder	Alternatively high resolution RVDT or LVDT (Rotary or Linear Variable Differential Transformer) coupled as above to surface reference frame. (radius arm mechanism would be required with the linear device).
Shear Coupling Key Displacement.	LVDT fitted inside fixed keys at both ends of the coupling cylinder/s. 24 LVDT's per coupling cylinder.
Lateral Jacking Pressure	Miniature strain gauge diaphram pressure tranducer plumbed into the hydraulic system as close as possible to the coupling cylinder/s.
Cutting Tip Thrust	"Doughnut" type low profile multi-element strain gauge force transducer mounted behind the rim blade of the self-boring head.
Auger and Breaker Tip Drive Torque	Probably most conveniently instrumented at the surface (at least for preliminary trials). Conventional slip-ring coupled strain gauge torque transducer.
Axial (Placement) Displacement	Again, probably most conveniently instrumented at the surfaces. Conventional long-stroke linear potentiometer displacement transducer.
Pore Water Pressure and Total Stress Gauge	Flush contoured, strain-gauge diaphram type pressure transducers, inset int. thick conic section of rim blade due to axial thrust.
Plane Strain Penetrometer. Force/ displacement measure-ments. (see Section 5.6.2)	One LVDT and one strain gauge force transducer channel per plane strain penetrometer probe.

Table 10. Miscellaneous services for the BSD apparatus

	Single Cylinder BSD	Two Cylinder BSD
Bailer Tank Lifting Gear	Bailer tank not necessary for Single Cylinder BSD	Wire line used to hoist bailer tank up hole.
Deadload Relief	Deadload of torsion tube can be relieved by pull applied directly to tubing at surface.	Wire line
Flushing/Lubricating Fluid	If required temporarily or continuously during self boring, flushing/lubricating fluid can be pumped down the centre of the auger drive shaft.	

5.5.4 Practical Aspects Of The Single And Two Cylinder BSDs

The most significant difference between the single and two cylinder BSDs in terms of handling and placement procedures, is the means by which power for the torsional drive is transmitted down hole. The single cylinder system employs a torsion tube which is driven from a surface mounted actuator. Reaction torque is provided by a system of ground anchors and the torsion tube can be used either as a direct coupling or as part of a resonant coupling which would be able to magnify the torque developed. Drive torque for the coupling mechanism is derived from a motor or set of motors mounted on the reaction frame and coupled directly to the torsion tube. The system is shown in Fig 32 as an electrohydraulic control system which would typically be comprised of a two stage flapper/spool servo valve driving a vane type torque motor. Hydraulic power would be developed at the system pressure by a screw or piston type pump. Since the dynamic load history to be applied to the soil in any one test is relatively short, the possibility exists for accumulator storage of the total energy for each test. In this case, hydraulic power could be developed slowly from a high pressure pump which might ultimately be powered by, say, a vehicle battery. This latter feature obviously applies to both the single and two cylinder BSD's.

The single cylinder BSD system however is not limited to the use of hydraulic actuators as is the two cylinder device. The actuator is surface mounted and hence is not constrained by problems of limited space. It may be more appropriate to use electric torque motors with switching drive for the high torque and linear drive for smooth control at low torque. A decision on the type of drive most suited to this system is,

however, not critical to this design study since it does not influence significantly the concept of the single cylinder BSD. It is better relegated to a subsequent phase of the BSD development following a detailed study of these devices.

The torsion tube in the single cylinder BSD, fulfills a number of roles. Firstly, and most obviously, it transmits the main drive torque for the coupling mechanism. Secondly, it forms a catch tank to retain soil cuttings. Finally it allows direct transmission of axial thrust to the cutting tip during the self boring operation. The chief penalty inherent in this simple configuration, however, is the necessity for couplings in the system. The torsion tube must obviously be sectioned, the most appropriate length being determined by factors such as convenience of handling in the field and by the resolution or minimum spacing of the measurement locations. These joints in the torsion tube must be able to transmit the design drive torque without introducing significant backlash compared with the rotation of the coupling mechanism. This may not seem at first sight to be a reasonable requirement since the drive torque and angular displacement of the coupling cylinder are instrumented directly at the measurment location. The problem arises, however, in the control system which under torque control, experiences a loss or deterioration in the linearity of the transfer characteristics when the torque is small or at the point of reversing. This region is precisely the point where a well-behaved system is required, at least for the lower strain stage of the test. The high loop gains required to compensate for such non-linearities would certainly add to any problems with stability of the control system.

The two cylinder system, on the other hand, is not rigidly coupled to the surface. It is suspended on an umbilical line which is comprised of hydraulic power and instrumentation cables linked to a strain relief wire.

Drive torque for the coupling cylinders is derived from a centrally located torsional actuator coupled directly to the two cylinders. Some of the practical difficulties inherent are two cylinder BSD configurations have already been discussed, notably, those associated with the incorporation of the self-boring equipment. The actuator in the two cylinder BSD would almost certainly have to be a hydraulic motor. The extremely limited radial space and the high drive torque required of the actuator are constraints that only a high pressure hydraulic system could meet unless some system of gearing is also incorporated. In the absence of radial space the length of the motor increases, leading to further drawbacks with the two cylinder BSD. It is only reasonable to expect that the coupling mechanisms, upon expanding in the locking-on operation, will become slightly misaligned. This will result in bending moments applied to the motor shaft which, of course, increase with the length of the motor. Thus it is likely that a system of coupling would be required between the motor and the coupling cylinders to isolate or reduce this bending. Those couplings, however, should not significantly degrade the torsional stiffness of the driving system, otherwise reactive power consumption of the system would be increased. Reactive power is here defined as the power observed into strain energy in the BSD system. It is wasted power since the electrohydraulic systems do not recover power returned from the load, and the low stiffnesses which are characteristic of their systems limit the performance obtainable from the control system.

A fundamental problem of the two cylinder BSD concept is that of limiting the dynamic range of operation. As discussed above, there is little choice in the type of actuator that can be used and little space available in which to tandem devices, or to incorporate alternative drive systems to extend the dynamic range of operation. Furthermore, the actuator is operating under relatively adverse conditions which may include bending and lateral shaft loading. The dynamic range of controlled torque available from the device corresponds directly to the range of shear stress coupled to the soil and hence to the range of soil properties that the BSD can cope with.

Common to both systems is the requirement to relieve dead weight loading in order to avoid inducing unwanted shear stresses in the soil. This dead weight is partly contributed by the in-situ apparatus, and, in the case of the single cylinder system, by the torsion tube string. If instrumentation is incorporated in the downhole equipment to measure the cutting tip thrust, it may well serve also as a monitor for the deadload applied to the coupling mechanism/s.

The technique proposed for the measurement of angular displacement is again the same for both the single and two cylinder BSDs (See section 5.5.4). The displacement reference for the system is derived from a rigid rod lowered through the apparatus and attached to a reference frame at the surface. This rod does not couple directly to the apparatus, it is linked via the angular displacement transducer and an expansion mechanism to the central access bore in the coupling mechanism/s.

The final part of this section is a summary comparison of the single cylinder (SC) and two cylinder (TC) BSD systems. A comparison of the principal characteristics of the two systems is given in Table 11 and the points discussed previously in the section, along with some additional factors, are summarized.

5.5.5 Summary Comparison Of The Single And Two Cylinder BSDs

Two basic concepts for the borehole shear device are proposed:

(a) The double cylinder (DC) BSD: this utilises radially expanding cylinders providing complementary reaction torque for each other. This torque is generated by a hydraulic motor located in the borehole between the two shoes.

(b) The single-cylinder (SC) system: a single radially expanding shoe is coupled via a rigid or resonant system to an uphole torsional actuator.

Approximate characteristics of the two concepts are given in the following table.

Table 11. Comparison of estimated characteristics

	SINGLE CYLINDER (SC)	DOUBLE CYLINDER (DC)
LENGTH OF MEASURING DEVICE (m)	0.5	2.5
SELF-BORED LENGTH (m)	1.0	3.0
DYNAMIC RANGE (decades of controlled shear stress)	4	2-3
MAXIMUM FREQUENCY (Hz)	50	10
WEIGHT (Kg)	100+ coupling tubes	500

The following points discuss in more detail the relative merits of the two systems (SC=single cylinder, DC=double cylinder).

(a) PLACEMENT: The SC requires a substantially shorter self-bored length This expedites and reduces the cost of the field procedures. Also, in the DC it is almost certain that the upper cylinder will be required to contact soil somewhat more disturbed than the lower one.

(b) MEASUREMENT RESOLUTION AND EFFECTS OF SOIL PROPERTIES: The SC provides a single test at a time, performed at one depth and repeatable at approximately 1 metre intervals. The DC could provide two simultaneous tests at 2 metres from each other, repeatable every 3 or more metres. When each shoe is in a different layer, or at shallow depths in soils with depth dependent properties, the interaction between the two shoes may be difficult to analyze, particularly when the constitutive non-linearities induce deviations from the sinusoidal shape of the actuator output. In other words, the input to one shoe is affected not only by the actuator and the soil surrounding a particular shoe, but also by the soil around the other one. Furthermore, if the material at one shoe is significantly weaker than that at the other one, large strains will not be obtainable at that shoe. Hence, the DC performance grows worse as gradients of soil strengths increase. This problem is not shared by the SC configuration.

(c) DYNAMIC RANGE OF OPERATION: The large strain operations require torques which generate stresses close to the producing soil failure. Since shear strengths are likely to increase more or less linearly with depth, the torque required will have to change over a range at least similar to that of depths of operation (2 to 50 metres).

Since it would be ideal to be able to use the BSD for a large range of soils (from shallow and soft to deep and stiff), and also since a minimum range of strains has to be examined at each depth, it is apparent that a wide dynamic range of controlled output is an important requirement of the BSD. The advantages of the SC with respect to the DC are obvious in this respect. The hydraulic motor in the DC system would have a probable dynamic range of torque on the order of or little above two decades. This system is very difficult to improve or change since it is specially developed and located within the confines of a borehole. The SC on the other hand is powered by a motor on the surface. This actuator is not confined by the borehole and allows the freedom to choose between a number of systems (electro-hydrualic or electromagnetic), or indeed a combination of systems. By this means the dynamic range can be extended and much less special systems development is involved.

(d) FREQUENCY OF OPERATION: The upper frequency attainable with the SC system approaches 50Hz, the only theoretical limitation being given by the resonant frequency of the coupling between the resonant mechanism and the BSD. However, in the case of the DC the torque-frequency curve is fixed; the maximum frequency is determined by the peak angular amplitude, the torque and the available power. This frequency is not expected to approach 10Hz at the maximum design torque.

(e) HANDLING IN THE FIELD: The SC requires a special torsional tube coupling with backlash-free connections in order to transmit the torque. This tubing has to be transported and handled carefully. The DC on the other hand is a more compact system which is suspended and powered by means of a flexible line. However, the DC is a far heavier single unit than the SC increasing problems with handling and transportation.

(f) HARDWARE DEVELOPMENT: The SC can be more readily produced and involves less special component development that the DC. In particular, the TC requires a specially developed hydraulic motor which is both costly and complex in design.

5.6 PLACEMENT

Following discovery of the fact that the allowable dimensionless frequencies were small and the BSD could not properly be considered as a wave generating device, it became evident that placement would be a critical factor affecting the test. This is because the zone of high strain is highly localized at the coupling cylinder. Hence, it becomes important to minimize the disturbance to the in-situ stress state and fabric of the soil immediately surrounding the apparatus is required.

To assist with these problems, the following features were incorporated into the design of the BSD.:

(a) A self-boring mechanism which, as an integral part of the downhole equipment, is arranged to advance into the soil ahead of the coupling cylinder.

(b) A precision engineered, multi-element concept has been used for the design of the coupling cylinder, in which the device is capable of making some sensitive changes in surface profile to achieve uniform contact with the soil.

5.6.1 Self-Boring Operation

The self boring attachment, a schematic drawing of which can be seen in Figure 32 is based on the system developed at Cambridge University for placement of in-situ stress gauges and pressuremeter testing apparatus. The process is a highly controlled and steady removal of soil in a manner similar to a tunnelling machine. By careful control of certain parameters in the

apparatus and in the drilling procedures, it is possible to obtain extremely small zones of disturbance in the soil and very little modification from the undisturbed stress state.

A thin-walled circular blade or cutting tip is mounted on the end of the downhole assembly the outside profile of which is a smooth and continuous cylinder. Axial thrust is applied to advance the blade into the soil and the isolated central core is broken up by a rotating blade located behind the tip.

The total thrust required to advance the apparatus below the borehole casing will be comprised of the following components:

(a) A net cutting force developed over the tip of the rim cutting blade

(b) Adhesion or friction forces developed over the surface of the in-situ equipment by contact with the soil under lateral stress.

The maximum friction or adhesion forces will be the greatest component of the two above (see section 5.7.7); these forces depend heavily upon the type of soil, the depth of the selected measurement location and, of course, on the distance of placement below the borehole casing. The rim blade of the self boring equipment is conic within the cutting head leading past the breaker blade. The blade is designed such that the stresses in the soil ahead of the blade are changed as little as possible. Since the amount of load applied to advance the cutter is critical, it becomes convenient to include some form of monitoring and control for the force developed at the cutting head.

The soil cuttings are conveyed by the advancing core pressure to a throated section at which point they are picked up by a helical auger. The auger is housed in a concentric bore which runs through the entire length of the apparatus and opens into a catch tank located at the top of the downhole assembly. Hence the auger drive is used both to power the core breaker blade and to lift the soil cuttings through the apparatus. It is conceivable that it could also be used to transmit the axial thrust required on the rim blade during the placement operation. In Figure 32 the drive rod is shown socketed into a drive coupling within the cutting head. This arrangement allows for the auger to be withdrawn after self-boring leaving an uninterupted central bore through the downhole assembly. This feature assists not only in helping to remedy problems with jamming or fouling of the placement equipment, but as discussed in section 5.8.1, it permits the use of a very convenient means of instrumenting the rotation of the coupling cylinder.

For clayey soils, the auger may not be the most appropriate means for lifting the cuttings. Without lubricating and flushing with water, it is highly possible that these soils could gather in coagulated masses with sufficient adhesion and strength to foul the auger. To overcome this problem conventional flush boring methods can easily be employed; indeed, with the detachable auger system already described, it would be possible to change boring techniques even during a particular placement. Flushing water could be pumped through the centre of the auger drive rod and the slurry returned via the annular space between the rod and the bore of the coupling cylinder. This space would have to be reduced in order to raise the fluid velocity but, again, the means for achieving this could be incorporated onto the hollow drive rod assembly to allow simple conversion of the downhole equipment to water flush boring.

The self-boring operation is likely to be the longest and most in need of careful control of the complete testing procedure. It would be worth attempting to make some assessment of the likelihood of an acceptable placement and of the soil quality and uniformity, whilst the self boring process is in progress. Hence it is suggested that at least for the initial trials of the field equipment, the principal parameters associated with the placement equipment be instrumented and provision be made so that they can be monitored directly on site. If, for instance, a simple stripchart type record is produced during self-boring operations showing penetration, tip thrust, auger drive speed and torque, it is probable that an immediate on-site impression could be gained concerning the progress of the placement. Under certain conditions these data might be used to test the suitability of a given location or to determine whether or not to abort a particular placement.

5.6.2 Coupling to the Soil

Having reached the desired measurement location in the virgin soil, the final phase of the placement process occurs: that of jacking-out or locking-on to the borehole wall. Because of the sensitivity of the test to the state of soil immediately in contact with the coupling cylinder, the apparatus must replace as closely as possible the in-situ or undisturbed lateral stress condition. In this respect, two factors are of prime importance:

(a) The cylinder, should achieve upon jacking out a contact pressure with the soil as uniform as possible. Thus, the shoe should be able to adhere closely to the uniform cylindrical cavity produced by the self boring operation and, if necessary, should also be able to distort slightly in order to accommodate small anomalies or gradients in the properties of the surrounding soil.

(b) A means must exist to determine the undisturbed lateral stress in the soil, so that the correct jacking pressures can be applied.

To achieve uniform contact stress with the soil, the surface of the cylinder is composed of a large number of shoe segments. These segments act entirely independently and are free to both tilt and displace radially. The large number of shoes employed ensures that the cylinder can, if necessary, maintain a close approximation to the cylindrical profile, whilst the independent movement of the segments allows the system some tolerance to variations in the soil properties. For the undisturbed lateral stress in soil, the following is a list of viable techniques:

(a) By using a plane-strain or other type of horizontal penetrometer probe.

(b) By monitoring the total stress and the pore water pressure, and subsequent calculation based on these data and correction factors

(c) By calculation or estimation based on experience and/or site data.

(d) By observation of the pressure-displacement curve during radial expansion of the shoe.

The penetrometer test, conducted using horizontally action probes located behind the self boring head, would load the soil entirely through the range of lateral stress from the initial stress up to yield. The resultant stress-strain characteristic would provide the required soil data.

The stress gauge is a more simple expedient than the penetrometer and requires no intricate mechanics and little or no control procedures. The measurement is subject to errors, however, principally arising from disturbance or stress relief due to placement and to the well-known phenonomen of soil arching over the gauge. With experience, the output of the stress gauges could no doubt be used to achieve quite reasonable results for a majority of cases.

Without any measurements, it is felt that little better than 20% accuracy could be achieved in the determination of the undisturbed lateral stress. This, it should be emphasized, assumes a uniform uncomplicated site with well known geology. It may occur that under certain conditions this would be a perfectly adequate method, but for the analysis of early data from the BSD test, such lack of certainty can only hinder the rate at which familiarity with the procedure grows.

As a further indication of the quality or state of coupling to the surrounding soil, it is proposed that displacements of the expanding elements of the coupling cylinder be instrumented. In the coupling cylinder design described in this report, expansion is achieved by means of rigid continuous keys moving in slots in the surface of a central cylindrical core (see Fig 32). Displacement of these keyways is instrumented at both ends of the coupling cylinder giving information on the mean displacement and tilt of the moving elements. Jacking force is achieved by a system of hydraulic pistons and cylinders and hence the mean lateral jacking stress can easily be determined from the pressure in the hydraulic system.

As described in Section 4.5, it is also possible to choose an optimum point at which the mean lateral stress on the coupling cylinder is close to the original undisturbed stress; this is done by monitoring the pressure/displacement function during jacking out. Should there be an inclusion or gross discontinuity in the soil which results in correspondingly erratic shoe displacements, the proposed monitoring system will readily indicate this and allow a quick decision to be made concerning the success or otherwise of a particular placement. This method has the advantage of providing the same data during expansion of the shoe that existing self-boring pressuremeters produce. The procedure hence gives more information about the soil and creates at the same time one more link between the new data and other results which already count with years of expertise.

5.7 SYSTEMS DESIGN SPECIFICATION

5.7.1 Size Of The Coupling Cylinder

Probably one of the most fundamental questions that could be asked concerning the design of a practical BSD is what are the factors which govern the physical size of the coupling mechanism. Clearly the dimensions are limited at the lower extremes by the particle size of the soils in which the device is expected to work. For the upper bound, two significant limitations arise: these are the cost of the preliminary boring and casing operations, and the increasing power requirements of the system. The dimensions finally chosen for the coupling cylinder were arrived at by the reasoning that the larger the device, the more representative the test and the greater the range of materials in which it could operate. This, however, was tempered by the correspondingly higher power requirements and the fact that use of the apparatus might be limited if non-standard or prohibitively expensive borings were required. Thus it was decided that design specifications should be based on the largest readily available cased borings that could be produced without using specialised equipment. This requirement seems to be satisfied by 200 mm (eight inch) boreholes and hence the design specifications and the design of the prototype coupling mechanism are based on this size of boring.

5.7.2 Operational Specifications

The specifications for the power supplies to the equipment and for the coupling cylinder design, are based on the following worst case assumptions for the operational conditions:

(a) The maximum depth of operation of the equipment is 50 metres.

(b) The water table is not lower than 25 metres.

(c) The maximum coupling cylinder drive torque is determined by that required to fail the soil in shear.

(d) The coupling system is to be operated at contact pressures close to the original undisturbed lateral stress.

For the parameters of the different soil types in which the BSD has potential for testing, the spread of values is large. A number of practical disadvantages weigh against a totally worst case choice for the values of these parameters and it was decided that calculations should be based on nominal values only. This is justified to a certain extent in that, should a worse case or extreme value situation arise, the effect on the testing program is not catastrophic. Testing can still proceed although some limitation will occur on the depth to which the apparatus can be operated and the maximum strain at which the test can be run. Furthermore, since the dynamic range is finite, design for an extreme worse case decreases the resolution of the system thus losing some of its small strain capabilities.

5.7.3 Calculation of Maximum Drive Torque

The effective lateral stress in the soil before placement of the coupling cylinder is:

$$\sigma'_h = gK_o((\rho_s - \rho_w)\, d + \rho_w d_w) \qquad (12)$$

where σ'_h = effective lateral stress (N/m^2)

g = gravitational constant (m/sec^2)

K_o = lateral earth pressure coefficient

ρ_s = mean density of soil overburden ($10^3 Kg/m^3$)

ρ_w = density of water

d = depth of measurement from the soil surface

d_w = depth of measurement from the water table

Neglecting soil adhesion to the shoe and assuming that the friction coefficient at the shoe-soil interface is equal to the angle of internal friction, the torque required to yield the soil approximately is given by:

$$T_m = 2\pi r_o^2 h \sigma_h' \tan \phi \qquad (13)$$

where : T_m = peak torque applied to the coupling cylinder (Nm)

r_o = radius of the coupling cylinder

h = height of the coupling cylinder

ϕ = internal friction angle of the soil

Assuming the following values for the variables in the above equations: $\tan \phi = 0.5$, $K_o = 1.0$, $\rho_s = 1.8 \times 10^3$ Kg/m^3, $r_o = 0.1$ m and h = 0.5 m, a maximum design torque $T_m = 1 \times 10^4$ Nm results.

5.7.4 Calculation Of Maximum Jacking Pressure

For the lateral jacking pressure, the mean lateral stress at the surface of the coupling cylinder must equal the total applied stress. Hence, assuming a saturated overburden density of 2.0×10^3 Kg/m^3 and $K_o = 1.0$, this gives a maximum jacking pressure of:

$$\sigma = 1 \times 10^6 \text{ N/m}^2$$

5.7.5 Calculation of Maximum Range of Rotation

Using the hyperbolic soil model developed in Section 4.3 to describe the non-linear behaviour of the soil at high strains, an approximate calculation for the range of rotations occuring at the coupling cylinder can be derived. The relationship between shear stress at the cylinder surface and rotation of the cylinder has been found to be:

$$\tau_o = \tau_m \left(1 - e^{\frac{2\mu_o \theta_o}{\tau_m}} \right)$$

where τ_o = shear stress at the cylinder/soil interface

τ_m = yield shear stress of the hyperbolic soil

μ_o = elastic shear modulus of the soil

θ_o = rotation of the cylinder

For a maximum value of shear stress $\tau_o = 0.8\ \tau_m$, the rotation is :

$$\theta_{om} = \frac{\tau_m}{2\mu_o} \ln 5$$

Substituting for τ_m and μ_o gives

$$\frac{T_m}{\theta_{om}} = \frac{3.2\pi r_o^2 h \rho_s v_s^2}{\ln s}$$

Hence, the apparent rotational stiffness of the in-situ coupling cylinder at $\tau_o = 0.8\ \tau_m$ is:

$$\frac{T_m}{\theta_{om}} = 5.62 \times 10^1\ v_s^2 \text{ Nm/rad}$$

Given the maximum design torque derived earlier of $T_m = 1 \times 10^4$Nm and assuming a range of shear wave velocities $100 \leq v_s \leq 500$m/sec, the corresponding range of maximum rotation is:

$$7.12 \times 10^{-4} \leq \theta_{mo} \leq 1.78 \times 10^{-2} \text{ rad}$$

or $$0.04 < \theta_{mo} < 1.0 \text{ degrees}$$

5.7.6 Calculation of Drive Power

Assuming a sinusoidal drive function and a purely elastic load, the peak mechanical power required to drive the coupling cylinder is:

$$P_m = \pi T_m \theta_{om} f \tag{14}$$

where f = frequency (hertz)

For the range of maximum rotations given above the peak drive power is:

$$22.5 < P_m < 560 \text{ Watts/Hertz}$$

For the power absorbed in strain energy in the BSD apparatus, the major component is due to the twist in the torsion coupling tube in the single cylinder system. The torsional stiffness of a hollow tube is given by:

$$K_t = \frac{\pi \mu_t (r_2^4 - r_1^4)}{2L_t} \tag{15}$$

where:

K_t = torsional stiffness of the tube

r_1, r_2 = inside and outside radi of the tube

μ_t = shear modulus of the tube material

L_t = length of the tube

For a sinusoidal torque function applied to the torsion tube, the peak power exchanged between the torsion tube and the actuator (i.e.: non contributory or reactive power) is:

$$P_m = \frac{2 T_m^2 L_t f_o}{\mu_t (r_2^4 - r_1^4)} \tag{16}$$

where f_o = frequency of operation of the torsional drive (Hertz)

Assuming a torsion tube of 150mm outside diameter, 10mm wall thickness (34.5 kg/m tubing) with a nominal μ_t of 8×10^{10} N/m^2, the maximum reactive power (i.e. at the maximum drive torque $T_m = 10^4$ Nm) due to the torsion tube coupling is:

$$P_m = 131 \text{ watts/metre hertz} \quad (0.24 \text{ h.p./metre hertz})$$

The total theoretical energy required assuming the drive system is incapable of recovering the reactive energy stored in the tube is:

$$E_m = P_m \text{ Joules/cycle metre}$$

which, at the system maximum torque of $T_m = 1 \times 10^4$ Nm and at the maximum depth of operation of 50 metres is 9.0×10^3 Joules/cycle.

It must be remembered that this figure is an upper bound and that only a small number of cycles involving energies approaching this figure are required in the BSD test. If, as suggested in an earlier section, an accumulator storage system is used to provide hydraulic power, then the power supply system will not have to be generating and damping the maximum required power Although efficiencies will be low, the total energy required for the test will not be inordinately high and could, it is felt be stored in a high pressure of gas bladder type.

If the torsional coupling is operated at resonance, the power required will effectively be divided by Q, the resonant magnification of the system. Under these conditions the torsion tube would be thin-walled and an approximate expression for the resonant frequency of the system is:

$$f_r = \sqrt{\frac{r_m^3 \, r_t \, \mu_t}{2\pi L_t \, I_s}} \qquad (17)$$

where f_r = resonant frequency of the coupling in Hertz

r_m, r_t = mean radius and wall thickness of the coupling tube

I_s = lumped moment of inertia of the coupling tube and drive system

The above analysis assumes a much greater stiffness for the in-situ coupling cylinder than for the torsion tube, hence the tube is effectively fixed at one end with a lumped mass attached to the free end. To serve as an example, a torsion tube of 2.5mm wall thickness, and a lumped moment of inertia I_s = 10 Kg m^2, the resonant frequency of operation at L_t = 50 metres is:

$$f_o = 5.18 \text{ Hz}$$

Hence, at resonance, an approximate expression for the peak reactive power due to the coupling is:

$$P_{mo} = \frac{T_m^2}{Q} \sqrt{\frac{L_t}{8\pi \, \mu_\tau \, r_m^3 \, r_t \, I_s}} \qquad (18)$$

where:

P_{mo} = peak power at resonance (watts)

Q = resonant torque magnification of the system.

In terms of the linear damping, either inherent in the drive system or artificially introduced by means of feedback, a simple relationship exists for systems with low damping:

$$\zeta = \frac{1}{2Q} \tag{19}$$

where:

ζ = coefficient of viscous damping in the overall transfer function of the torque control system associated with the peak due to resonance of the torsional coupling.

By controlling certain terms of the feedback signal in the torque control system it would be reasonable to expect a range of Q values between:

$$1 < Q < 25$$

The main drawback of the resonant coupling method would be the fact that the buildup of torque at the output of the system would depend upon the characteristic damping. If a constant amplitude sinusoidal command signal is applied to the system, the output torque will build up exponentially. The time constant of this response in terms of the system damping and resonant frequency is:

$$t_c = \frac{1}{2\pi f_u \zeta} \tag{20}$$

where:

t_c = time constant of the exponential envelope of the response

f_u = undamped resonant frequency of the system

5.7.7 Calculation of Placement Forces

As mentioned previously, the nett thrust applied to advance the apparatus, into the ground during the self-boring operation is comprised of two components:

(a) a tip thrust due to the action of the cutting head

(b) a frictional force developed on the walls of the in-situ apparatus due to contact with the soil.

In order to disturb the material ahead of the cutter as little as possible, the nett tip force must be close to the in-situ vertical stress times the sectional area of the apparatus, i.e.:

$$f_t = \pi r_o^2 g \left[(\rho_s - \rho_w)\, d + \rho_w d_w \right] \qquad (21)$$

where f_t = tip force

thus giving a maximum tip force $f_t = 2 \times 10^4$ N

Taking the case of sand as providing the greatest frictional forces on the surface of the in-situ apparatus:

$$f_s = 2\pi r_o h_t \sigma_n \tan\delta \qquad (22)$$

where f_s = force developed by frictional contact with soil

h_t = self-bored depth

δ = friction angle at the soil-shoe interface governing vertical relative measurement

Assuming $\tan\delta = 0.3$ and $h_t = 1.0$ metres, the component of thrust due to friction between the in-situ apparatus and the surrounding soil is:

$$f_s = 1.4 \times 10^5 \text{ N}$$

Hence, the approximate total thrust required for a self-bored depth of one metre is 1.4×10^5 N.

5.8 INSTRUMENTATION

5.8.1 Measurement of the Rotation of the Coupling Cylinder

The system employed for measurement of the small angular displacements of the in-situ coupling mechanism must fulfill the following requirements:

a) It must have an inherently broad dynamic range. Particularly for the single cylinder BSD, the limit to the dynamic range of the test could be imposed by instrumentation of the cylinder rotations.

b) The system must be compact and rugged. Space is limited in the in-situ apparatus, and the requirement for through access for removal of the soil while self boring is an added complication.

c) The rotations of the coupling cylinder are small. The measurement system must obviously be appropriately scaled to resolve these movements, but must also be tolerant of large rotations and displacements prior to placement.

The method proposed here is a novel solution whereby the instrumentation is added to the down-hole apparatus when the placement procedure is completed. Following the self-boring and jacking-out phases, the coupling cylinder is at a zero reference point for the ensuing dynamic bading history. It is only

at this point that it is necessary or indeed relevant to begin to measure the rotations of the coupling cylinder. Unless a technique such as this is employed, the rotation transducer must be capable of handling significantly larger rotations during general handling and placement than will be realized during the measurement process. Optical transducers in general posseses this ability, and they can even tolerate the unwanted displacement as an arbitrary offset or bias to the measurement range in which they are required to operate. They are, however, expensive and, for the very high resolution required in the BSD test, they are also bulky and fragile.

An appealing solution, which is in fact the one proposed in this study, is to couple the transducer into the in-situ apparatus immediately before the dynamic loading history is to begin. By this method, the only offsets introduced will be those inherent in the transducer itself and any contribution that may arise from the system employed to couple the transducer to the apparatus. The transducer would include a self locking attachment which would radially expand to grip the inside of the central bore in the coupling cylinder. Being a frictional coupling, the device would require no initial orientation or location and it would simply assume a zero displacement for the cylinder with respect to the reference system, at the point of locking on to the coupling cylinder. The displacement reference for the system is derived from a rigid rod coupled to an anchored frame at the ground surface. The transducer and locking system are mounted directly on the reference rod and are lowered into the in-situ apparatus following the removal of the auger or flush boring equipment.

The design suggested for the transducer employs a series of strain gauged cantilevers as displacement sensors. The cantilevers would be arranged as radial web type members coupling the reference rod to an outer cylinder (see Fig. 37). This outer cylinder is attached to or in part of the locking mechanism and hence follows the rotations of the coupling cylinder. The required gain of the transducer, determined by the strain in the cantilever surfaces for a given rotation, can be achieved in a given design by varying the length of the cantilevers and their radial position.

With the method proposed here, the sensitivity of the system could be changed very easily by replacement of the rotation transducer assembly. Alternatively it would be possible to employ transducers of different sensitivites in parallel to extend the dynamic range of measurement, although it should be remembered that the higher sensitivity device would have to be decoupled beyond a certain amplitude of rotation.

5.8.2 Measurement of the Coupling Cylinder Drive Torque

Here again, a strain gauge transducer is proposed. The most suitable location of the gauges would depend on the BSD configuration, i.e. the single or double cylinder device, but in any case the transducer would be configured on the shaft or tube driving the coupling cylinders on a uniform or gauge section close to the cylinder. Since the dynamic range required at this measurement is more a function of the depth of operation of the equipment, it is likely that adequate dynamic range will be provided at any given measurement location by a single transducer system. For the generally increasing drive torque required with increased depth of the test, it would be a simple matter to change transducers between tests. This would not significantly inconvenience the testing procedure since the entire

BSD apparatus is extracted from the boring between measurements in order that the cased hole can be achieved.

5.8.3 General

Much of the remaining instrumentation of the BSD apparatus, although operating in what may be described as harsh environmental conditions, is not regarded as particularly critical. Many of the measurements can be achieved using standard process control or geotechnical instrumentation equipment and therefore a discussion of the methods is not attempted here.

6.0 COUPLING CYLINDER DESIGN

6.1 INTRODUCTION

The design of the coupling mechanism with the corresponding investigation into the practical problems of operating and handling the proposed device in the field, has proved an invaluable exercise. Much discussion has taken place on matters such as the influence of soil properties, drilling procedures and instrumentation problems; the findings of this work have often resulted in modifications to the course of the project development. Equally, the findings of the analytical work have had direct and significant influences in the hardware design.

The following section presents a discussion of these developments and their influence on the prototype hardware design. Later, the overall design considerations for the coupling mechanism are listed and discussed, and the final design of the coupling mechanism is described. Aspects of the design affecting performance and manufacture are then dealt with and finally, a description of the laboratory testing apparatus is given.

6.2 DESIGN CONSIDERATION

As originally conceived, the BSD operated in a constrained system where two coupling cylinders provided complementary reaction torques for each other. The region in which high strains were to be induced was the space surrounding the borehole between the two cylinders. Hence a major portion of the coupling surface was distant from the zone of high strain and the effects of both

non-uniformity of contact and of hysterysis or backlash in the coupling cylinders were controllable in that they were dependent on the spacing of the cylinders.

However it was found that for most realistic configurations of the double cylinder BSD, $\tau_{r\theta}$ strains predominate over the $\tau_{\theta z}$ strains. Hence, as discussed earlier, the thrust of the study of the BSD test was directed towards the $\tau_{r\theta}$ strain and its effect on the design specifications for the apparatus.

6.2.1 Coupling Characteristics

For inducing strain the dominant $\tau_{r\theta}$ plane, the characteristics of the coupling mechanism become critical: the zone of high strain in the soil is small in relation to the coupling cylinder and the maximum value occurs at the interface between the soil and the cylinder. The state of stress or strain in the surrounding soil can only be inferred from measurement of applied torque and the resultant rotation of the cylinder. Hence the limit of resolution or dynamic range of the measurement is directly linked to the mechanical characteristics of the coupling cylinder. Of particular importance is the degree of backlash or hysteresis exhibited by the system under the reversing drive torque.

Backlash or hysteretic effects in the torque/displacement characteristics of the cylinder are likely to arise mainly from the mechanism which allows radial expansion of the cylinder. Some clearance must exist to permit this movement and, although it is proposed that a viscous lubricant be used between the moving surfaces, it must be accepted that some non-linear behavior will occur. In the section on design specifications, the range of maximum rotations of the coupling cylinder under the design maximum torque were found to be:

$$7.12 \times 10^{-4} < \theta_{01} < 1.78 \times 10^{-2} \text{ (rad)}$$

The radial movement which allows expansion of the coupling cylinder occurs near the surface and a tolerable lateral movement or clearance in this system can be determined from an equivalent rotation. The tangential displacements u at the surface of the coupling cylinder corresponding to the above rotations are

$$0.07 < u < 1.8 \text{ (mm)}$$

The required resolution of measurement must be applied to these displacements in order to determine the allowable lateral movements due to clearance in the coupling cylinder jacking system. The upper bound to the maximum displacements requires a total movement of less than 0.02 mm for 1% resolution which is not a particularly difficult accuracy to achieve in the manufacture of the coupling cylinder, but nonetheless falls within the realm of close-tolerance engineering. Clearly, for the lower bound, it would be highly impractical to expect to be able to achieve so small a backlash from purely machined and fitted components. Thus the coupling cylinder will rely heavily on the ability of the lubricant film on the jacking system bearing surfaces to take up the manufacturing clearances.

The critical effects of disturbance due to placement have been mentioned earlier. The T/θ relation derived from the apparatus will depend heavily on the state of the soil immediately surrounding the coupling cylinder, hence the magnitude and the extent of the disturbance are important factors.

For the jacking-on part of the placement procedure, the major contribution to disturbance is likely to arise from non-uniformities on the contact stresses at the soil/cylinder interface. The cylinder profile must be as regular and continuous as possible in order to minimize the effects of local yielding and

weakening. Such effects will certainly limit the degree of coupling attainable with the soil and, being in the critical measurement zone, could result in anamolous or unrepresentative data. To achieve the desired highly uniform contact with the soil, the mechanism which allows radial expansion of the cylinder must be comprised of a relatively large number of elements. Thus the departure from the ideal circular section with expansion will be minimized at least to the extent that manufacturing costs allow.

6.2.2 Torsional Stiffness

Finally, the discussion in this section on fundamental design considerations for the coupling cylinder, is the question of torsional stiffness of the device. In the process of coupling shear stress into the soil, the coupling cylinder will itself twist under the applied torsion. Hence a rotation along the cylinder will occur which will in effect reduce the nett stress applied to the soil. If not held to admissable limits, the effect would certainly degrade the measurements, particularly since it would be difficult to compensate for it in the analysis of the field data.

In order to assess the influence of twist in the cylinder, the ratio of twist in a non-rigid cylinder with one end fixed, to the rotation of a perfectly rigid cylinder in an elastic space (see section 3) is formulated. For a perfectly rigid cylinder bonded to the walls of a continuous hole in an elastic space, the ratio of rotation to applied torque is given by:

$$\frac{\theta_o}{T} = \frac{1}{2\pi\mu r_o^2 hF} \qquad (1)$$

For a non-rigid solid cylinder of shear modulus μ_t, the angular twist along the cylinder under an applied torque T (assuming that the cylinder is laterally free and fixed at one end) is given by:

$$\frac{\alpha}{T} = \frac{2h}{\pi \mu_t r_o^4} \tag{2}$$

Hence the ratio of twist to rotation is:

$$\frac{\alpha}{\theta_o} = \frac{4F\mu}{\mu_t} \left[\frac{h}{r_o}\right]^2 \tag{3}$$

This analysis is conservative. It neglects the effect of reducing torque in the cylinder away from the driving point. Furthermore, using the elastic modulus for the soil, the worse case or maximum soil stiffness is assumed. The analysis shows the simple ratio $\frac{h}{r_o}$ to be most critical in determining an acceptable stiffness for the coupling cylinder.

For worse case calculations,; $\mu = 5 \times 10^8$ N/m^2, $\mu_t = 8 \times 10^{10}$ N/m^2 and F = 2.3. this gives:

$$\frac{\alpha}{\theta_o} = 5.75 \times 10^{-2} \left[\frac{h}{r_o}\right]^2$$

The above result shows that the ratio of twist to rotation approaches 0.06 for a height to radius ratio of unity. The choice of the height to radius ratio is bounded on the othe. nand by consideration of end effects. These, it is felt, would be unacceptable for height to radius ratios less than 4. Hence using $\frac{h}{r_o} = 5$ the actual ratio for the prototype coupling cylinder:

$$\frac{\alpha}{\theta_o} = 1.44$$

which is felt to be a reasonable starting point in view of both the highly conservative nature of the calculations and of the worst case assumptions in the values used for the soil properties.

6.2.3 Summary Of Fundamental Design Considerations

The following list summarizes the fundamental design considerations discussed above together with additional practical considerations relevant to the design of a system suitable for operation in the field.

(a) Coupling to the soil: the coupling cylinder must be able to expand radially under controlled lateral stress. This feature allows the system to accommodate soil compaction and deformation under the combined static lateral and dynamic shear stresses.

(b) Torsional stiffness: In order to comply with the analytical model the cylinder should be torsionally rigid.

(c) Load characteristics: The design should yield minimal interaction between the dynamic shear stress and the static lateral stress applied to the soil.

(d) Coupling characteristics: non-linear hysteretic or backlash effects in the coupling cylinder load at least over the range of operation of the test, should be small in relation to the rotations inducing strain in the soil.

(e) Loading considerations: the coupling cylinder must withstand the loads applied during and resulting from the self boring operation. Principally,

these are the axial thrust transmitted through the cylindrical core to the cutting tip, and the shear forces acting on the cylinder surface due to adhesion and frictional contact with the surrounding soil.

(f) Surface profile: the desig1 should allow for interchangeable shoe-type segments to be fitted to the cylinder; different surface profiles can then be used to enhance coupling for a range of different soil types.

6.3 DESIGN OF THE PROTOTYPE COUPLING CYLINDER

The object of the hardware design and construction aspect of the project was to produce a prototype version of the coupling cylinder, upon which laboratory tests could be performed to investigate the more basic characteristics of the mechanism. Apart from the inherently enlightening process of design and manufacture, the exercise was aimed at producing some hardware which hopefully can be used in subsequent field trials. Certain features essential to the field version of the coupling cylinder are not incorporated in the first prototype. These features, it was felt, did not present a significant challenge in their design or manufacture and were better relegated to subsequent phases of the BSD development. The prototype described here, however, has been designed with many of these considerations in mind and should require no major modifications to incorporate any additional features required by the field version.

The design finally chosen for the coupling cylinder utilises a series of beams keyed into the surface of a hollow cylinder (see Fig. 37). The keys are rectangular in section and are ground to a precision fit with mating grooves in the surface of a thick walled cylinder. Lateral jacking forces are derived from a system of single-acting hydraulic pistons and cylinders located within the body of the keys and arranged at regular intervals along their length. Shear stress is coupled from the keys to the cylinder/soil interface by means of shoes which are attached to the outer faces of the keys. These shoes are curved in outside profile to achieve uniform contact with a circular opening, and are provided with a fine splined surface in order to enhance frictional coupling capabilities.

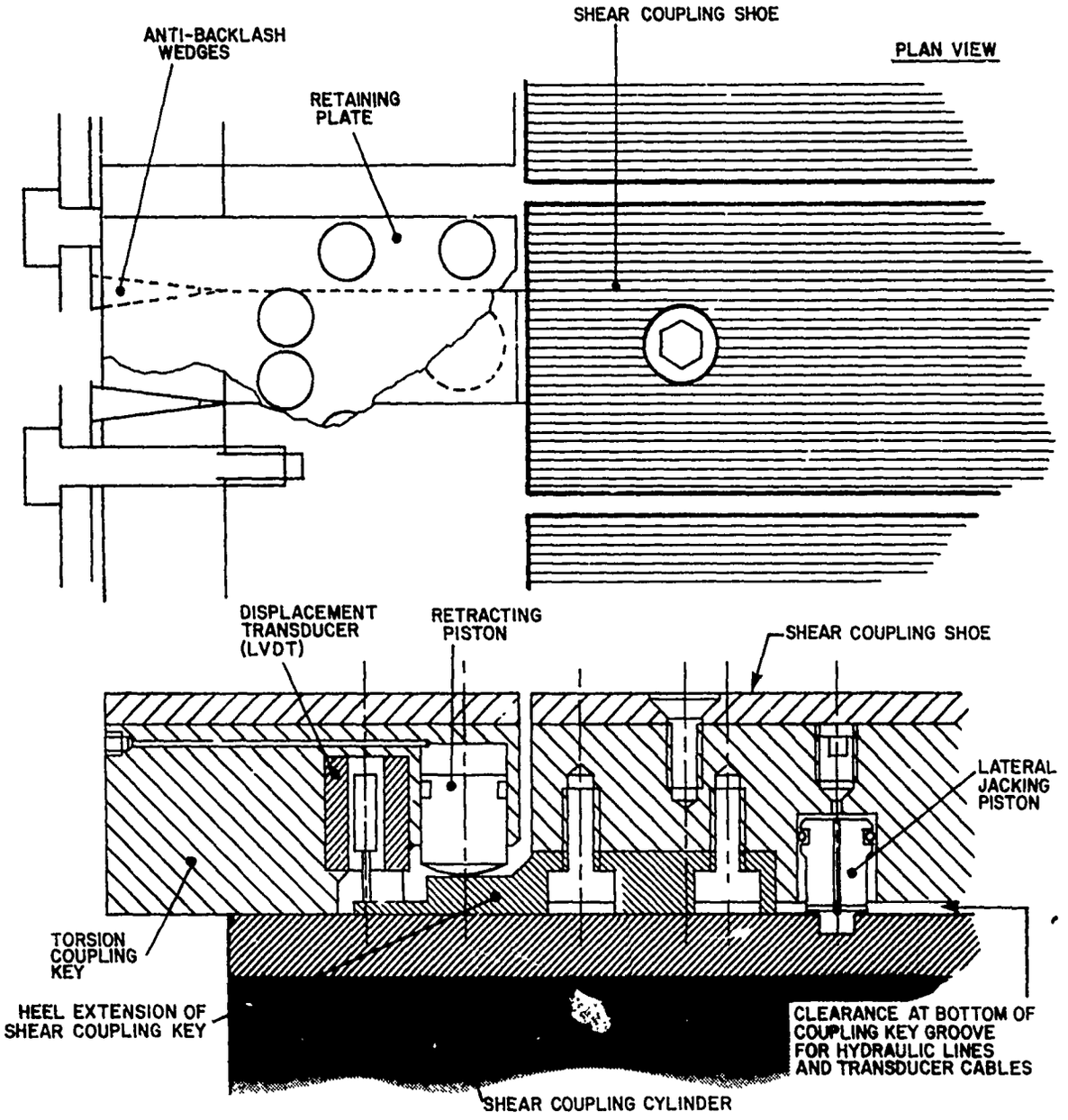

Figure 37. Plan view of the laterally moving keys

The concept of this design evolved from the reasoning that the maximum strength and torsional stiffness would be realized from a mechanism that approaches as closely as possible the optimum configuration of a thick walled hollow cylinder. Apart from the locations of the jacking pistons, the section of the design described above is a continuous, virtually solid thick-walled tube. Shear and compressive forces are applied to the components of the cylinder uniformly and over large contact areas. Hence the design attempts to minimize stress concentrations with their inherent penalty of inefficiency of load rating and reduced service life.

Torsion is applied by means of another set of keys located at one end of the grooved cylinder. These keys are similar in section to the laterally moving keys, but they are force-fitted into the cylinder and are utlised only in coupling load to the walls of the cylinder grooves. The keys are tapered in section leading axially out of the cylinder, the taper forming part of an anti-backlash high torque coupling which employs wedges to eliminate clearances. These wedges normally bear on the walls of the keys protruding from the cylinder and are normally preloaded by means of sprung plates.

For retracing the laterally moving keys, an arrangement similar to the integral jacking pistons mentioned earlier is proposed (see Fig 37.) This would again be a single-acting piston and cylinder arrangement machined into the fixed keys and arranged to apply load laterally inwards. The scheme suggested for the final design utilizes a domed headed piston acting on a heel extension of the laterally moving keys. Provision has been made in the design of the prototype coupling cylinder to incorporate this system and a means of measuring the positions of the ends of the moving keys into the apparatus.

A clearance is deliberately provided between the laterally moving keys and the bottom of the grooves in the central cylinder. This space, being relatively distant from the surface of the cylinder does not significantly degrade the torsional stiffness; it does, on the other hand, serve a number of practical uses:

(a) It allows a loose tolerance on the depth of the grooves and also allows that the close tolerance on the groove width does not have to be maintained to the bottom.

(b) The bottom corners of the groove can be rounded to minimize stress concentrations.

(c) Transducer cables and small hydraulic pipes can be routed through the cylinder and afforded good protection.

The lateral jacking pistons are mushroom shaped structures protruding from the bottom of the cylinder grooves. The necking or relief away from the sealing ring on the piston allows the key to tilt whilst requiring only a minimum of radial clearance. Five pistons are arranged along the keys to distribute the jacking load and each unit is through-fed on a common hydraulic line. For the laboratory prototype coupling cylinder, no provision has been incorporated to isolate these pistons from the shear stresses that would result from any loads applied to the keys in the direction of the axis of the coupling cylinder. These loads, as mentioned in the section on design considerations, will arise from frictional contact of the shoe segments of the cylinder surface with the surrounding soil. It may be that for most soil conditions encountered in

testing, these shear stresses may not damage the pistons and that no special clamps or stops are required to absorb the load. However, if required, it is suggested that for the field design the fixed keys in the top of the cylinder be closely butted to the moving keys to form a stop. Obviously this technique cannot also be used to absorb loads due to extraction of the apparatus, however, it is likely that upon retraction of the coupling keys, the frictional contact with the soil will be considerably reduced. Under these circumstances, it is almost certain that the jacking pistons will easily withstand the axial loads on the shoe segments.

6.4 ASSEMBLY AND TESTING OF THE PROTOTYPE COUPLING CYLINDER

Assembly

The mechanical functions of the coupling cylinder are threefold; to supply a radial pressure to the soil to restore the lateral in-situ stresses, to key into the soil so that torsional loads may be applied and then to transmit those loads. The complete set of design drawings are included in Appendix VI together with a set of photographs of the device and test equipment. The reimposition of the radial soil stresses and the keying are both achieved by the radial expansion of the twelve shoes, whilst the torque is transmitted by imposing a small rotation about the vertical axis. These two mechanical actions are mutually conflicting in the configuration adopted. Radial movement is accommodated by the provision of slides which must have some circumferential clearance to avoid binding through metal-to-metal welding. On the other hand, the anticipated rotations of the cylinder when applying a couple to the soil would be of the order of 0.03 degrees, corresponding to an absolute movement at the circumference of the cylinder of about 0.05 mm, comparable with the clearance

necessary to ensure satisfactory slide operation. The slides therefore had to be manufactured with minimal clearance, necessitating careful hand fitting and scraping. Because of the length of these slides the accuracy of the final result was dependent upon the straightness of the slots and of the slide bars. Inevitably each bar had to be selectively fitted into a specific slot.

The workmanship was to a high standard. Only two bar and slot pairs showed any circumferential clearance which could be detected by hand when clean and oil-free. The others tended to bind when dry but moved smoothly and progressively with steady resistance when lubricated (there qualitative observations were made before the six pistons were inserted). It is therefore concluded that the cylinder was manufactured to a standard which closely matched the fine tolerances demanded by the design.

The fix pistons were found to be in accurate alignment with the cylinders on each of the sliding bars (a total of 60) and no problems were encountered with their operations. Nevertheless, it is now realized that the pistons should be re-designed because, to avoid alignment problems, they were manufactured 0.08 mm under-size on this diameter with the result that the 'O' ring seals would be intruded at hydraulic pressures in excess of 35 MPa.

Testing

The objective of the mechanical testing of the coupling cylinder was to simulate its operation under laboratory conditions so that potential problems could be identified. The tests were conducted using a dummy borehole fabricated from a length of 203 mm (8 inch) bore mild steel tube with support flanges welded at each end.

In the initial stages of testing, the tube was lined with wooden strips to reduce its internal diameter to 185 mm and to provide a deformable material into which the shoes could key. To contact the wood each shoe had to be jacked out through a mean radial distance of 6 mm. These tests proved that the radial loading system worked satisfactorily and, once all hydraulic leaks had been located, it was possible to hold hydraulic oil pressures of 14 MPa in the shoe rams for periods of several hours. All rams functioned smoothly at pressures above 700 KPa without undue sticking.

Torque loading was applied to the coupling device by a pair of hydraulic rams, bolted to the top flange of the dummy borehole. These acted tangentially onto a reaction plate bolted to the cylinder. To ensure that the torque was transmitted uniformly to each shoe, this reaction plate was positively keyed to each of the radial slide slots by a series of metal wedges. These torque rams were loaded by a hand operated hydraulic pump with a pressure gauge to monitor the applied load.

When attempting to apply significant torque loads to the device it was found that slipping occurred between the wood and the shoes because of their failure to key by mechanical identation. Methods of enhancing the coefficient of friction between the two, such as interposing a thin rubber sheet, proved unsuccessful. These difficulties were overcome by using sand as the locking mechanism, an approach which was taken with reluctance because this prototype cylinder incorporated no design features for excluding sand from the precision sliding surfaces.

Prior to exposing the cylinder to the sand, the gaps between the shoes were packed with mastic sealing strip. The cylinder was supported concentrically within the dummy borehole and a simple annular seal was made with modelling clay at the bottom of the borehole tube, between the wood lining and the shoes. Dry sand was poured

down the annular gap and manually compacted. The shoes were then radially expanded to key intc the sand and further compact it. With this system it was found that slipping occurred at a torque which was proportional to the radial jacking pressure. At the maximum hydraulic pressure which could be applied to the shoes (18.5 MPa, an effective radial pressure on the sand of 0.49 MPa) slipping occurred at an applied torque of 5×10^3 Nm.

Short of setting the cylinder in concrete or epoxy-resin, the testing has demonstrated that the cylinder is well able to operate over the range of applied loads which will normally be encountered in service and the sufficient confidence has been gained to extrapolate that, where a positive key can be made with the soil, the device will operate satisfactorily at its maximum torque.

7.0 CONCLUSIONS AND RECOMMENDATIONS

A concept has been proposed for an in-situ measurement device designed to determine the soil secant modulus as a function of strain for levels up to failure. This device first bores itself into the soil with minimal disturbance; it then lays itself into the soil and at the same time re-imposes the lateral stresses by radially expanding a number of axial shoes against the sides of the bored hole. A harmonic rotation of increasing amplitude is then applied and the torque and corresponding angular rotation are measured to determine the stiffness characteristics of the soil. The apparatus has been named the Borehole Shear Device (BSD).

Based on the authors' assessment of the state-of-the-art, such a device is presently required for producing reliable soil properties for site characterisation and subsequent analysis. Existing procedures for determining the soil modulus over the required range of strains suffer important drawbacks; past attempts to produce a device able to operate in-situ over the complete range of strains have not been totally successful.

This report summarises the research efforts conducted during the first phase of work orientated towards production of an operational BSD. The activities undertaken were:

- A literature search and critical assessment of the state-of-the-art
- Analytical and numerical studies to predict the characteristics of the BSD operation and the effects on the soil; also to aid the configuration of the test and the instrumentation required.

- The specification of a procedure to derive the value of the soil secant shear modulus as a function of the shear strain level, based on the values of the torque and the rotation measured in the field. This procedure attempts to minimise possible errors which might result from the presumed constitutive behaviour of the soil.
- A conceptual design of the BSD, its instrumentation requirements and mode of operation.
- Detailed design, construction and laboratory testing under the design torque of the radially expanding cylinder.

All of the above tests have been duly completed. As a consequence of this work, a number of conclusions have been reduced. They can be summarised thus:

1 From the theoretical studies conducted and the analysis of the hardware required, the construction and operation of the BSD seems to be feasible and desireable.

2. A single-point measurement technique appears more adequate, rather than uphole, crosshole or other alternative test configurations. This refers only to normal operation of the device; it will probably be convenient though to install extra instrumentation during initial field trials with the purpose of confirming particular details of the operation of the BSD.

3. Two concepts have been provided: a double-cylinder and a single-cylinder operation. Although no decisions on this matter were required during the present phase of the work, the latter seems to be more advantageous both technically and economically; hence the full development of the single-cylinder BSD is that proposed for future work.

4. At the design frequencies of the BSD (about 10 Hz), wave-lengths are large compared to all the dimensions of the test. Also, contrary to the initial concept and the test in which it was expected to impose major $\varepsilon_{\theta z}$ strains, the main component of the strain was found to be $\varepsilon_{r\theta}$ and the shear modulus corresponds to this type of deformations.

5. It is important to minimise the disturbance of the soil around the BSD. As a consequence, the latter has been provided with a self-boring tool.

6. A procedure has been devised for deriving other shear modulus as a function of strain from torque and rotation measurements. The procedure is based in progressive hyperbolic approximations and has been successfully tested for hyperbolic and non-hyperbolic soil constitutive laws.

7. It is also concluded from the analysis that stiffer or softer layers close to the BSD will affect the measurements by very small amounts. In soils of low sensitivity, the effect of disturbance around the borehole will also be small due to the self-boring placement and to the fact that the lateral normal stresses are theoretically recovered.

8. Close-form solutions reported include: full dynamic long-cylinder solutions for several constitutive laws; full dynamic long-cylinder solutions for elastic soil (with or without damping); and torque-rotation relationships for the case of a finite cylinder at finite depth in elastic soil.

9. Numerical solutions were based on the finite element method; an equivalent linear procedure was implemented to produce solutions in the frequency domain. Non-reflecting boundaries of the Lysmer-Waas and Lysmer-Kuhlemeyer types were included in the model. Excellent

agreement was shown with existing close-form solutions. Numerical solutions were used for all non-linear dynamic cases and some elastic ones. At the frequencies of interest, the real part of the dynamic solutions essentially coincides with the static one; this is particularly important for constructing the procedure for derivation of the shear modulus from the field data.

10. Displacement and strain distributions have been obtained for the cases of interest. Although those have not provided quantitative data in usable form, they have produced essential qualitative information, such as the relative importance of $\tau_{r\theta}$ versus $\varepsilon_{\theta z}$ strains, the progressively faster decrease of the strain level away from the BSD as the soil becomes more non-linear, etc.

11. The cylinder and radially expanding keys were designed and built. Laboratory expansion and torsion tests showed this part of the BSD to perform adequately for the purposes intended up to the design radial pressures and torques.

It is recognised that the work reported here constitutes only a first step towards the solution of a difficult problem. In order to continue this effort in the most appropriate manner, several recommendations are proposed here based on the results and experience achieved to this point:

1. The work should continue towards production and operation of the BSD. No more theoretical work is deemed necessary at this point, at least until the device starts undergoing field tests.
2. It is recommended that the single-cylinder concept be preferred instead of the double-cylinder one because of the reasons stated in the report.

3. Due to the unknowns present in all development work it is proposed that on the basis of experience gained to date the remaining work be tackled in two separate phases: to design and manufacture the mechanical system relating to the torque loading so that the concept can be tested and developed under more realistic conditions and, the final phase, to manufacture the self-boring device and fit all instrumentations so that full field trials can be performed.

8. REFERENCES

1 Schnabel, P.B., Lysmer, J., Seed, H.B., (1972) "SHAKE a Computer Program for Earthquake Response Analysis of Horizontally Layered Sites", Report No. EERC 72-12, University of California, Berkeley, Dec. 1972

2 Seed, H.B., Idriss, I.M, (1970) "Soil Moduli and Damping Factors for Dynamic Response Analysis", Report No. EERC 70-10, University of California, Berkeley, Dec. 1970.

3 Stokoe, K.H., Arnold, E.J., Hoar, R.J., (1978) "Development of a Bottom-hole Device for Offshore Shear Wave Velocity Measurement", Offshore Tech. Conf. paper 3210, May 1978

4 Stokoe, K.H. Richart, F.E., (1973) "Shear Moduli of Soils, In-Situ and from Laboratory Tests", Proc. of the Fifth World Conf. on Earthquake Eng., Vol. 1, Rome, Italy, (1973), pp. 356-359

5 Anderson, D.G., Stokoe, K.H., (1978) "Shear Modulus, A Time-Dependent Material Property", "Dynamic Soil and Rock Testing in Field and Laboratory for Seismic Studies",ASTM STP, (1978)

6 Anderson, D.G., Woods, R.D., (1976) "Time-Dependent Increase in Shear Modulus of Clay", Journal of the Geotechnical Eng. Div., ASCE, May 1976, pp. 525-537

7 Timoshenko, S.P., Goodier, J.H., (1951) "Theory of Elasticity", Third Edition, McGraw Hill, New York.

8 Ewing, W.M., Jardetzky, W.S., Press, T., (1957) "Elastic Waves in Layered Media", McGraw-Hill, New York

9 Duke, M., (1969), "Techniques for Field Measurement of Shear Wave Velocity in Soils", Fourth World Conf. in Earthquake Eng., Santiago, Chile, 1969

10 Richart, F.E., Hall, J.R., Woods, R.D., (1970) "Vibrations of Soils and Foundations", Prentice Hall, 1970

11 Mooney, H.M., (1974) "Seismic Shear Waves in Engineering", Jour. of Soil Mech and Found. Div., ASCE, Aug 1974, pp. 905-923

12 Schwarz, S.D., Conwell, P.R., (1974) "A Technique for In-Situ Measurement of Shear Wave Velocities (Vs) for Deep Marine Foundations", Offshore Tech. Conf., paper 2014, May 1974

13 Lande, G., (1974) "Seismologisk Metod for In-Situbestamaning av Jord- och Bergdynamiska P[illegible]ter", Bjerking Ingenjorsbyra, Uppsala, Sweden

14 Kurzeme, M., (1971) "In-Situ Investigations Using SH-Waves", J. of the Soil Mech. and Found. Div., ASCE, Feb. 1971, pp. 341-356

15 Jones, R., (1960) "Measurement and Interpretation of Surface Vibrations on Soil and Roads", Highway Research Board Bulletin, 1960

16 Jones, T.R., (1962) "Surface Wave Technique for Measuring the Elastic Properties and Thickness of Roads: Theoretical Development", Brit. J. Appl. Physics, 1962, Vol. 13, pp. 21-29

17 Fowler, J., (1972) "An Evaluation of an Existing Procedure for Determining Shear Moduli at Depths by In Situ Vibration Technique", Technical Report S-72-5, WES, Vicksburg, Mississippi, April 1972

18 Ballard, R.F., McLean, F.G., (1975) "Seismic Field Methods for In Situ Moduli", Proc. of the Conf. on In Situ Measurement of Soil Properities, ASCE, June 1975, Vol. 1, pp. 121-150

19 Stokoe, K.H., Woods, R.D., (1972) "In-Situ Shear Wave Velocity by the Cross-Hole Method", J. of Soil Mech. and Found. Div. ASCE, May 1972, pp. 443-460

20 Swain, R.J., (1962) "Recent Techniques for Determination of In-situ Elastic Properties and Measurement of Motion Amplification in Layered Media", Geophysics, Vol. 27, No. 2, April 1962, pp. 237-241

21 Tanimoto, K., Kurzeme, M., (1973) Discussion of Stokoe et al, J. of Soil Mech. and Found. Div., ASCE, April 1973, pp. 351-353

22 Auld, B., (1977) "Cross-Hole and Down-Hole vs by Mechanical Impulse", Journal of the Geotechnical Eng. Div., ASCE, Dec. 1977, pp. 1381-1398

23 Ballard, R.F., Leach, R.E., (1969) "Development of a Vibropacker System for Inducing Polarize Shear Waves and Compression Waves at Depth", S-69-30, WES, Vicksburg, Mississippi, July 1969

24 Miller, R.P., Brown, F.R., (1972) "Shear Modulus Determination of Soils by In-Situ Methods for Earthquake Engineering", Proc. of the Int. Conf. of Micromization for Safer Construction, Research and Application, Seattle, Washington, Nov. 1972, pp. 319-335

25 Miller, R.P., Troncoso, J.H., Brown, F.R., (1975) "In-Situ Impulse Test for Dynamic Shear Modulus of Soils", Proc. of the Conf. on In Situ Measurement of Soil Properties, ASCE, June 1975, Vol 1, pp. 319-335

26 Troncoso, J., (1975) "In-Situ Impulse Test for Determination of Soil Shear Modulus as a Function of Strain", Ph.D. Thesis, Dept. of Civil Eng., University of Illinois at Urbana-Champaign, 1975

27 Boyer, G.R., Oien, M.A., (1972) "Steady Motion of a Torsional Oscillator Clamped in a Borehole", Journ. of Sound and Vibration, (1972) 23 (2), pp. 175-186

28 Lysmer, J., Waas, G., (1972) "Shear Waves in Plane Infinite Structures", Journ. of Eng. Mech. Div., ASCE, Feb. 1972, pp. 85-105

29 Lysmer, J., Kuhlemeyer, R.L., (1969) "Finite Dynamic Model for Infinite Media", Journal of Eng. Mech. Div., ASCE, Aug. 1972, pp. 859-877

30 Hughes, J.M.O., Wroth, C.P., Windle, D., (1977) "Pressuremeter Tests in Sands", Geotechnique 27, No. 4, pp 455-477

31 Windle, D., Wroth, C.P., (1977) "The Use of Self-Boring Pressuremeter to Determine the Undrained Properties of Clays", Ground Engineering, Sept. 1977

APPENDIX A

LIST OF SYMBOLS

b	height of rectangular finite element
d	depth from the soil surface
d_w	depth from water table
D	normalized depth from the soil surface
E	Young's modulus
E_m	reactive energy
f	frequency
f_I	imaginary part of the influence function
f_o	frequency of operation of the torsional drive
f_r	resonant frequency of the coupling cylinder
f_R	real part of the influence function
f_s	vertical force developed by friction
f_t	tip force
f_u	undamped resonant frequency of the system
F	influence function
F_E	influence function for the elastic soil
F_H	influence function for the hyperbolic soil
g	gravitational constant
h	height of the BSD's snoe
h_t	height of the self boring
$H_1^{(1)}$	Hankel function of the first kind and order one
$H_2^{(2)}$	Hankel function of the second kind and order one
$H_2^{(2)}$	Hankel function of the second kind and order two
i	complex constant

I_s	lumped moment of inertia of the coupling tube and drive system
J_o	Bessel function of the first kind and order zero
J_1	Bessel function of the first kind and order one
K_o	coefficient of lateral earth pressure
K_T	torsional stiffness of the hollow tube
L_T	length of the hollow tube
m_j	lumped mass in a finite element node
P_m	maximum reactive forces power
P_{mo}	peak power at resonance
Q	resonance magnification of the system
r	radial coordinate
r_o	radius of the borehole
r_1	internal radius of a hollow tube
r_2	external radius of a hollow tube
r_m	mean radius of the coupling tube
r_t	thickness of the coupling tube
R	normalized radius of the BSD
t	time
t_c	time constant of the exponential envelope of the response
T	torque per unit length
T_{EF}	torque per unit length in a finite cylinder with elastic soil
T_{EL}	torque per unit length in an infinite cylinder with elastic soil
T_F	torque per unit length in a finite cylinder

T_{HF}	torque per unit length in a finite cylinder with hyperbolic soil
T_{HL}	torque per unit length in an infinite cylinder with hyperbolic soil
T_{ℓ}	torque per unit length
T_L	torque for an infinite cylinder
T_m	maximum torque applied to the coupling cylinder
u	tangential displacement
u_j	tangential displacement at a FE node
u_o	tangential displacement at the borehole wall
u_r	radial displacement
u_θ	tangential displacement
v_p	velocity of compressional waves
v_R	velocity of Rayleigh waves
v_s	velocity of shear waves
Y_o	Bessel function of the second kind and order zero
Y_1	Bessel function of the second kind and order one
z	vertical coordinate
α	angular twist over the height of the cylinder
δ	friction angle in the soil-shoe interface
ϵ	shear strain
ϵ_e	equivalent strain
ϵ_o	shear strain in the borehole wails

$\varepsilon_{r\theta}$, $\varepsilon_{\theta z}$	shear strain components
ζ	coefficient of linear viscous damping
θ	rotation angle
θ_o	rotation angle at the borehole wall
θ_{om}	maximum rotation angle in the borehole
ϕ	internal friction angle of the soil
λ	Lame constant
μ	secant shear modulus
μ_t	secant shear modulus of the tube
μ_j	shear modulus of the soil in the finite element zone
μ_o	shear modulus of the soil at low strain (elastic)
μ_r	reference shear modulus
ν	Poisson's ratio
ρ	density of the material
ρ_s	density of the soil
ρ_w	density of water
σ_{lm}	maximum lateral jacking pressure
σ_r	radial normal stress
σ'	effective confining pressure
σ'_h	effective lateral stress
σ'_{rf}	reference effective confining pressure
τ	shear stress
τ_m	limiting shear stress
τ_o	shear stress at the cylinder-soil interface

$\left.\begin{matrix}\tau_{r\theta}\\ \tau_{\theta z}\end{matrix}\right\}$	shear stress components
ω	angular velocity

APPENDIX B

NON-REFLECTING BOUNDARIES

As mentioned in Chapter 4, two different non-reflecting boundaries have been used:

- A permanent non-reflecting boundary of the Lysmer-Waas type has been provided at the cylindrical boundary.
- An optional non-reflecting boundary of the Lysmer-Kuhlemeyer type was implemented at the upper boundary.

In either case, the purpose of such boundaries is to guarantee that the phenomena predicted inside the finite domain modelled are those which would be observed if the domain modelled extended to infinity. That is to say, that the relatively arbitrary location of the boundaries does not affect in any way the calculations.

B.1 THE LYSMER-WAAS AXISYMMETRIC BOUNDARY

The basic assumptions embodied in the axisymmetric version of this boundary are:

- The soil properties outside the boundaries are linear and change only with depth.
- The particle velocity takes place only in the θ direction.
- Waves arriving at the boundary are locally cylindrical.

The implementation of the Lysmer-Waas boundary requires the determination of the following:

- The stiffness matrices at the boundary elements, that is, the relation between forces and displacements at the boundary nodes accounting for the fact that the soil extends all the way to infinity.

- The forces introduced at the boundary of the finite domain due to the presence of the external soil which is not modelled by the mesh.

The following derivations will be pursured in parallel with those presented in the original plane-strain version of this boundary (Lysmer and Waas, 1972)[28]. Figure B 1 shows the finite-element mesh.

Due to one of the basic assumptions of the FE method, the displacement at any point of a rectangular axisymmetric element are (since only out of plane displacements occur):

$$\delta\ (r,z) = \|d\| \ \{\delta\} \tag{1}$$

where $\|d\| = \frac{1}{hb} \ \|(b-z)\ (h-r) \quad z(h-r) \quad zr \quad r(b-z)\|$

$\{\delta\}$ is the matrix of the displacements at the four corners (Fig. B 2)

The strains can be be derived from the displacements:

$$\begin{Bmatrix} \varepsilon_{r\theta} \\ \varepsilon_{z\theta} \end{Bmatrix} = \begin{Bmatrix} \frac{\partial}{\partial r} - \frac{1}{r + r_o} \\ \\ \frac{\partial}{\partial z} \end{Bmatrix} \delta(r,z) = \left[D \right] \ \{\delta\} \tag{2}$$

$$\left[D \right] = \frac{1}{hb} \begin{bmatrix} \frac{-(b-z)(r_o+h)}{r_o+r} & \frac{-z(r_o+h)}{r_o+r} & \frac{zr_o}{r_o+r} & \frac{(b-z)r_o}{r_o+r} \\ \\ -(h-r) & h-r & r & -r \end{bmatrix}$$

All other strain conponents vanish everywhere.

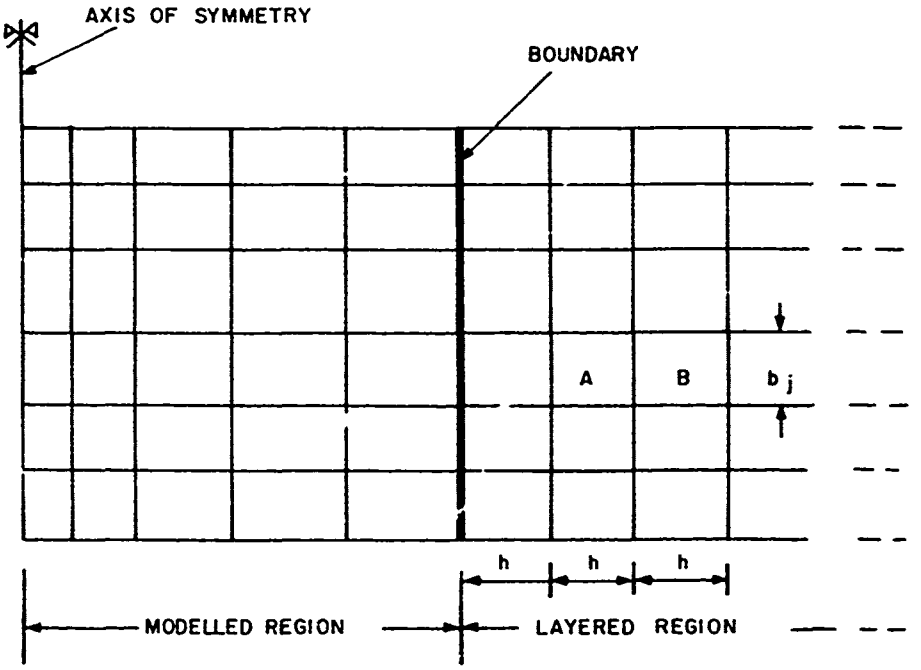

FIG. B.1 FE MODEL AND OUTSIDE REGION

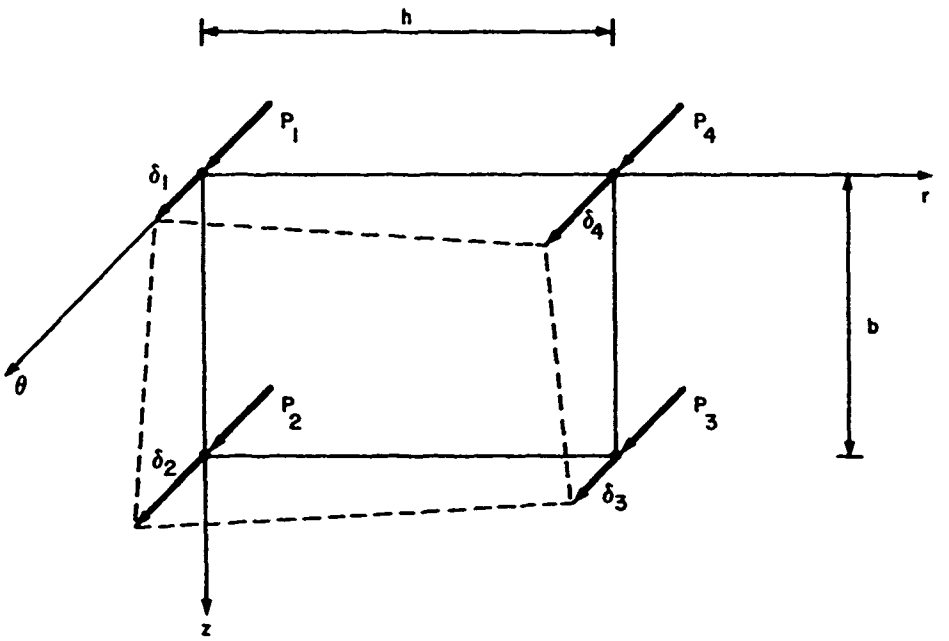

FIG. B.2. FORCES AND DISPLACEMENTS OF A RECTANGULAR AXISYMMETRIC ELEMENT.

The stress components are:

$$\begin{Bmatrix} \tau_{r\theta} \\ \tau_{z\theta} \end{Bmatrix} = \mu_j \begin{Bmatrix} \varepsilon_{r\theta} \\ \varepsilon_{z\theta} \end{Bmatrix} = \mu_j \left[D \right] \{ \delta \} \qquad (3)$$

where μ_j is the corresponding shear modulus.

The forces per unit radian acting on the corners of each element can then be related to the nodal displacements:

$$\{ \quad \} = \left[K \right]_j \{ \delta \} \qquad (4)$$

where $\left[K \right]_j = \mu_j \iint [D]^T [D] \; (r_o + r) \; dr \; d\theta$ is called the stiffness matrix of the element.

When the above integration is carried out, the stiffness matrix can be derived.

$$\left[K \right]_j = \frac{\mu_j}{h^2 b} \left[\begin{array}{c|c|c|c} \frac{m}{3}(1+\alpha)^2 + \frac{p}{3} + \frac{q}{12} & & & \\ \hline \frac{m}{6}(1+\alpha)^2 - \frac{p}{3} - \frac{q}{12} & \frac{m}{3}(1+\alpha)^2 + \frac{p}{3} + \frac{q}{12} & & \\ \hline -\frac{m}{6}(1+\alpha) - \frac{p}{6} - \frac{q}{12} & -\frac{m}{3}(1+\alpha) + \frac{p}{6} + \frac{q}{12} & \frac{m}{3} + \frac{p}{3} + \frac{q}{4} & \\ \hline -\frac{m}{3}(1+\alpha) + \frac{p}{6} + \frac{q}{12} & -\frac{m}{6}(1+\alpha) - \frac{p}{6} - \frac{q}{12} & \frac{m}{6} - \frac{p}{3} - \frac{q}{4} & \frac{m}{3} + \frac{p}{3} + \frac{q}{4} \end{array} \right] \qquad (5)$$

where $m = b^2 r_o^2 \ln(1+\alpha)$

$p = r_o h^3$

$q = h^4$

$\alpha = \frac{h}{r_o}$

B .1.1 Stiffness Matrix for External Elements

Let us now concentrate in the region outside the boundary. In any two elements (A and B in Fig. B.3).

$$\{\delta\}_A = \begin{bmatrix} D' & O \\ O & D' \\ O & 1 \\ 1 & O \end{bmatrix} \begin{Bmatrix} u_j \\ u_{j+1} \end{Bmatrix} \tag{6}$$

$$\{\delta\}_B = \begin{bmatrix} 1 & O \\ O & 1 \\ O & D \\ D & O \end{bmatrix} \begin{Bmatrix} u_j \\ u_{j+1} \end{Bmatrix}$$

The coefficients D and D' are easily obtained from the solution for cylindrical Love-wave propogation in the positive r-direction:

$$u = u_o(z)\, H_1^{(2)}(kr) e^{i\omega t} \tag{7}$$

where $u_o(z)$ is an amplitude depending on depth

k is the wave number (ω/v_s)

$H_1^{(2)}$ is the Hankel function of second kind and order 1.

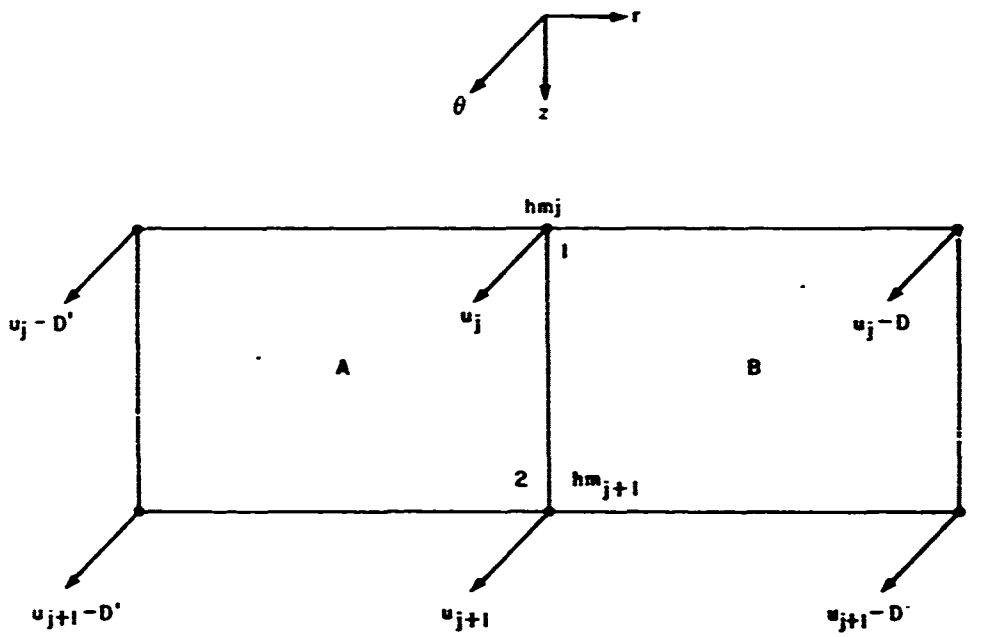

FIG. B.3. DISPLACEMENTS OF ELEMENTS A AND B

Then:

$$D = \frac{H_1^{(2)}\left[k(r_o+h)\right]}{H_1^{(2)}(kr_o)}$$

$$D' = \frac{H_1^{(2)}\left[k(r_o-h)\right]}{H_1^{(2)}(kr_o)} \tag{8}$$

... all values of h:

$$D = 1 + khF + (kh)^2 S$$

$$D' = 1 - khF + (kh)^2 S \tag{9}$$

where

$$F = \frac{1}{H_1^{(2)}(kr_o)} \left.\frac{dH_1^{(2)}(\alpha)}{d\alpha}\right|_{\alpha = kr_o}$$

$$S = \frac{1}{2H_1^{(2)}(kr_o)} \left.\frac{d^2H_1^{(2)}(\alpha)}{d\alpha^2}\right|_{\alpha = kr_o}$$

In order to derive the forces in the two nodes common to A and B (nodes 1 and 2):

$$Q_{j1} = \left\|K_4\right\|_A \{\delta\}_A + \left\|K_1\right\|_B \{\delta\}_B$$

$$Q_{j2} = \left\|K_3\right\|_A \{\delta\}_A + \left\|K_2\right\|_B \{\delta\}_B \tag{10}$$

where $\left\|K_r\right\|_A$ stands for the r^{th} row of the stiffness matrix of element A.

By performing the operations indicated above and taking h→0, the following expression can be obtained relating the force and the displacements at nodes 1 and 2.

$$\begin{Bmatrix} Q_{j1} \\ Q_{j2} \end{Bmatrix} = \frac{\mu_j h r_o}{b} \begin{bmatrix} 1 + \frac{1}{3}M & -1 + \frac{1}{6}M \\ -1 + \frac{1}{6}M & 1 + \frac{1}{3}M \end{bmatrix} \begin{Bmatrix} u_j \\ u_{j+1} \end{Bmatrix} \qquad (11)$$

where $M = \left(\frac{b}{r_o}\right)^2 \left[1 - kr_o F - 2(kr_o)^2 S\right]$

It can be readily seen from the recurrence formulae between Hankel functions that:

$$1 - kr_o F - 2(kr_o)^2 S = (kr_o)^2$$

which substituted above, yields:

$$\begin{Bmatrix} Q_{j1} \\ Q_{j2} \end{Bmatrix} = \frac{\mu_j h r_o}{b} \begin{bmatrix} 1 + \frac{1}{3}(bk)^2 & -1 + \frac{1}{6}(bk)^2 \\ -1 + \frac{1}{6}(bk)^2 & 1 + \frac{1}{3}(bk)^2 \end{bmatrix} \begin{Bmatrix} u_j \\ u_{j+1} \end{Bmatrix} \qquad (12)$$

B .1.2 External Boundary Forces

Consider again Fig. B.3 where the boundary now splits the two zones A and B (Fig. B.4).

From equation (3), for z = 0 and r = 0.

$$\tau'_{r\theta} = \frac{\mu_j}{r_o h b} \left\| -b(r_o+h) \quad 0 \quad 0 \quad br_o \right\| \begin{Bmatrix} u_j \\ u_{j+1} \\ \Delta u_{j+1} \\ \Delta u_j \end{Bmatrix}$$

$$= \frac{\mu_j u_j}{r_o h} \left[r_o D - r_o - h \right] \qquad (13)$$

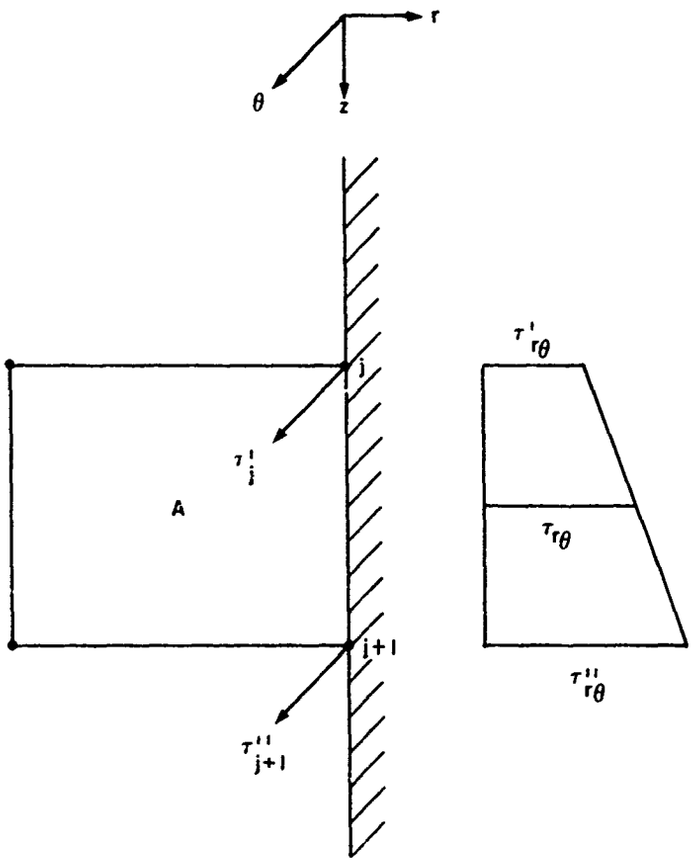

FIG. B.4. STRESS DISTRIBUTION ON CYLINDRICAL BOUNDARY

where $D = 1 + Kh\ F$ since second order terms can now be neglected.

$$F = \frac{1}{H_1^{(2)}(kr_o)} \left. \frac{dH_1^{(2)}(\alpha)}{d\alpha} \right|_{\alpha = kr_o}$$

$$= -\frac{1}{kr_o} + \frac{H_o^{(2)}(kr_o)}{H_1^{(2)}(kr_o)} \qquad (14)$$

which substituted into (13) yields:

$$\tau'_{r\theta} = \frac{\mu_j u_j}{r_o} \left[-2 + Kr_o \frac{H_o^{(2)}(Kr_o)}{H_1^{(2)}(Kr_o)} \right] \qquad (15)$$

As a matter of interest, note that the static solution can be derived from equation (15) by taking the limit when $k \to o$. Then, the same result provided in Table 2 is obtained:

$$\tau'_{r\theta} = -\frac{2\mu_j u_j}{r_o}$$

Similarly, the plane-strain solution is recovered at the limit when $r_o \to \infty$. In this case, the solution obtained is identical to that found by Lysmer and Waas (1972)[28]:

$$\tau'_{r\theta} = \mu_j u_j k \lim_{r_o \to \infty} \frac{H_o^{(2)}(kr_o)}{H_o^{(2)}(kr_o)} = -ik\mu_j u_j$$

Equation (15) gives the stress at the top of layer j. At the bottom:

$$\tau''_{r\theta} = \frac{\mu_j u_{j+1}}{r_o} \left[- 2 + kr_o \frac{H_o^{(2)}(kr_o)}{H_1^{(2)}(kr_o)} \right] \tag{16}$$

The forces per unit radian at both nodes can then be obtained:

$$T'_j = \frac{\mu_j b_j}{6} \left[- 2 + kr_o \frac{H_o^{(2)}(kr_o)}{H_1^{(2)}(kr_o)} \right] (2u_j + u_{j+1})$$

$$T''_j = \frac{\mu_j b_j}{6} \left[- 2 + kr_o \frac{H_o^{(2)}(kr_o)}{H_1^{(2)}(kr_o)} \right] (u_j + 2u_{j+1}) \tag{17}$$

B.1.3 Concluding Remarks

Equations (12) and (17) provide the stiffness matrix of the boundary elements and the equivalent boundary forces, respectively. The problem can then be completely solved with the aid of those expressions. It is interesting to notice that, although the eigenvalues (k^2) of the resulting problem are all real, some of them are positive and some are negative. The positive eigenvalues yield real wave numbers which correspond to travelling waves; the sign of the square root must be selected so that the wave propagates away from the axis.

Negative eigenvalues generate imaginary wave numbers, which correspond to standing waves; the sign of the square root should be taken such that the standing wave decays towards infinity.

B .2 THE LYSMER-KUHLEMEYER PLANE BOUNDARY

The full discussion of this boundary can be found in the original paper by Lysmer and Kuhlemeyer (1969)[29]. The reader is referred there for details on the characteristics and behaviour of the boundary.

For the purpose of the present report it is sufficient to state that the boundary consists of a series of dashpots connected to the boundary nodes. The viscous constants of these dashpots are taken:

$$C = \rho V A$$

where ρ is the density.

V is the velocity of propagation of the radiated pulse (shear waves in this case).

A is the area lumped in the boundary node to which the dashpot of constant C is connected.

Dashpots chosen in such way dissipate exactly all the energy carried by waves in the case of one-dimensional propagation. For this case it constitutes a perfect non-reflecting boundary. In the case of more than one dimension, some of the incoming energy is reflected back into the domain.

The following figure, taken from the referenced paper, shows the ratio of reflected to incident energy ratio as a function of the angle of incidence.

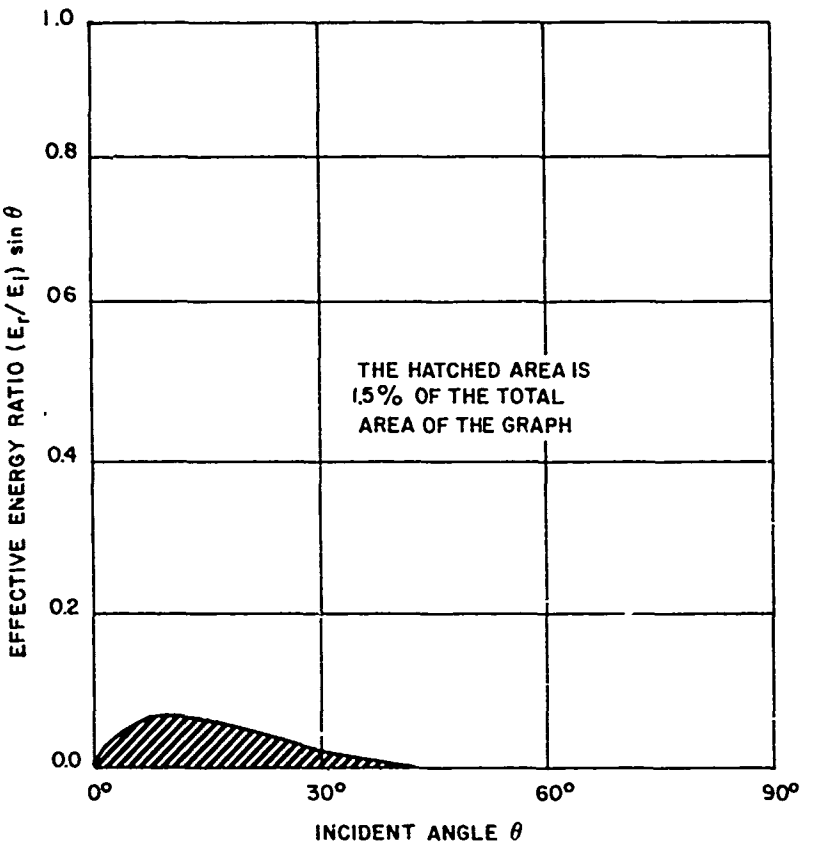

FIG. B.5. EFFECTIVE ENERGY RATIO FOR INCIDENT P-WAVE (AFTER LYSMER AND KUHLEMEYER, 1972)

Given the facts that in the finite element model proposed the angle of incidence is never small and that the effects of the BSD vanish rapidly above and below the depth of operation, the proposed form of viscous boundary is thought to be sufficiently accurate to simulate the radiation of energy across the norizontal boundaries of the model.

APPENDIX C

MISCELLANEOUS CALCULATIONS

C.1 ELASTIC DISPLACEMENT DISTRIBUTION

From Chapter 3, equation (9) is:

$$\frac{du}{dr} - \frac{u}{r} = \frac{\tau_o r_o^2}{\mu_o r^2}$$

where the partial has been replaced by an ordinary derivative. This equation is subjected to the boundary condition:

$$\lim_{r \to \infty} u = o$$

The general solution to the above linear equation can be obtained as:

$$u = e^{-\int_{r_o}^{r} -\frac{ds}{s}} \left[u_o - \int_{r_o}^{r} -\frac{\tau_o r_o^2}{\mu_o s^2} e^{\int_{r_o}^{s} -\frac{dt}{t}} ds \right]$$

$$= \frac{r}{r_o} \left[u_o + \frac{\tau_o r_o^3}{\mu_o} \left(\frac{1}{2r_o^2} - \frac{1}{2r^2} \right) \right]$$

The boundary condition requires:

$$u_o = -\frac{\tau_o r_o}{2\mu_o}$$

Hence the final solution is:

$$u = \frac{\tau_o r_o^2}{2\mu_o r}$$

C .2 HYPERBOLIC DISPLACEMENT DISTRIBUTION

The equation to be intergrated (Chapter 3, eq. 11) was:

$$\frac{du}{dr} - \frac{u}{r} = \frac{\tau_o r_o^2}{\mu_o} \frac{1}{r^2 - \frac{\tau_o r_o^2}{\tau_m}}$$

subject to the boundary condition:

$$\lim_{r \to \infty} u = o$$

The general solution is:

$$u = e^{\int_{r_o}^{r} -\frac{ds}{s}} \left[u_o - \int_{r_o}^{r} -\frac{\tau_o r_o^2}{\mu_o} \frac{1}{s^2 - \frac{\tau_o r_o^2}{\tau_m}} e^{\int_{r_o}^{s} -\frac{dt}{t}} ds \right]$$

$$= \frac{r}{r_o} \left[u_o + \frac{\tau_o r_o^3}{\mu_o} \int_{r_o}^{r} \frac{ds}{s\left(s^2 - \frac{\tau_o r_o^2}{\tau_m}\right)} \right]$$

The integral is easily obtained by expressing the integrand as a sum of irreducible fractions. Then:

$$u = \frac{r}{r_o}\left[u_o + \frac{\tau_m r_o}{2\mu_o} \ln\left(\frac{1 - \frac{\tau_o r_o^2}{\tau_m r^2}}{1 - \frac{\tau_o}{\tau_m}} \right) \right]$$

The boundary conditions require:

$$u_o = \frac{\tau_m r_o}{2\mu_o} \ln\left(1 - \frac{\tau_o}{\tau_m}\right)$$

And hence the final solution for the displacement is:

$$u = -\frac{\tau_m r}{2\mu_o} \ln\left(1 - \frac{\tau_o r_o^2}{\tau_m r^2}\right)$$

APPENDIX D

GENERAL DESCRIPTION OF FINEL

D.1 INTRODUCTION

FINEL is a finite-element system which has been designed to meet the requirements of teaching and research establishments. It has been developed over a period of years by the Department of Aeronautics, Imperial College, London. The system has most of the features found in large general purpose finite-element programs, but also has additional facilities allowing the user to add features pertinent to his own requirements. In adding these, the interfacing between the user and the program is a minimum and occurs in such a way that it is not possible for any user to alter permanently the system.

The FINEL input has been designed to be of a general form such that it is capable of being adapted to suit any problem which can be solved by the finite-element method. This ensures that it is completely compatible with the open-endedness built into the system. The input is also of such a form that it is readily understood, making the system easy to use.

A further feature of the system is that it has been specifically designed to fit into small core, shorttime partitions within a computer, but with the user able to expand core allociation at run time for large analyses. This feature is essential for a teaching and research orientated program since a large amount of its usage will involve debugging, requiring a rapid turnaround time.

D.2 SPECIAL FEATURES OF FINEL

FINEL can be used in the same way as other finite element systems for analysing structures and other problems. In addition to this it has particular features which enable it to be used in a rather more general fashion. The most important of these are:

a) It has a highly modular structure, including sub-modules (termed libraries within FINEL).

b) A general form of free format data input using the command and label concept to define a block of data.

c) A central data filing system, forming a problem data base. This has a two level structure of files and pages within files. Only one subroutine is used to control the data base and this of such a form that it is easy for the user to employ.

d) There are no assumptions built into the system that fix it to a particular type of analysis. This applies to both the input formats and the execution sequence.

During the analysis carried out for the BSD project, several features were added to the program:

- An optional axisymmetric, plane, non-reflecting boundary of the Lysmer-Kuhlemeyer type.
- An axisymmetric, cylindrical, non-reflecting boundary of the Lysmer-Waas type.

- A procedure to incorporate "equivalent-linear" calculations for frequency-domain solution of non-linear problems.

D.3 EXECUTION SEQUENCE OF A FINEL RUN

The basic execution sequence of a FINEL is shown in Figure D.1. If the user is adding facilities to the basic program then the routines describing these are compiled first. These are written in FORTRAN.

A large amount of data checking is carried out at the preprocessor stage. An interactive form of this is available for on line data input and correction.

The finite-element analysis is carried out in the FINEL main program. This is structured in a highly modular form. Each module is only entered through the control program. The modules which are called, and their calling sequence, are basically defined at runtime but there are facilities for altering this depending upon intermediate results. This allows iterative and non-linear analysis to be performed.

The modular structure has various advantages. It enables simple overlay sequences to be set up, allowing FINEL to be run on a relatively small machine. More importantly, for a research orientated system, modules can be added at runtime. This allows the user to modify the system to suit his own requirements without actually altering any part of the system. The modules are written as essentially independent programs (Fig. D.2).

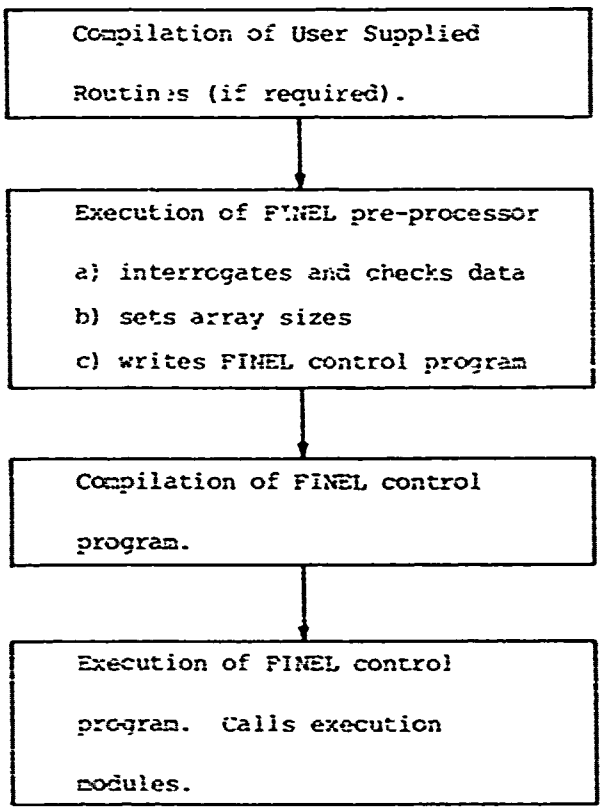

FIG.D.I. EXECUTION OF SEQUENCE OF FINEL

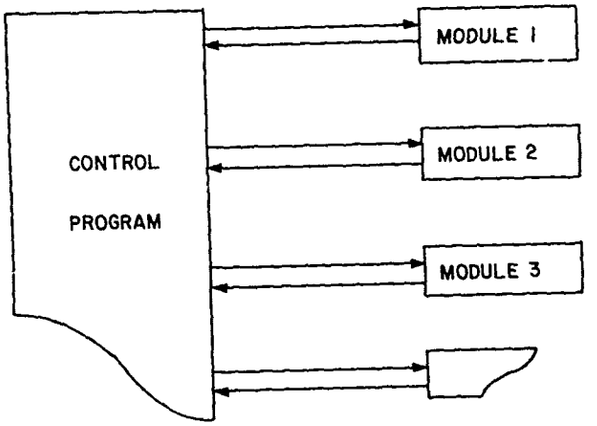

FIG. D.2. FINEL PROGRAM STRUCTURE

The modular concept is repeated at a lower level in the form of FINEL libraries. These have the access structure shown in Figure D.3. The libraries contain a series of standard entries which can always be used. There are also facilities for the user to add to his own entries are runtime.

FINEL contains six libraries, these being:

a) Element library.

b) Load library.

c) Mesh generation library.

d) Plotting library.

e) Program library.

f) Module library.

All libraries have the same form and are used in the same way. For teaching purposes students can, typically, add their own elements to gain practical experience in F.E. theory. The coding required for this is minimal.

D.4 FINEL DATA INPUT

Data is inputted to FINEL in free format. Each block of data consists of a command word, a label and numerical data. The commands and labels are usually English words, making the input itself explanatory in most cases. This form of input was chosen since it is adaptable to any type of problem. The command word is usually defined by F.E. theory, whereas the label can be chosen to suit the problem nomenclature.

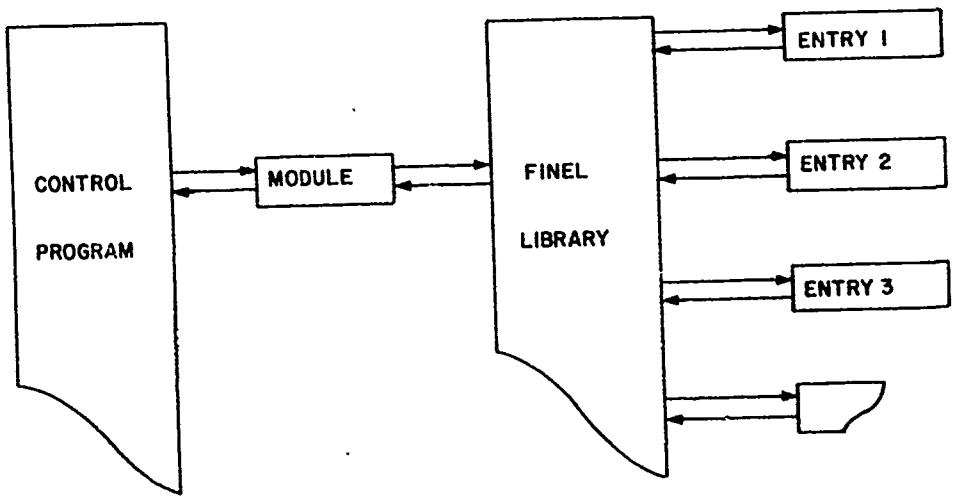

FIG. D.3. FINEL LIBRARY STRUCTURE

A simple stress analysis problem, together with the FINEL input is shown in Figure D.4.

D.5 THE FINEL FILING SYSTEM

Data is transferred within FINEL either in labelled common areas for small (single words) amounts of data or through a direct access filing system (data base) for large blocks of data. The data base comprises a two level system of files and pages with files. This is illustrated in Figure D.5.

A set of files are dedicated to storing blocks of data that are always generated, by the nature of the F.E. method. Other files are available to the user for intermediate scratch use.

Any operation on the filing system is carried out through a single routine called ZFILE. This is called as:

```
CALL ZFILE  (VAR,NVAR,NFILE,NPAGE,IWTRD)
```

where VAR is the first word address for the data transfer

NVAR is the number of words transferred on page NPAGE of file NFILE.

IWTRD is set to 1 for writing and 2 for reading.

The filing system has proved to be easy to use and efficient in operation. Since all data base operations are controlled through a single routine it becomes easy to transfer the system to other computers. The filing routine can then be written separately for each machine to give optimum efficiency. The rest of FINEL is in standard ASA FORTRAN so that no other changes have to be made when transferring to other machines.

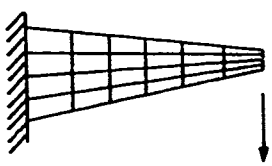

```
*TAPERED CANTILIVER BEAM
PROGRAM STRESS
MATERIAL STIFNESS 30.0E6
ELEMENT QDUB 1.0
REGIONAL COORDINATES  0.  0.  10.  2.  0.  4.  10.  3.
REGION SQUD  1  3  2  4  4  6
FIXED DISPLACEMENT  1  0  2  0  3  0  4  0  5  0
LOAD POINT  -1.0E3  31  7
END JOB
```

FIG D.4. EXAMPLE
OF FINEL INPUT

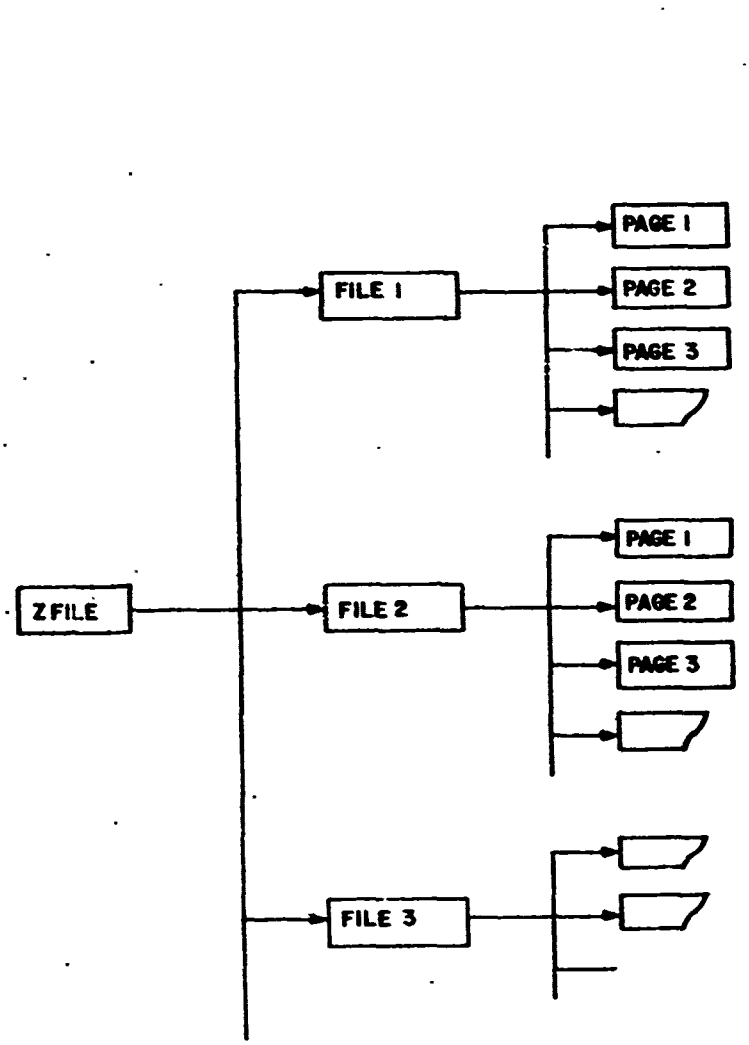

FIG. D.5. FINEL FILING SYSTEM

D.6 ASSUMPTIONS WITHIN FINEL

Every attempt has been made to make FINEL free from any restrictive asumptions. The data input allows problems to be specified in their natural form. Elements can be used to define up to ten types of coefficient matrices, although only up to four can be used in any one run. It is assumed that every node on an element, for a given matrix type, has the same number of freedoms per node and this is not always so, however in such cases dummy freedoms can be specified without loss of efficiency. There is no restriction upon the number of freedoms per node, or the types of freedoms. The pre-processor automatically allocates core, optimizing array sizes to suit the problem. The largest single problem is dictated by the requirement to hold a completed load vector in core, but the use of sub-structuring allows any size problem to be solved.

D.7 SOLUTION PROCEDURE IN THE PRESENT FINEL VERSION

The calculation procedure employed in FINEL is based on the technique of modal decomposition which is the general scheme normaly used in other structural dynamics frequency domain computer routines. The principles of the technique are illustrated in Figure D.6 in which the logical sequence of the main operations are shown.

To expand upon this illustration, it was shown in Appendix B that the values of displacement, strains and stresses at any point in an element can be derived as a function of the displacements of the nodes of that element:

$$\delta\ (r,z) \quad = \| d \| \{ \delta \} \qquad (1)$$

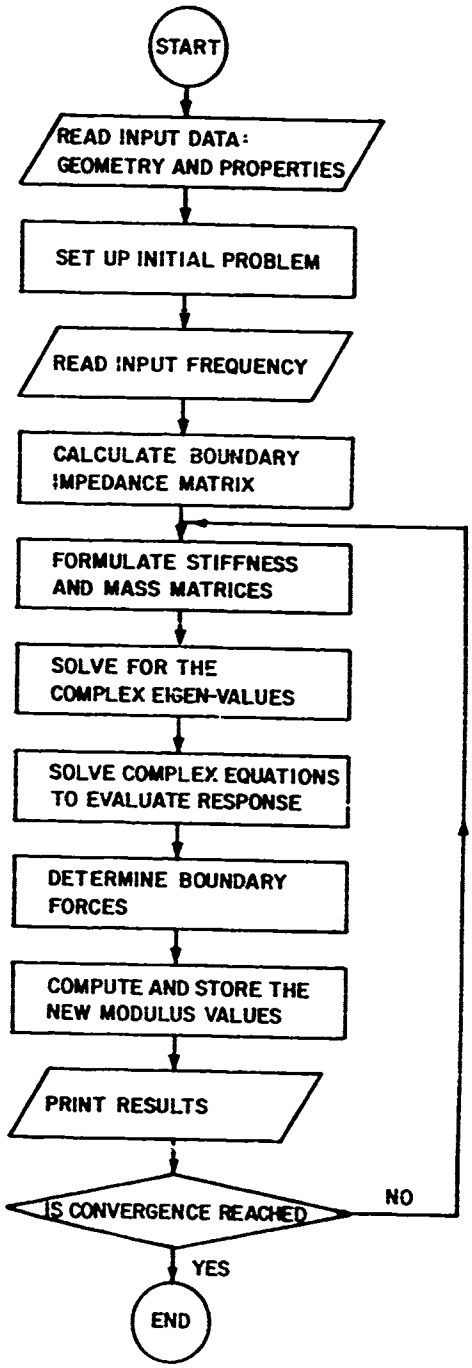

FIG. D.6. GENERAL FLOW-CHART FOR FINEL VERSION IN THE BSD PROJECT.

$$\{\varepsilon\} = [D]\ \{\delta\} \qquad (2)$$

$$\{\tau\} = \mu_j[D]\ \{\delta\} \qquad (3)$$

where $\|d\|$ and $[D]$ are the matrices introduced in the equations (1) and (2) of Appendix B

$\{\delta\}$ is a column vector representing the displacement in the element nodes.

Likewise, the stiffness and mass matrices for the elements of the soil can be defined:

$$[K]_j = \int_V \mu_j\ [D]^t\ [D]\ dV \qquad (4)$$

$$[M]_j = \int_V \rho_j\ \|d\|\ \{d\}\ dV \qquad (5)$$

The soil will in general display some internal damping characteristics. In FE calculations, the stiffness matrix of the soil is often expressed as a linear combination of the mass and stiffness matrices (Rayleigh damping). Such is the procedure used in FINEL. However, preliminary estimates showed internal damping to be unnecessary in the BSD runs. This is due to the small size of the domain modelled compared to the wave lengths induced by the device.

Radiation damping is however important. It appears in the formulation through the complex stiffnesses associated with the non-reflecting boundaries, both the Lysmer dashpots and the Lysmer-Waas boundary.

The equations can then be formulated as:

$$\left[K + i\omega C - \omega^2 M\right]\left\{r\right\} = \left\{R\right\} \qquad (6)$$

Where K is composed of the soil stiffness matrix plus the real part of the stiffness contribution of the non-reflecting boundaries

C is the damping matrix, composed of possible internal damping plus that arising from the formulation of the non-reflecting boundaries.

M is the mass matrix of the soil elements

R is the input force vector

r is the resulting displacement response vector

Both R and r can be complex, the ratio of real to imaginary parts representing the phase angle relative to some reference. The elements of R are point forces applied on nodes.

If some pre-defined input displacements are to be applied, the displacement vector is divided in two parts r_1 and r_2 representing the unknown and the constrained displacements respectively.

$$r = \left\{ r_1 , r_2 \right\} \tag{7}$$

The response equation takes the form:

$$\begin{bmatrix} D_{11} & D_{21} \\ D_{12} & D_{22} \end{bmatrix} \quad \begin{bmatrix} r_1 \\ r_2 \end{bmatrix} = \begin{bmatrix} R_1 \\ R_2 \end{bmatrix} \tag{8}$$

Solving the first of these equations for r_1, the unknown forces R_1 necessary to produce the constrained deflections r_1 can be determined. Once

a global displacement vector r has been obtained it is then possible to deduce the strains in every element.

The constitutive non-linearity is introduced approximately via the equivalent linear method. This method has been generalized to two dimensions by assuming that the shear modulus is only a function of position and time and is related to the strain level ε_e via

$$\mu = \mu(\alpha\varepsilon_e) \tag{9}$$

where α has been taken as 1

ε_e is the maximum value of the shear strain at the point (in any direction at any time).

APPENDIX E

SET OF PHOTOGRAPHS OF THE PROTOTYPE COUPLING MECHANISM AND TESTING EQUIPMENT

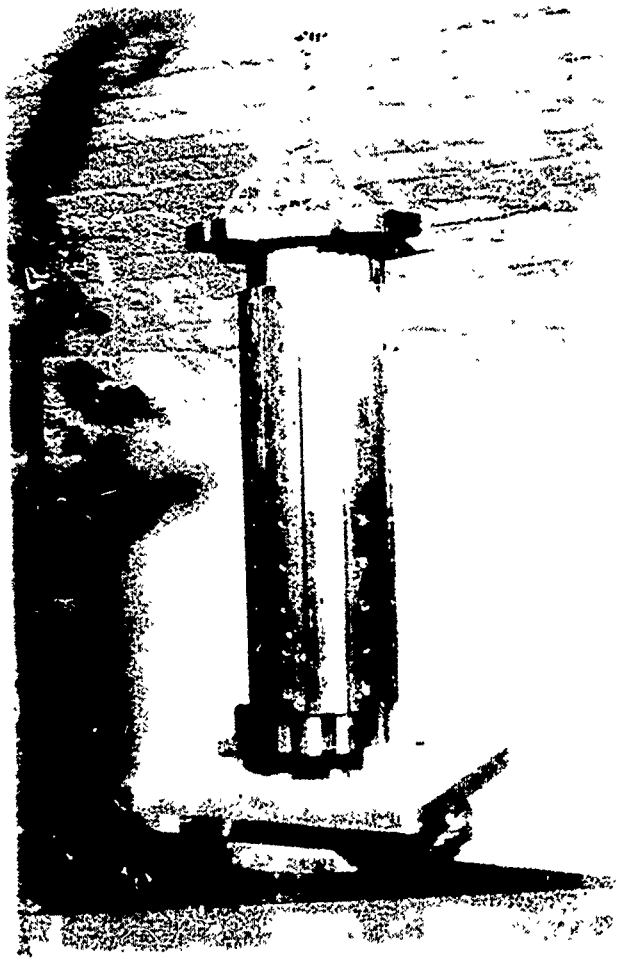

E.1 GENERAL VIEW OF THE COUPLING MECHANISM

E.2 VIEW OF THE COUPLING MECHANISM IN WHICH ONE OF THE SHOES HAS BEEN REMOVED

E.3 VIEW OF THE COUPLING MECHANISM IN WHICH ONE OF THE SHOES AND ITS CORRESPONDING COUPLING KEY HAS BEEN REMOVED

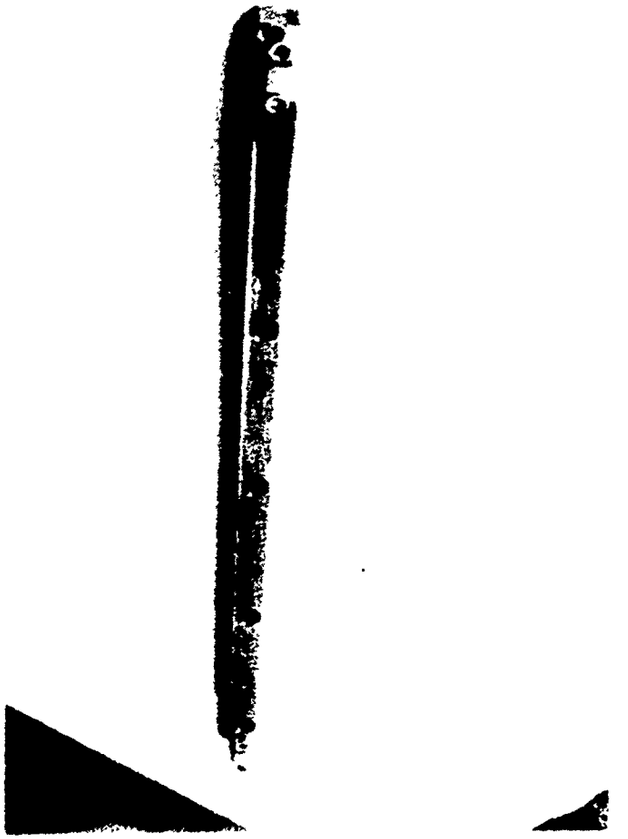

E.4 VIEW OF A COUPLING KEY

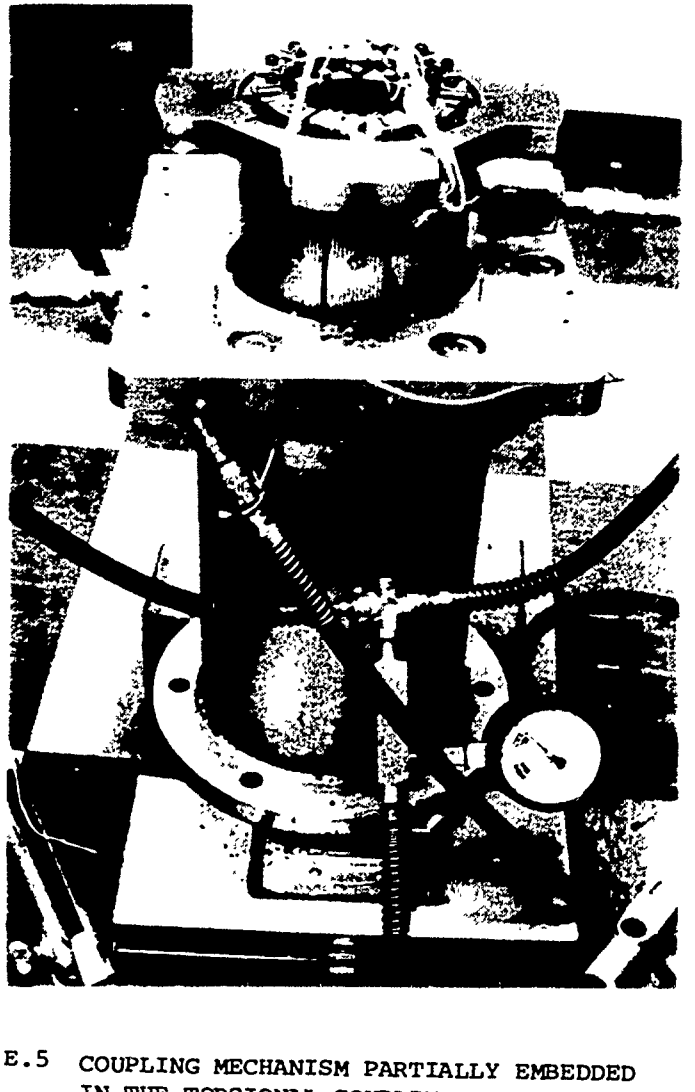

E.5 COUPLING MECHANISM PARTIALLY EMBEDDED IN THE TORSIONAL COUPLING TUBE

E.6 DETAILED VIEW OF HOW THE TORSIONAL INPUT IS TRANSMITTED TO THE COUPLING PLATE

E.7 TOP VIEW OF THE COUPLING PLATE

APPENDIX F

SET OF DRAWINGS OF THE PROTOTYPE COUPLING MECHANISM AND TESTING EQUIPMENT

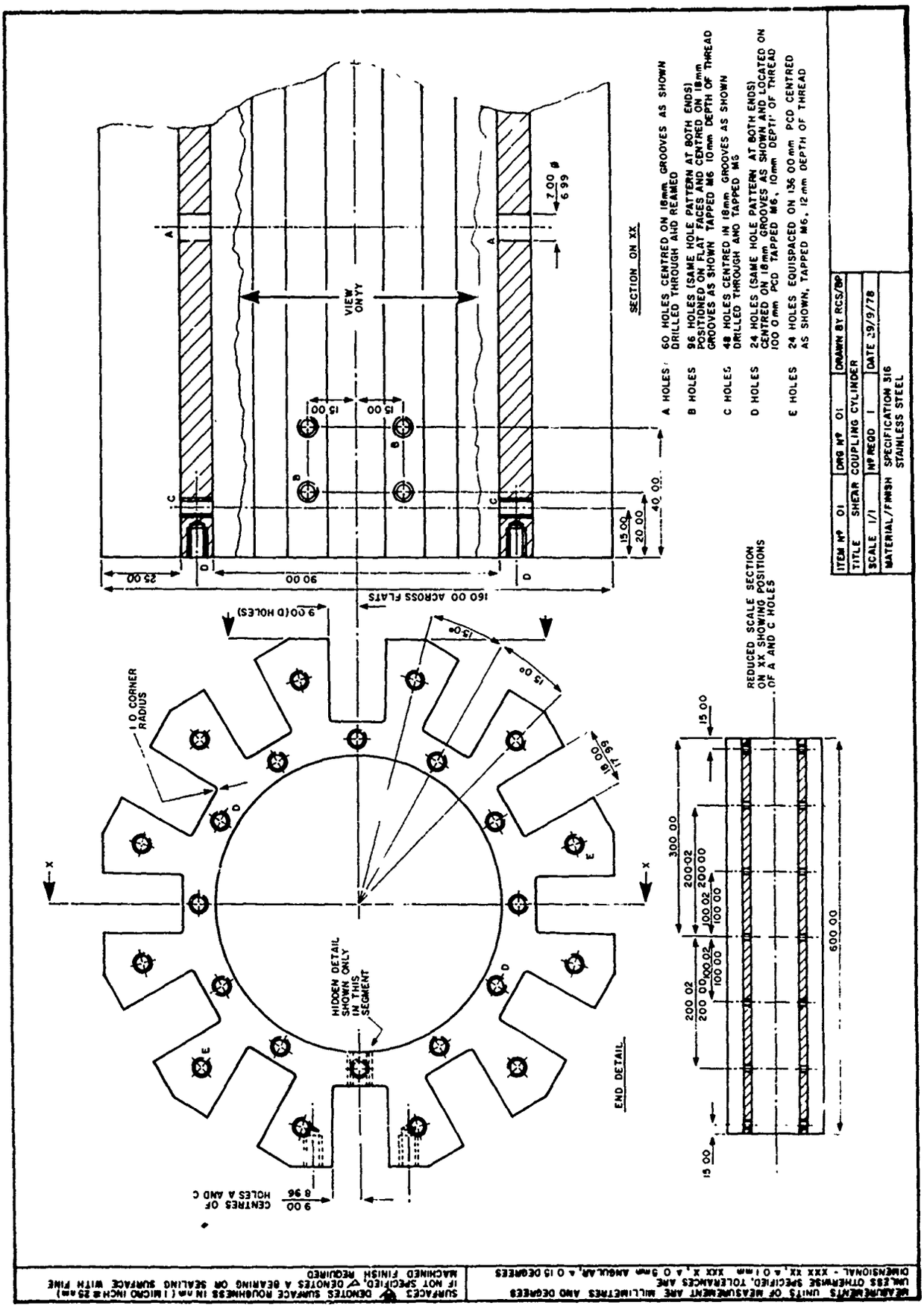

Drawing No. F1

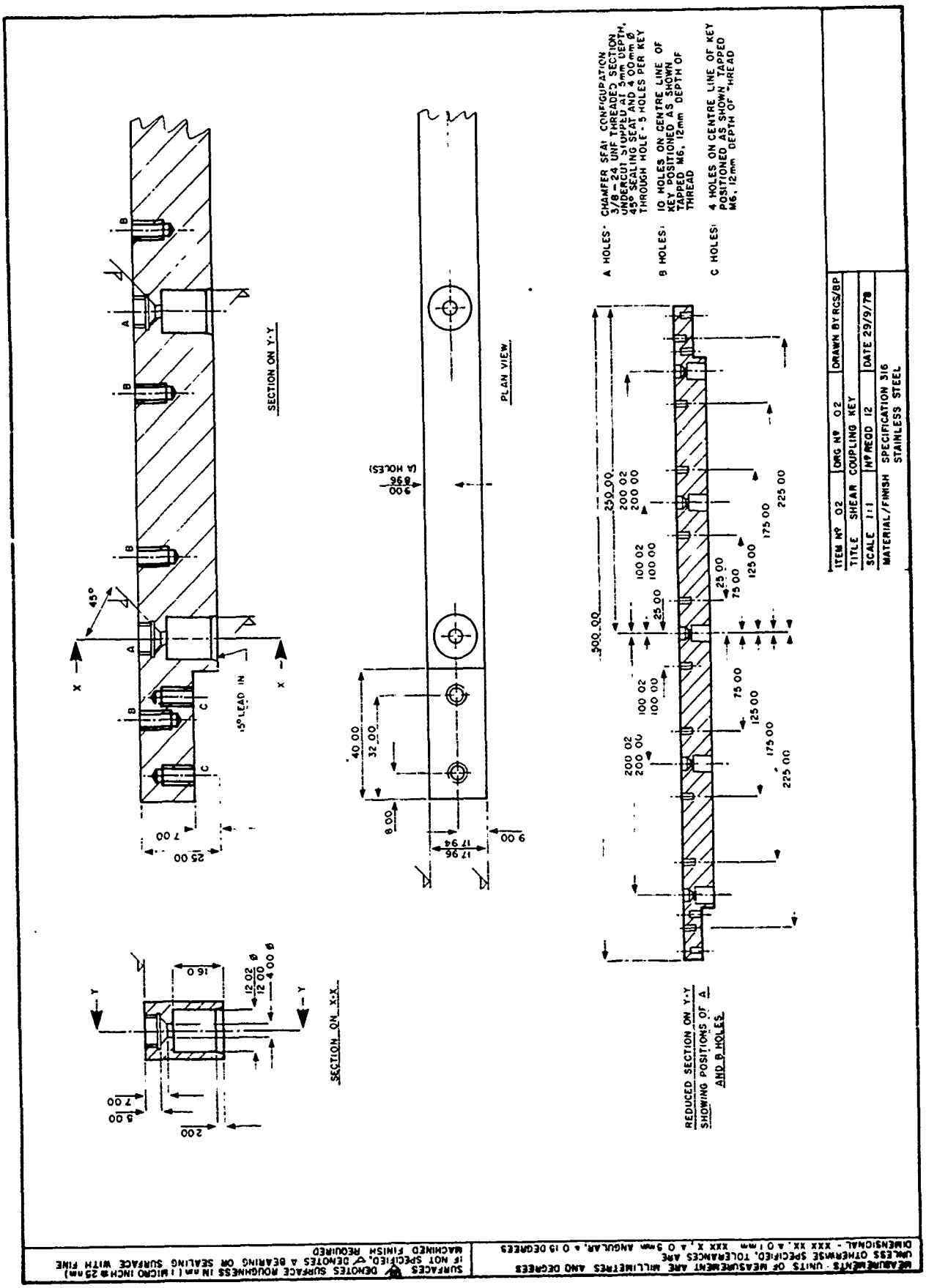

Drawing No. F2

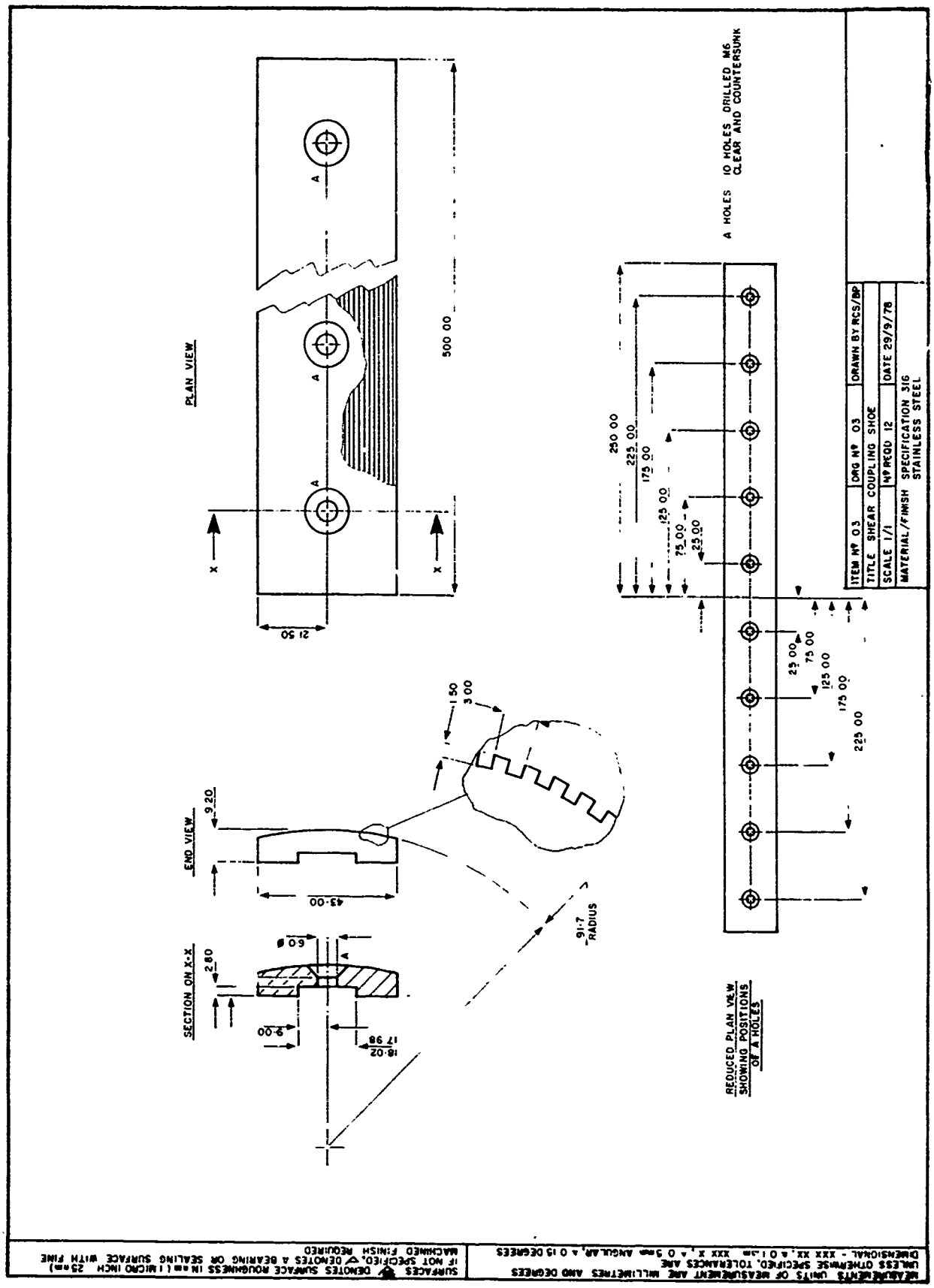

Drawing No. F3

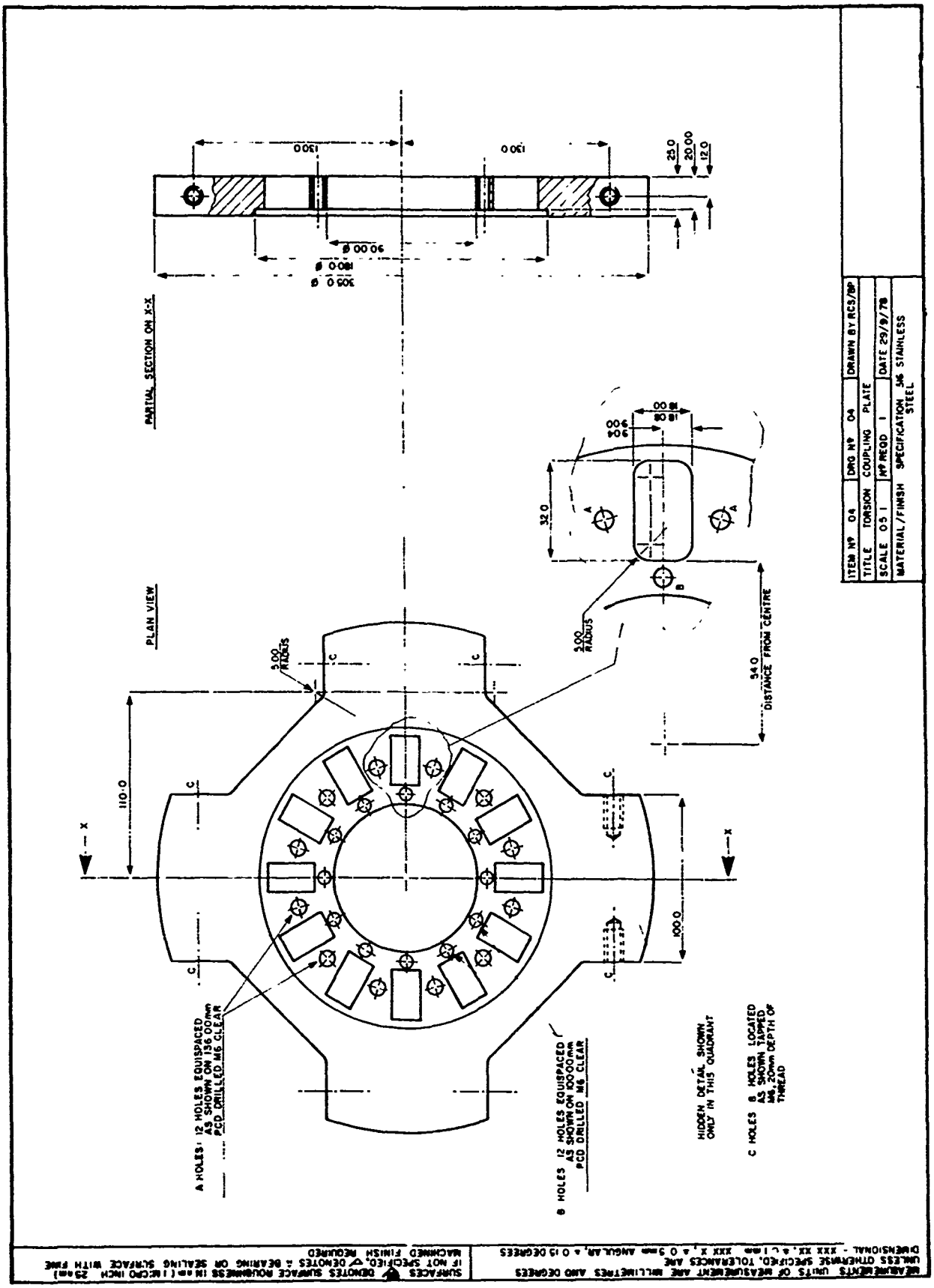

Drawing No. F4

MEASUREMENTS · UNITS OF MEASUREMENT ARE MILLIMETRES AND DEGREES
UNLESS OTHERWISE SPECIFIED, TOLERANCES ARE
DIMENSIONAL - XXX·XX, ± 0·1 mm XXX·X, ± 0·5 mm ANGULAR, ± 0·15 DEGREES

SURFACES: ▽ DENOTES SURFACE ROUGHNESS IN nm (1 MICRO INCH 25 nm)
IF NOT SPECIFIED, ▽ DENOTES A BEARING OR SEALING SURFACE WITH FINE
MACHINED FINISH REQUIRED

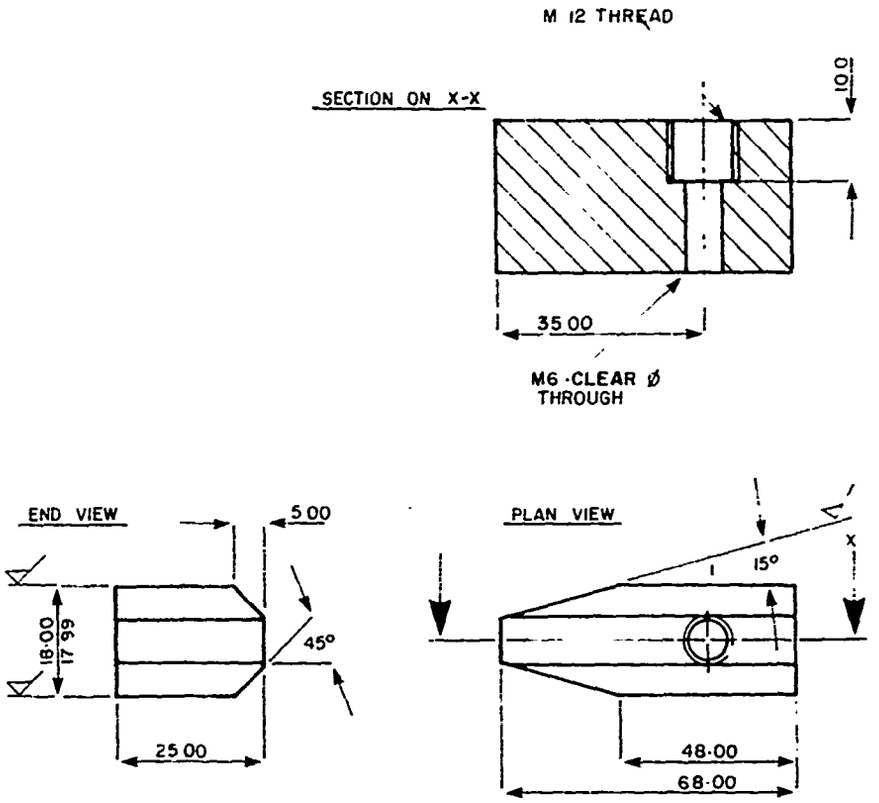

ITEM Nº 05	DRG Nº 05	DRAWN BY RCS/BP
TITLE TORSION COUPLING KEY		
SCALE 1:1	Nº REQD 12	DATE 29/9/78
MATERIAL/FINISH SPECIFICATION 316 STAINLESS STEEL		

Drawing No. F5

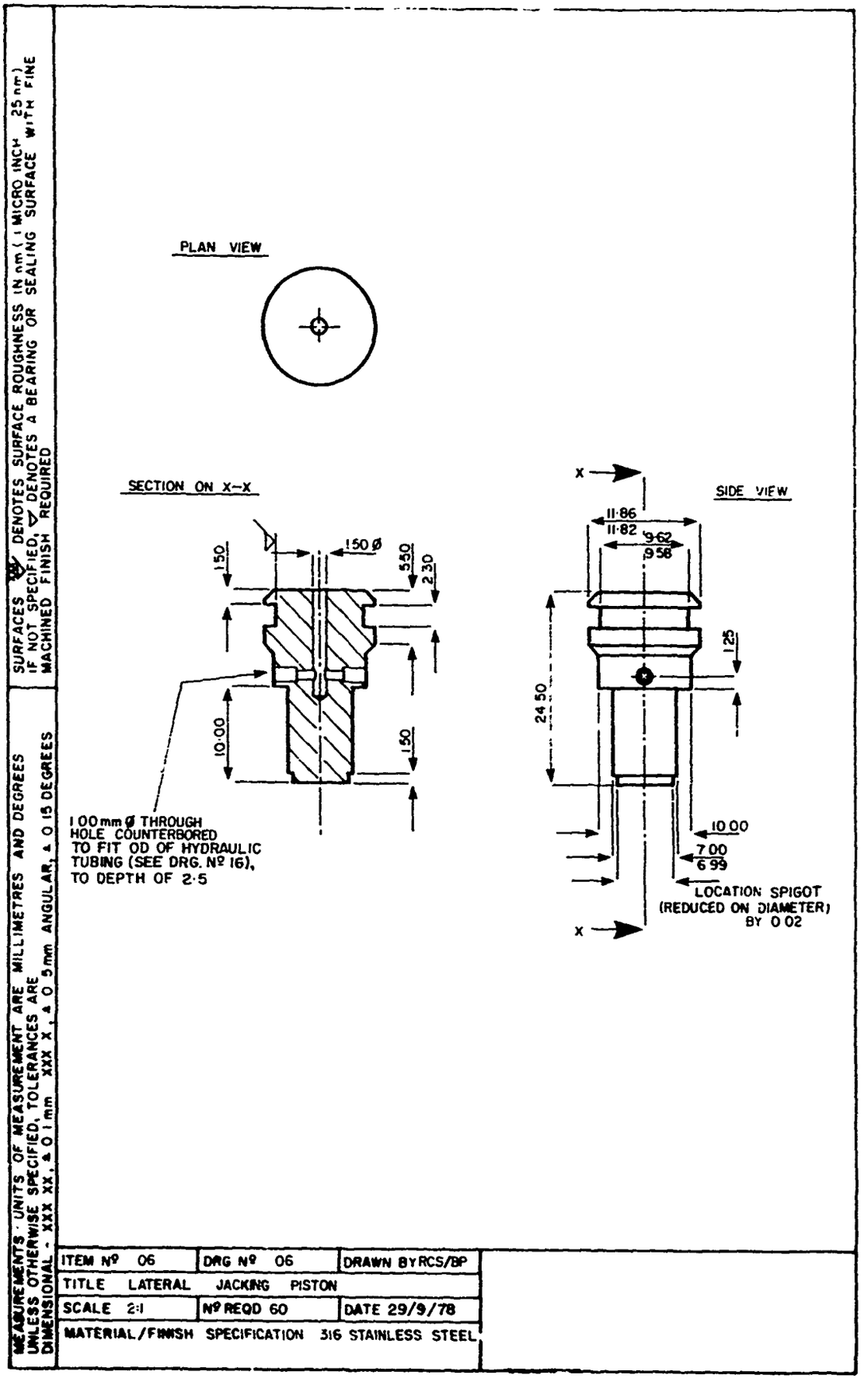

Drawing No. F6

MEASUREMENTS - UNITS OF MEASUREMENT ARE MILLIMETRES AND DEGREES
UNLESS OTHERWISE SPECIFIED, TOLERANCES ARE:
DIMENSIONAL - XXX·XX, ± 0·1 mm. XXX X, ± 0·5 mm. ANGULAR, ± 0·15 DEGREES

SURFACES ▽ DENOTES SURFACE ROUGHNESS IN nm (1 MICRO INCH ≏ 25 nm)
IF NOT SPECIFIED, ▽ DENOTES A BEARING OR SEALING SURFACE WITH FINE
MACHINED FINISH REQUIRED

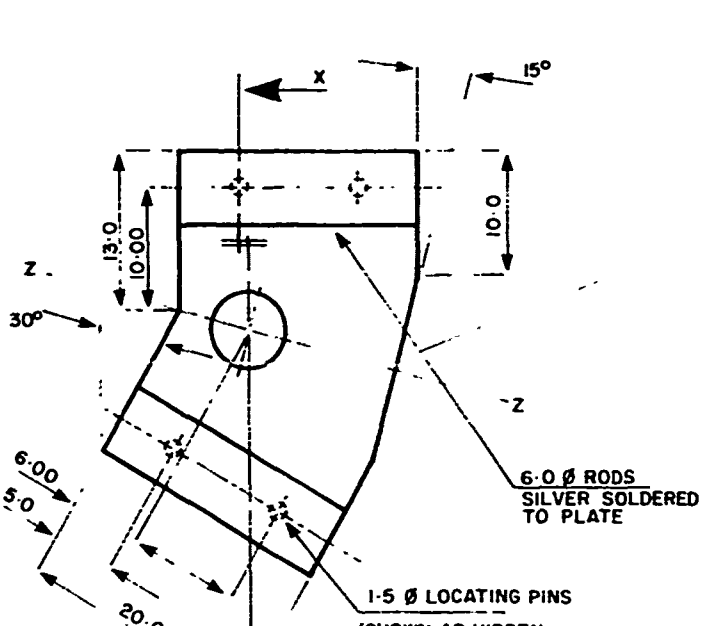

PLAN VIEW
(SYMMETRIC ABOUT Z-Z)

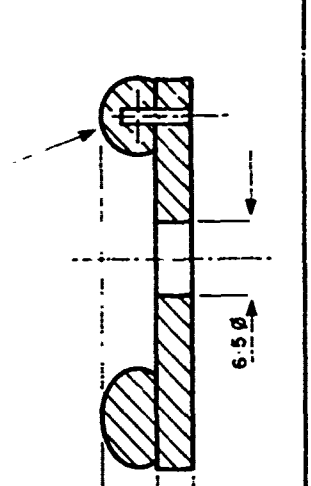

SECTION ON X-X

ITEM Nº 07	DRG Nº 07	DRAWN BY RCS/BP
TITLE COUPLING WEDGE LOADING PLATE		
SCALE 2/1	Nº REQD 12	DATE 29/9/78
MATERIAL/FINISH SPECIFICATION 316 STAINLESS STEEL		

Drawing No. F7

MEASUREMENTS: UNITS OF MEASUREMENT ARE MILLIMETRES AND DEGREES
UNLESS OTHERWISE SPECIFIED, TOLERANCES ARE
DIMENSIONAL - XXX XX, ± 0·1 mm. XXX X, ± 0·5 mm ANGULAR, ± 0·15 DEGREES

SURFACES: ✓ DENOTES SURFACE ROUGHNESS IN nm (1 MICRO INCH = 25 nm)
IF NOT SPECIFIED, ✓ DENOTES A BEARING OR SEALING SURFACE WITH FINE
MACHINED FINISH REQUIRED

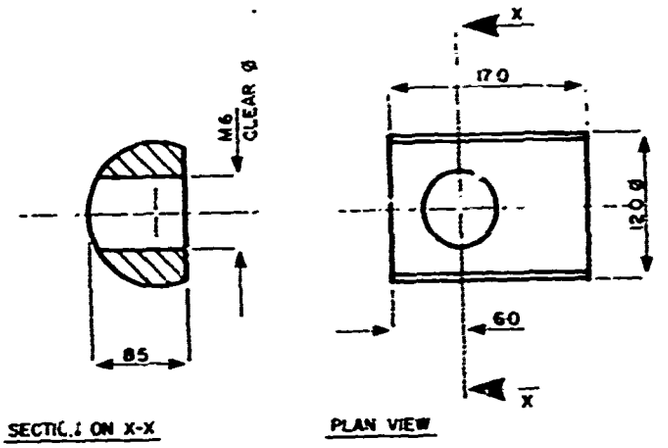

ITEM Nº 08	DRG Nº 08	DRAWN BY RCS/
TITLE WEDGE LOAD BOLT SEATING		
SCALE 2/1	Nº REQD 12	DATE 2^/9/78
MATERIAL/FINISH SPECIFICATION 316 STAINLESS STEEL		

Drawing No. F8

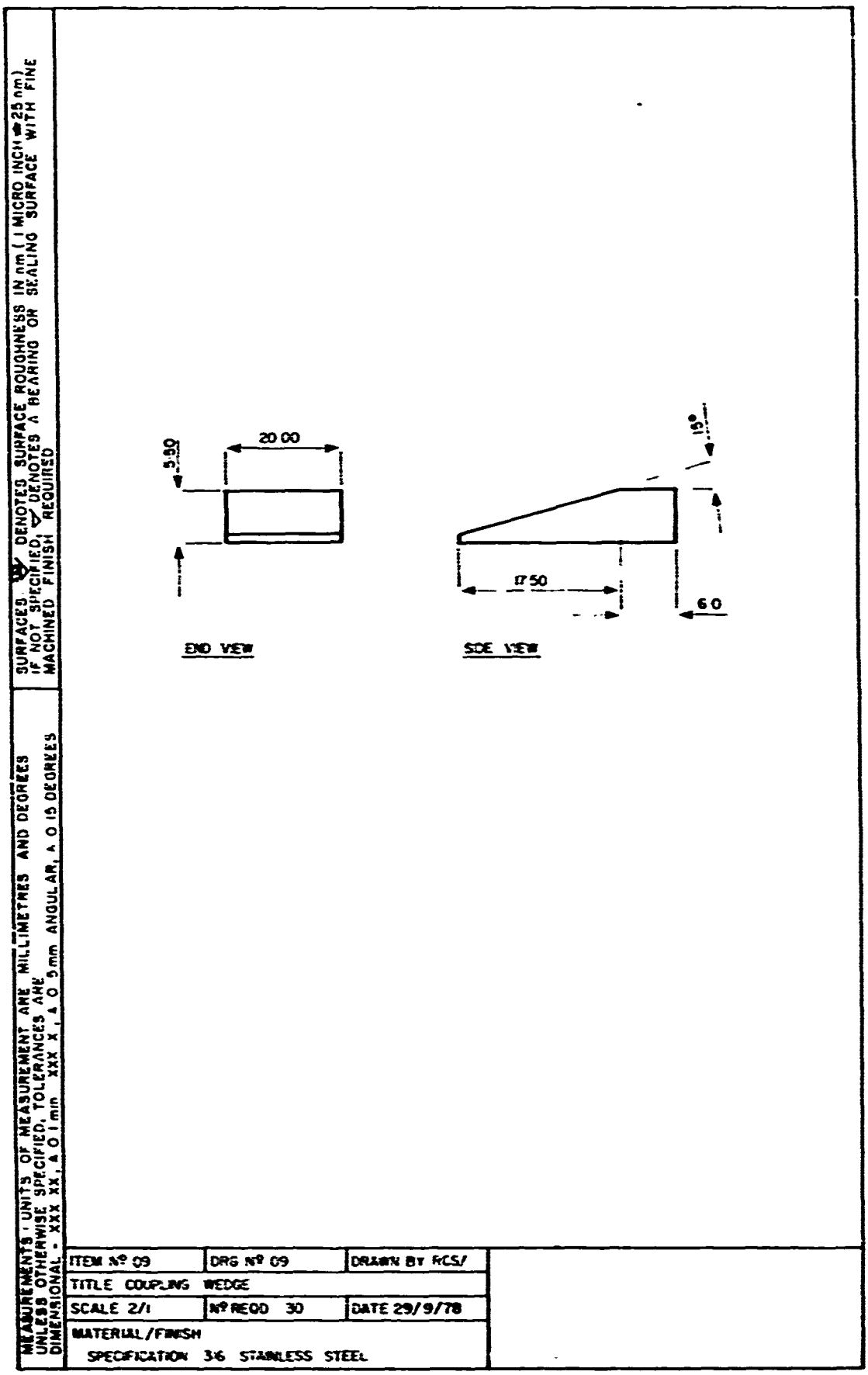

Drawing No. F9

MEASUREMENTS: UNITS OF MEASUREMENT ARE MILLIMETRES AND DEGREES.
UNLESS OTHERWISE SPECIFIED, TOLERANCES ARE:
DIMENSIONAL - XXX·XX, ± 0·1 mm XXX X, ± 0·5 mm ANGULAR, ± 0·15 DEGREES

SURFACES. $\sqrt{XX}$ DENOTES SURFACE ROUGHNESS IN nm (1 MICRO INCH ≙ 25 nm)
IF NOT SPECIFIED, $\sqrt{}$ DENOTES A BEARING OR SEALING SURFACE WITH FINE MACHINED FINISH REQUIRED

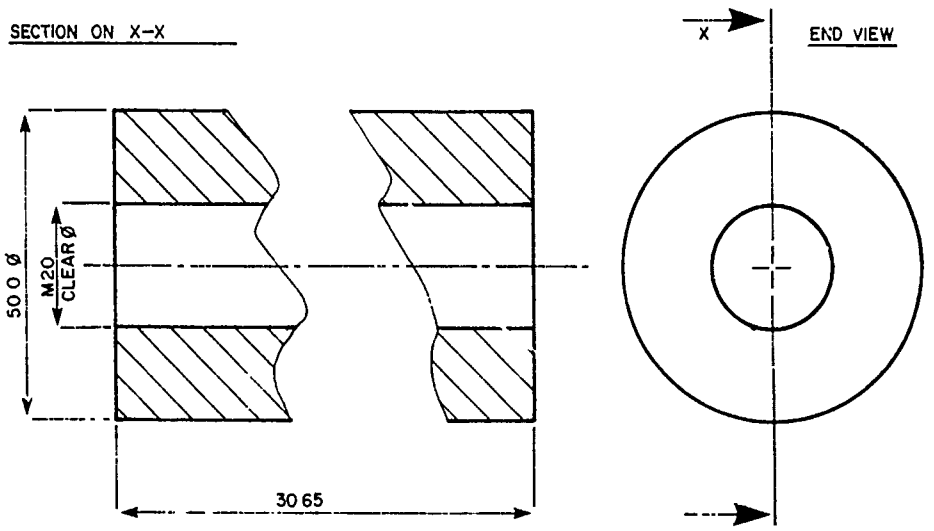

ITEM Nº 10	DRG Nº 10	DRAWN BY RCS/
TITLE TORSION FIXED SPACER A		
SCALE 1/1	Nº REQD 6	DATE 29/9/78
MATERIAL/FINISH	MILD STEEL, CADMIUM & PASSIVATE PLATE FINISH.	

Drawing No. F10

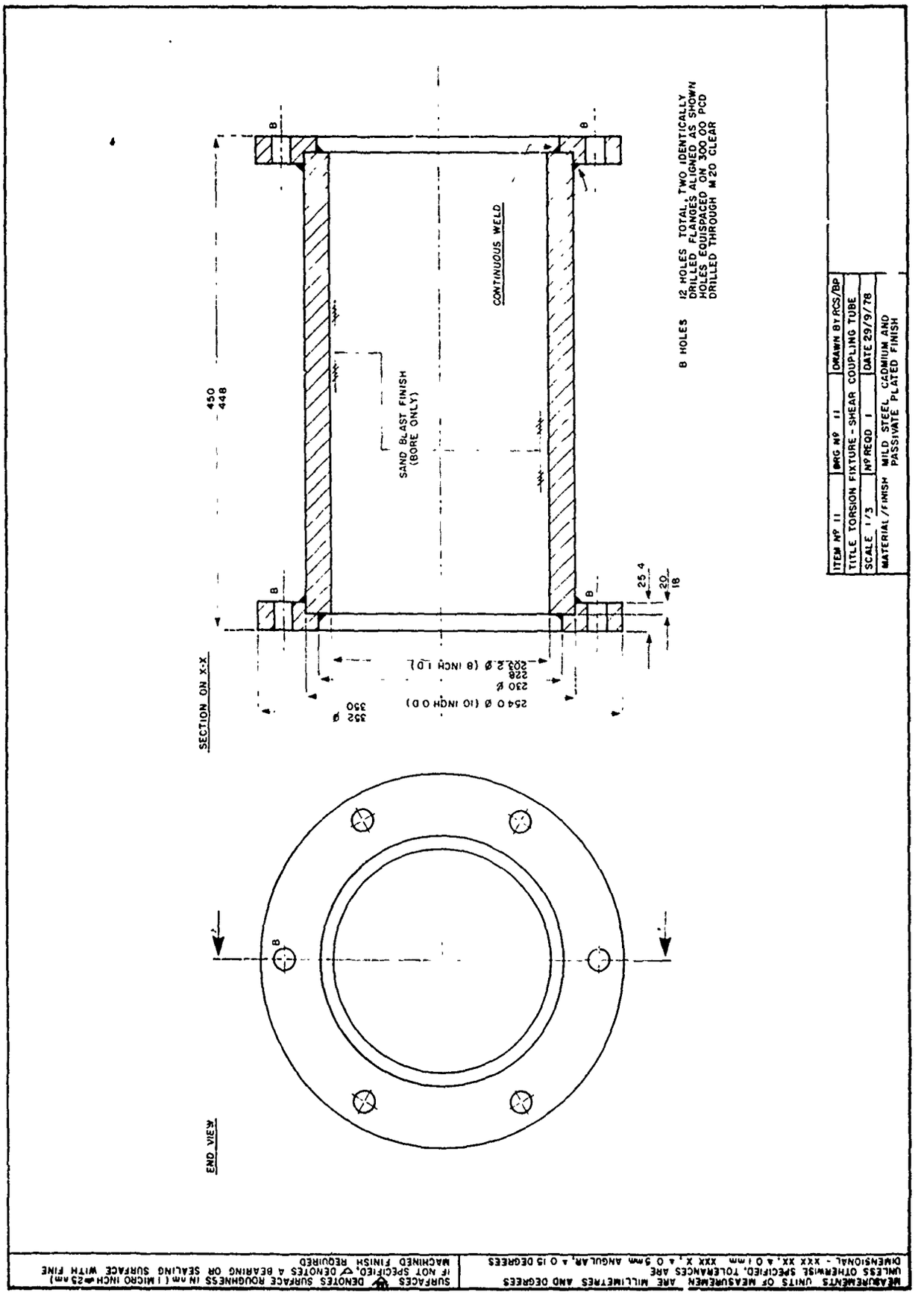

Drawing No. F11

Drawing No. F12

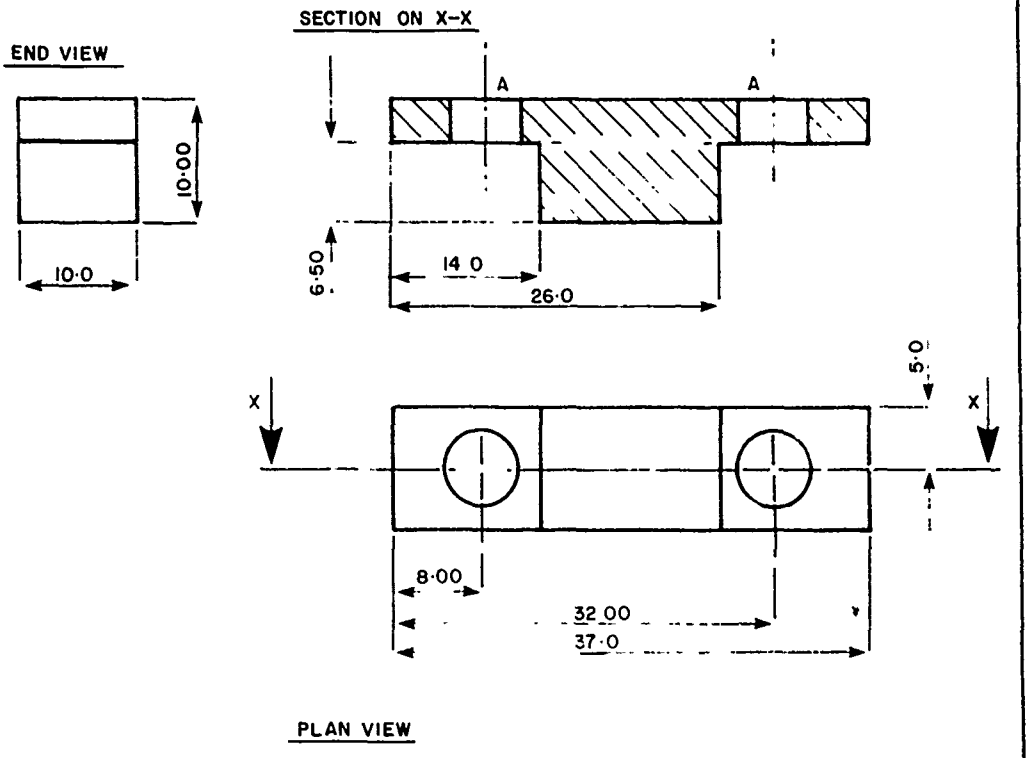

A HOLES : M6 CLEAR

SURFACES. $\sqrt{xx}$ DENOTES SURFACE ROUGHNESS IN nm.(1 MICRO INCH ≈ 25 nm)
IF NOT SPECIFIED, ∇ DENOTES A BEARING OR SEALING SURFACE WITH FINE MACHINED FINISH REQUIRED

MEASUREMENTS : UNITS OF MEASUREMENT ARE MILLIMETRES AND DEGREES
UNLESS OTHERWISE SPECIFIED, TOLERANCES ARE:
DIMENSIONAL - XXX XX, ± 0·1 mm XXX X, ± 0·5 mm ANGULAR, ± 0·15 DEGREES

ITEM Nº 13	DRG Nº 13	DRAWN BYRCS/BP
TITLE SHEAR COUPLING KEY HEEL		
SCALE 2/1	Nº REQD 24	DATE 29/9/78
MATERIAL/FINISH SPECIFICATION 316 STAINLESS STEEL		

Drawing No. F13

MEASUREMENTS · UNITS OF MEASUREMENT ARE MILLIMETRES AND DEGREES
UNLESS OTHERWISE SPECIFIED, TOLERANCES ARE
DIMENSIONAL - XXX XX, ± 0 1 mm XXX X, ± 0 5 mm ANGULAR, ± 0 15 DEGREES

SURFACES ▽▽▽ DENOTES SURFACE ROUGHNESS IN nm (1 MICRO INCH ≈ 25 nm)
IF NO SPECIFIED, ▽ DENOTES A BEARING OR SEALING SURFACE WITH FINE
MACHINED FINISH REQUIRED

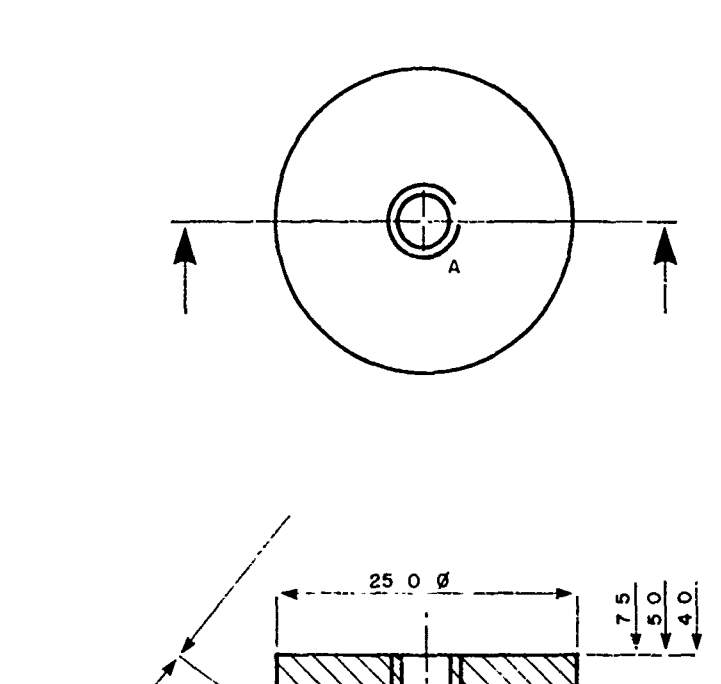

A HOLE : 1 HOLE DRILLED BLIND AND TAPPED M6
TO BOTTOM, 4·0 DEPTH OF THREAD

ITEM Nº 14	DRG Nº 14	DRAWN BY RCS/BP
TITLE TORSION JACK SEATING		
SCALE 2/1	Nº REQD 4	DATE 29/9/78
MATERIAL/FINISH SPECIFICATION 316 STAINLESS STEEL		

Drawing No. F15

MEASUREMENTS: UNITS OF MEASUREMENT ARE MILLIMETRES AND DEGREES
UNLESS OTHERWISE SPECIFIED, TOLERANCES ARE
DIMENSIONAL - XXX·XX, ± 0·1 mm XXX X, ± 0·5mm ANGULAR, ± 0·15 DEGREES

SURFACES: ▽▽ DENOTES SURFACE ROUGHNESS IN nm (1 MICRO INCH ≙ 25 nm)
IF NOT SPECIFIED, ▽ DENOTES A BEARING OR SEALING SURFACE WITH FINE
MACHINED FINISH REQUIRED

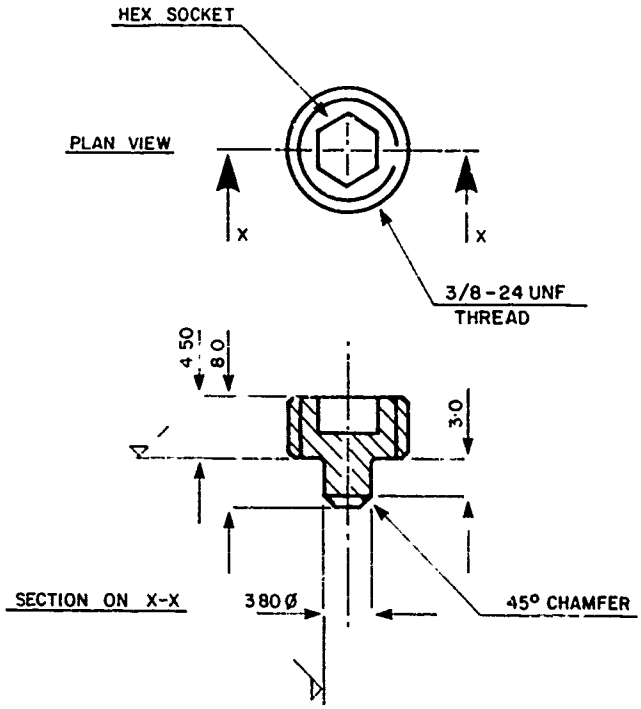

ITEM Nº 15	DRG Nº 15	DRAWN BY RCS/
TITLE LATERAL JACK BLEED SCREW		
SCALE 2/1	Nº REQD 64	DATE 29/9/78
MATERIAL/FINISH 10mm FINE THREAD SOCKET HEAD GRUB SCREW STOCK. HIGH TENSILE OR STAINLESS STEEL SCREW STOCK		

Drawing No. F15

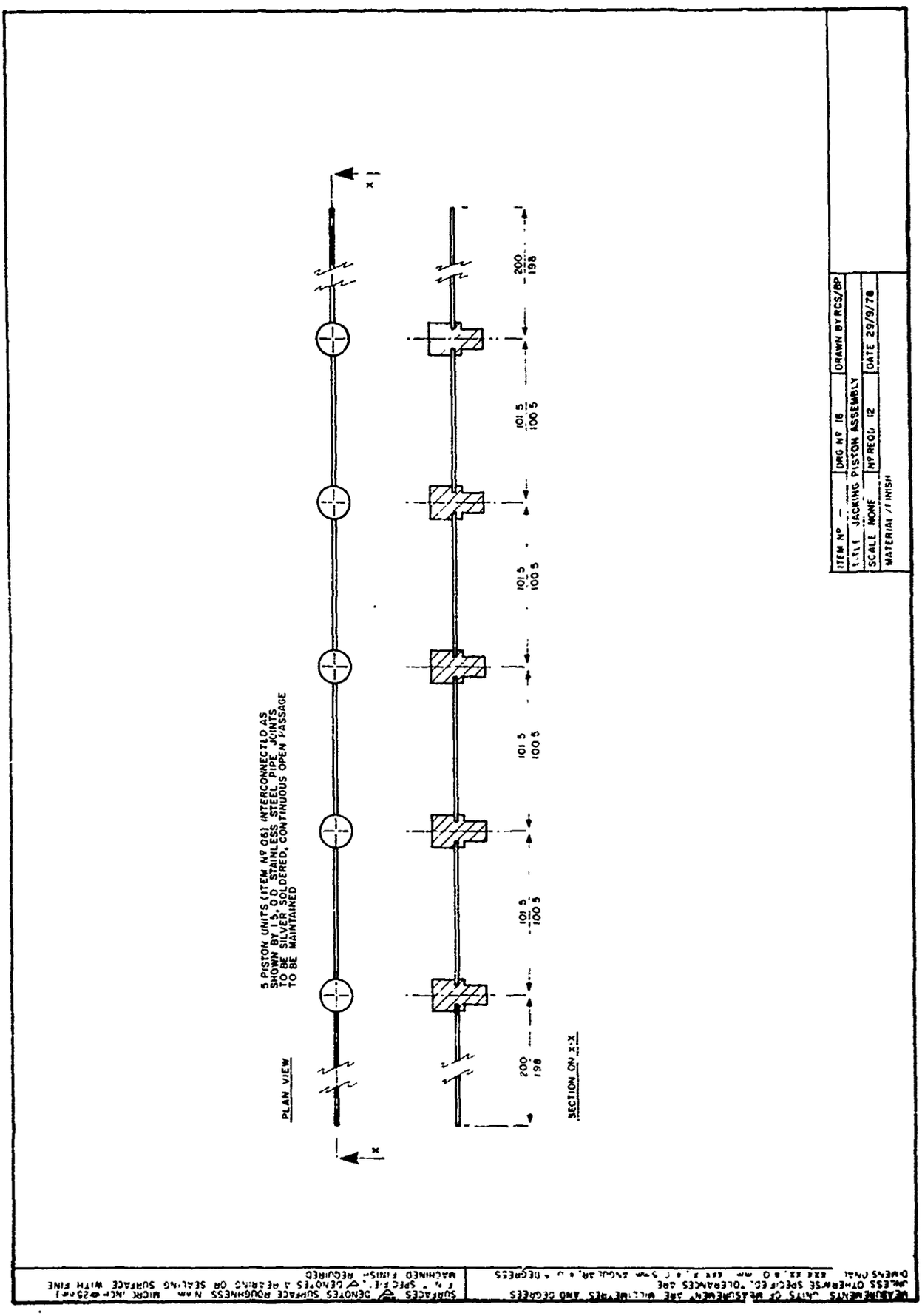

Drawing No. F16

DISTRIBUTION

Asst Secy Def/AE, Wash
DTIC/DDA, Alexandria
USDRE, Wash
DIA, Wash
H. Diamond Lab, Adelphi
DNA/TITL, Wash
(SPSS)
DNA, KAFB
AF Campridge Rsch Labs, Bedford
AFIT
AFSC/DLWM
(DLSP)
AUL
HQ USAF, Wash
BMO
Vela Seism Ctr, Alexandria
USA Engr WW Exp Sta, Vicksburg
NCEL, Port Hueneme
US Geol Surv, Wash
Sandia Nat'l Labs, Livermore
Sandia Nat'l Labs, KAFB
Aerospace Corp, Los Angeles
Analytic Svcs Inc, Falls Church
Applied Theory Inc, Los Angeles
Boeing, Seattle
CA Inst of Tech, Pasadena
CA Rsch & Tech Inc, Woodland Hills
Civil Sys Inc, Albuquerque
Civil Sys Inc, Royalton
Cons & Spec Engr Svcs, Redlands
Dames & Moore Ltd, London
GE-TEMPO, Santa Barbara
Higgins, Auld & Assoc, Albuquerque
IIT Rsch Inst, Chicago
Inst of Def Analyses, Arlington
LLL, Livermore
LASL, Los Alamos
MA Inst of Tech, Cambridge
McDonald-Douglas, Huntington Beach
Occidental College, Los Angeles
Pacifica Tech, Del Mar
Principia Mech Ltd, London
R&D Assoc, Marina del Rey
Physics Int'l Co, San Leandro
Karagozian & Case, Los Angeles
SW Rsch Inst, San Antonio
Stanford Rsch Inst, Menlo Park
Sys, Sci & Software, La Jolla
Sys, Sci & Software, Colton
Sys, Sci & Software, Reston
Teledyne, Brown Engr, Huntsville
Terra Tek Inc, Salt Lakr City
TRW Sys Grp, San Bernardino
TRW Sys Grp, Redondo Beach
Univ of IL, Champaign
Univ of OK, Norman
Univ of NM, Albuquerque
Univ of TX, Austin
VA Poly Inst, Blacksburg
Weidlinger, Paul Cons Engr, NY
Weidlinger Assoc, Menlo Park
J.H. Wiggins Co, Redondo Beach
AFWL/HO
(SUL)
(DE)
(DES)
Official Record Copy (AFWL/NTESG/
Capt Reed)